6-2012

Chlorophyll-based Approach for Remote Estimation of Crop Gross Primary Production: from In Situ Measurements to Satellite Imagery

Yi Peng
University of Nebraska-Lincoln, ypeng@huskers.unl.edu

CHLOROPHYLL-BASED APPROACH FOR REMOTE ESTIMATION OF CROP GROSS PRIMARY PRODUCTION: FROM IN SITU MEASUREMENTS TO SATELLITE IMAGERY

by

Yi Peng

A DISSERTATION

Presented to the Faculty of

The Graduate College at the University of Nebraska

In Partial Fulfillment of Requirements

For the Degree of Doctor of Philosophy

Major: Natural Resource Sciences

Under the Supervision of Professor Anatoly A. Gitelson

Lincoln, Nebraska

June, 2012

CHLOROPHYLL-BASED APPROACH FOR REMOTE ESTIMATION OF CROP GROSS PRIMARY PRODUCTION: FROM IN SITU MEASUREMENTS TO SATELLITE IMAGERY

Yi Peng, Ph.D.

University of Nebraska, 2012

Advisor: Anatoly A. Gitelson

The synoptic and accurate quantification of crop gross primary production (GPP) is essential for studying carbon budgets in croplands and monitoring crop status. The objective of this dissertation is to develop a quantitative technique to estimate crop GPP using remotely sensed data collected from close range to satellite altitudes. In this study, a model based on a recently developed paradigm, which relates crop GPP to a product of total crop chlorophyll content and incident radiation affecting vegetation photosynthesis, was justified for the remote estimation of GPP in crops. The model was tested with ground-observed incoming photosynthetically active radiation (PAR_{in}) and vegetation indices (VI), a proxy of total chlorophyll content, retrieved from *in situ* spectral reflectance collected at close range, for GPP estimates in maize-soybean croplands. The results showed that the VI-PAR_{in}-based model was able to provide accurate GPP estimates in maize and soybean under different crop managements, field history and climatic conditions. The algorithms using VIs with red edge spectral band were non-species-specific and yielded an accurate estimation of GPP in both crop types with contrasting canopy architectures and leaf structures (root mean square errors, RMSE, below 2.9gC/m^2/d and coefficients of variation, CV, below 21%). To estimate crop GPP

based solely on remotely sensed data, potential photosynthetically active radiation ($PAR_{potential}$), which is PAR_{in} under a condition of minimal atmospheric aerosol loading, was used. The model, relating crop GPP to a product of chlorophyll-related VI and $PAR_{potential}$, was applied to Landsat and MODIS 250 m data. The algorithms, based on this model, were calibrated over three Nebraska study sites and validated at AmeriFlux sites in Minnesota, Iowa and Illinois showing acceptable accuracy. This VI-$PAR_{potential}$-based model was capable of estimating GPP in both maize and soybean with CV below 16% for maize and 21% for soybean, and yielded higher accuracy than the VI-PAR_{in}-based model when concentrations of atmospheric gases and aerosols were low-to-moderate.

Dedicated with love and gratitude to

my dear mother and father.

谨以此文献给我最亲爱的爸爸妈妈

Acknowledgements

The completion of this dissertation has been one of the most challenges I have ever faced. This research is not possible without the help and support from many people. It is to them that I owe my deep gratitude.

I would like to express my deepest gratitude to my advisor and chairman of my supervisory committee, Prof. Anatoly A. Gitelson, for his great instructions, caring, patience, and providing me with an excellent atmosphere for doing research. He is a strong and supportive advisor to me throughout my graduate study, but he has given me great freedom to think independently. I really enjoyed discussing and debating the various aspects of research with him. As a famous scientist, he always respected my voice even my arguments. Dr. Gitelson helped and inspired me a lot to advance my research, and more importantly, he taught me an attitude to doing science passionately, creatively and critically.

I also acknowledge the valuable contributions from the other members of my supervisory committee: Prof. Donald C. Rundquist, Prof. Shashi B. Verma, Prof. Andrew E. Suyker and Prof. Timothy J. Arkebauer. They were very generous to provide the great data for my research, and were always kind and prompt in responding to my questions regarding to my research and reviewing my writings for publication. Their suggestions and comments helped me to understand my research from different perspectives.

I would like to thank Dr. Jeffery G. Masek, Dr. John M. Baker, Dr. Jerry L. Hatfield, Dr. Tilden Meyers and Dr. Toshihiro Sakamoto for providing and pre-processing the Landsat and MODIS images and field data concerning this research. I am also thankful to

Bryan Leavitt who was helpful and experienced to fix all the technical problems with my computer and instruments in the field.

I am deeply indebted to my dear teammates: Tony Nguy-Robertson, Daniela Gurlin and Tarlan Razzaghi. They not only helped me a lot on my graduate research, but also created a positive and friendly work environment. I will miss the time when we were debating with each other on group meetings for some research issues, the time when we were chatting and joking during the break, and the time when we were sharing our food and cultures on holidays. It would have been a lonely lab without them.

I am very thankful to all the staff and students associated with CALMIT and CSP. Your efforts to collect and maintain the data made my research possible.

I am also thankful to all my friends I met in Lincoln, Luan Pan, Ruopu Li, Leiming Zhao, Xueming Wu, Si Li, Yiyue Xu, etc. Your emotional and spiritual support was important to the successful completion of my research. I am fortunate to know you here.

I would like also to thank Professor Shenghui Fang, the advisor of my master and bachelor program, who opened my eyes to see the beauty of the world of remote sensing.

Finally, my sincerely gratitude goes to my dear mother and father. They are always patient to listen to my whining even woken up by me at midnight, and they are always there, ready to share my happiness and sorrow together.

Grant Information

This research was supported by NASA NACP grant no. NNX08AI75G and partially by the U.S. Department of Energy: (a) EPSCoR program, grant no. DE-FG-02-0ER45827 and (b) Office of Science (BER), grant no. DE-FG03-00ER62996. I sincerely appreciate the support and the use of facilities and equipment provided by the Center for Advanced Land Management Information Technologies (CALMIT) and Carbon Sequestration Program, University of Nebraska-Lincoln.

TABLE OF CONTENTS

LIST OF FIGURES

LIST OF TABLES

Chapter 1: Introduction

Terrestrial vegetation production is the basis of all the biosphere activities on the land surface that relate to global biogeochemical cycles of carbon and nitrogen (Lieth, 1975; Dixon et al., 1994; Schimel, 1998; Myneni et al., 2001). In terrestrial ecosystems, Gross Primary Production (GPP) is the total amount of carbon dioxide that is fixed by plants in photosynthesis. Currently approximately 12% of Earth's land surface is cultivated cropland (Wood et al., 2000). Croplands are both a unique resource and the product of a vital human activity, not only because of an increasing need to feed the world's seven billion people, but also because crops, as the most pervasive anthropogenic biome worldwide, impact environmental processes such as global carbon cycling and climate change (Malmstrom et al., 1997; Cassman and Wood, 2005). Crop GPP contributes approximately 15% of global carbon dioxide fixation (Malmstrom et al., 1997). In general, croplands can have equal or greater production than the natural ecosystems that were converted for crop production (e.g., Law et al., 2002; Barford et al., 2003; Hollinger et al., 2004). Recent study has shown that GPP estimation can be potentially used for evaluating crop yield and nitrogen content (Reeves et al., 2004; Kergoat et al., 2008). Therefore, an accurate and synoptic quantification of spatially distributed GPP in croplands is essential for monitoring crop growth and studying regional and global carbon budgets.

Field studies use tower eddy covariance systems (e.g., Baldocchi, 2003) to calculate seasonal and inter-annual dynamics of GPP in crops. Such micrometeorological approaches provide reliable and accurate estimates of GPP, based on measurements of the entire net CO_2 flux between the land surface and the atmosphere (e.g., Baker and

Griffis, 2005; Hollinger et al., 2005; Verma et al., 2005). Such a process involves building an extensive infrastructure that can be costly. And it measures CO_2 fluxes over a limited area, although at a high temporal resolution. The up-scaling beyond these small footprints is needed for regional and global carbon budget evaluations as well as for estimating crop yield.

Remote sensing is the technology by which the reflected and emitted radiation from the Earth in various wavelengths of the electromagnetic spectrum can be recorded by ground-mounted, airborne and satellite sensors. Since crop production is a result of the interception of solar radiation by the vegetation canopy, it is possible to use remotely sensed data as a powerful and expedient tool for assessing crop GPP over large areas.

The overall objective of this dissertation is to develop a quantitative technique to estimate crop GPP using remotely sensed data collected from close range to satellite altitudes, that is easy to implement, and robust for different crop species grown in the fields with different treatments and various weather conditions. The specific objectives of the study are to:

- Develop, calibrate and validate a model with data collected at close range for GPP estimation in maize-soybean croplands with different crop managements, field history and climatic conditions.
- Explore the possibility of using a unified algorithm, not requiring re-parameterization for different crop species, for GPP estimation in maize and soybean with contrasting leaf structures and canopy architectures.
- Develop, calibrate and validate a model based solely on satellite data for GPP estimation in maize-soybean croplands.

- Explore the possibility of using a unified algorithm based entirely on Landsat or MODIS 250 m data for GPP estimation in maize-soybean croplands that are different in geographic locations, crop management systems, and climatic conditions.

In Chapter 2, the background information regarding GPP estimation with remote sensing techniques is briefly presented. A new paradigm of GPP estimation in crops, based on total canopy chlorophyll content, is justified and compared with previous remote sensing techniques.

Chapter 3 includes the materials and methods used in this study.

In Chapter 4, the methodology is explained for the model that relates crop GPP to a product of vegetation index (VI), which is a proxy for total chlorophyll content, and incoming photosynthetically active radiation (PAR_{in}). This model was tested with ground-observed PAR_{in} and VI retrieved from *in situ* spectral reflectance collected at close range, for estimating GPP in maize and soybean fields over a period from 2001 through 2008. This model was able to provide the accurate estimation of the widely variable GPP in maize and soybean under different crop managements, field history and climatic conditions. And the algorithm using red edge spectral band was non-species-specific and yielded an accurate estimation of GPP in maize and soybean combined.

In Chapter 5, a model is proposed for GPP estimation using chlorophyll-related VI, retrieved from satellite data, and potential PAR_{in} ($PAR_{potential}$), which is PAR_{in} under a condition of minimal atmospheric aerosol loading. This model is based entirely on remotely sensed data, and it is capable of accurately estimating GPP with Landsat data in maize-soybean croplands. The algorithms established and calibrated over three Mead,

Nebraska study sites are validated at AmeriFlux sites in Minnesota, Iowa and Illinois showing acceptable accuracy.

In Chapter 6, the model with $PAR_{potential}$, proposed in Chapter 5, was applied for estimating GPP in maize and soybean with MODIS 250 m data. This approach allowed monitoring crop GPP accurately using solely MODIS 250 m data with high temporal resolution. The accuracy and uncertainties of GPP estimation models with PAR_{in} and $PAR_{potential}$ were also analyzed and compared.

Chapter 2: Estimation of crop gross primary production with remote sensing techniques and support for a new paradigm based on total crop chlorophyll content

This chapter is based on two published papers:

1. Peng, Y., Gitelson, A.A., Keydan, G., Rundquist, D.C. & Moses, W. (2011) Remote estimation of gross primary production in maize and support for a new paradigm based on total crop chlorophyll content. Remote Sensing of Environment, 115, 978-989.

2. Peng, Y., Gitelson, A.A., Keydan, G.P., Rundquist, D.C., Leavitt, B., Verma, S.B., & Suyker, A.E. (2010) Remote estimation of Gross Primary Production in Maize. Proceedings of 10th International Conference on Precision Agriculture, July 18-21, Denver, Colorado, USA, 10th ICPA Proceedings CD, pp. 1-15.

2.1 Background

The carbon exchange between the crop canopy and the atmosphere is mainly controlled by the amount of solar radiation absorbed as well as the efficiency of the plants in using this energy for photosynthesis. The former is expressed as the product of the incident photosynthetically active radiation (PAR_{in}) and the fraction of absorbed PAR_{in} (fAPAR). The latter is the light use efficiency (LUE), which is the efficiency with which the absorbed PAR_{in} is converted into biomass. However, not all light absorbed by the canopy is used for photosynthesis. Only the so-called 'photosynthetic' or 'green' part is absorbed by photosynthetically active vegetation. This component has been termed $fAPAR_{green}$ and defined as (Hall et al., 1992; Vina and Gitelson, 2005):

$fAPAR_{green} = fAPAR \times (\text{green LAI/total LAI})$ (2.1)

where total LAI is the leaf area index, a ratio of leaf surface area to unit ground area, which is widely used as a vital input in crop modeling (Bouman, 1995). Green LAI is the photosynthetically functional component of the total LAI (Barclay, 1998), which is directly expressive of the photosynthetic apparatus of the vegetation (Whittaker & Marks, 1975).

The estimation of crop productivity is based on a concept originally developed by Monteith (1972, 1977), who suggested that GPP can be expressed as:

$GPP = fAPAR_{green} \times PAR_{in} \times LUE$ (2.2)

This equation provides the linkage between GPP and vegetation biophysical characteristics, such as $fAPAR_{green}$ and/or green LAI, thus, forms the basis for quantification of GPP via estimation of biophysical characteristics by means of remote sensing. Biophysical characteristics of vegetation that relate to the amount of absorbed radiation (e.g., $fAPAR_{green}$, green LAI, chlorophyll content, vegetation fraction) can be measured remotely via transforms of spectral reflectance, allowing one to quantitatively connect remotely sensed data to plant productivity. The procedures developed so far can be classified into two broad categories according to the way the absorption of solar radiation and its conversion into dry matter are modeled (e.g., Ruimy et al., 1999):

(1) Production Efficiency Models (PEMs); and

(2) Canopy Photosynthesis Models (CPMs).

In the case of PEMs, $fAPAR_{green}$ is usually approximated by the Normalized Difference Vegetation Index - NDVI (Rouse et al, 1974). LUE is commonly regarded as a near constant value, though biome-specific (e.g., Ruimy et al., 1999). The problems in

using PEMs are: (a) a significant decrease in the sensitivity of NDVI to moderate-to-high vegetation density when $fAPAR_{green}$ exceeds 0.7 (e.g., Kanemasu, 1974; Asrar et al., 1984; Vina and Gitelson, 2005; Gitelson et al., 2006a), and (b) the species-specific rather than the merely biome-specific variation of LUE (e.g., Ahl et al., 2004). A certain variation of LUE is expected because GPP varies not only with APAR but also with other factors: e.g., soil water and nutrient availability, the ratio of direct to diffuse radiation, canopy age, and/or site history (Alton et al., 2007; DeLucia et al., 2007). LUE also varies considerably among vegetation types, in different phenological stages and under different environmental conditions (Prince, 1991; Ruimy et al. 1994; Medlyn 1998; Gower et al., 1999). Thus, there is little doubt overall that the assumption of a constant LUE does not provide an accurate description of terrestrial ecosystems (Binkley et al., 2004; Bradford et al., 2005; Kergoat et al., 2008). Recent analysis by Kergoat et al., (2008) strongly supports the view that LUE varies significantly not only both across and within biomes, but also among plant functional types.

The variations of LUE do need to be carefully considered, but a model that effectively accounts for the variations of LUE, resulting in a significant increase in the accuracy of GPP estimation, is yet to be developed. Many remote sensing models use look-up tables of maximum LUE for specific vegetation types. These values are then adjusted downward by considering environmental stress factors (Ruimy et al., 1994; Anderson et al., 2000; Running et al., 2004; Xiao et al., 2004; Yuan et al., 2007). Different approaches have arisen recently to remotely estimate LUE from a wide variety of wavelengths and sensor types. Among those approaches, climatic variables, like vapor pressure deficit, temperature, and water indices are widely employed as surrogates for

photosynthetic stresses (Running et al., 2004; Sims et al., 2008; Xiao et al., 2004). Because vapor pressure deficit, temperature and land surface water index are not always good surrogates of reduced efficiency, meteorologically based methods may not always explain efficiency variation (Garbulsky et al., 2010). While land surface temperature, derived from thermal wavelengths (Sims et al., 2008), and Vegetation Photosynthesis Model (Xiao et al., 2004) were successfully tested to estimate 16 day GPP from MODIS data, it would be inadequate to track short-term physiological variability.

The Photochemical Reflectance Index (PRI) was widely used as a proxy of LUE at different scales from leaves to entire canopies (Gamon et al., 1992). A recent review by Garbulsky et al., (2010) examined and synthesized the scientific literature on the relationships between PRI and several ecophysiological variables across a range of plant functional types and ecosystems at the leaf, canopy and ecosystem levels and at the daily and seasonal time scales. The authors demonstrated a consistency of the LUE–PRI relationship that suggests a surprising degree of functional convergence of biochemical, physiological and structural components affecting leaf, canopy and ecosystem carbon uptake efficiencies. It is underlined that PRI provides a useful tool for estimating seasonal carbon fluxes in evergreen plants because of its connection with LUE, whereas fAPAR as well as greenness (i.e., chlorophyll content) would presumably be less useful in this context since they change little over seasonal time scales. On the contrary, PRI may not be effective in detecting LUE in ecosystems where fAPAR closely follows the seasonal dynamic of CO_2 exchange. This seems to be the case in annual croplands and grasslands. In those ecosystems, fAPAR and LUE scale well with photosynthetic rates and chlorophyll content is closely tied to seasonal carbon dynamics and thus provides a

dominant indicator of ecosystem CO_2 uptake. No significant improvement was observed by the use of PRI as an approximation of LUE for GPP estimation in crops compared with the use of a constant LUE (Gitelson et al., 2006b; Wu et al., 2010b). The same is probably the case for the use of air temperature and water indices as input data to calculate LUE.

In the case of CPMs, GPP is first estimated at leaf level, and then integrated over the entire canopy. In these models, $fAPAR_{green}$ is expressed as a function of green LAI (e.g., Ruimy et al., 1999) in the form:

$$fAPAR_{green} = 0.95(1- \exp(-k \times \text{green LAI})) \quad (2.3)$$

where k is coefficient of light extinction. The probability of interception of solar radiation is related to foliage orientation and density, as well as the path length of light inside the canopy. So, the extinction coefficient is affected by many factors such as leaf structure and canopy architecture, both of which affect the rate and extent of the absorption of incoming radiation. Thus, the relationship $fAPAR_{green}$ vs. green LAI might be species specific and may vary even within a species, and the assumption that fAPAR is the radiometric equivalent of LAI is not valid in many cases.

A physically-based algorithm for estimating green LAI from NDVI observations has been developed (e.g., Myneni et al. 1997). However, the relationship between NDVI and green LAI is essentially non-linear and suffers a rapid decrease of sensitivity at moderate-to-high densities of photosynthetic green biomass; e.g., when LAI exceeds 3 (Kanemasu, 1974, Asrar et al., 1984, Myneni et al., 1997, Gitelson et al., 2003c).

2.2 Support for a new paradigm for estimating crop GPP based on total chlorophyll content

2.2.1 The basis for using total crop chlorophyll content as a proxy of GPP

Since the early 1960's, scientists have looked for natural short-cuts to estimating productivity based on the biophysical characteristics of vegetation related to photosynthesis. Among them was the total chlorophyll content per unit area (e.g., Whittaker and Marks, 1975). It was shown that canopy chlorophyll content is a very direct expression of the photosynthetic apparatus of a plant community, and it was found that for a given species or type of community, chlorophyll content may be strongly related to productivity. Medina and Leith (1964) found a very close linear relationship between chlorophyll content and productivity (as indicated by the seasonal maximum biomass) with determination coefficient (R^2) > 0.99. Chlorophyll content per unit area has been correlated with crop productivity, net photosynthesis and absorbance (Osborne and Raven, 1986 and references within). Since long- or medium-term changes in canopy chlorophyll content are related to both crop phenology and photosynthetic capacity, and may also be affected by water and thermal stresses (e.g., Ustin et al., 1998, Zarco-Tajeda et al., 2002), the canopy chlorophyll content is related to GPP. Houborg et al., (2010) indicated significant potential for using remotely sensed leaf chlorophyll content for quantifying variability of photosynthetic efficiency across a heterogeneous corn field that was exposed to severe environmental stresses. Wu et al., (2009) found a close relationship between GPP and total chlorophyll content, with R^2 > 0.87, for wheat encompassing three classes of canopy leaf orientation (erectophile, spherical, and planophile).

At the leaf level, numerous studies have demonstrated a strong link between nitrogen content and photosynthesis (Field and Mooney, 1986; Wullschleger, 1993). Kergoat et al., (2008) analyzed the relationship between foliar nitrogen content and eddy covariance CO_2 flux measurements, obtained at a range of diverse sites located in the mid to high latitudes, which encompass managed and unmanaged stands, mono- or pluri-specific canopies. They concluded that leaf nitrogen content is a strong factor influencing both optimum canopy LUE and canopy photosynthesis rate. On the other hand, Baret et al., (2007) found that canopy chlorophyll content is well suited for quantifying canopy level nitrogen content. They concluded that canopy chlorophyll content is a physically sound quantity since it represents the optical path in the canopy where absorption by chlorophyll dominates the radiometric signal. Thus, absorption by chlorophyll provides the necessary link between remote sensing observations and canopy state variables that are used as indicators of nitrogen status. Baret et al., (2007) claim that nitrogen status could only be assessed through chlorophyll estimates and showed that it can actually be retrieved with reasonable accuracy. A close relationship between contents of nitrogen and chlorophyll at canopy level rather than at leaf level was also clearly demonstrated in an experiment conducted over wheat crops subjected to a range of nitrogen stresses (Houles et al., 2006).

Recently, a new paradigm for GPP estimation in crops based on the assumption that total canopy chlorophyll content is the main driver of crop GPP has been proposed (Gitelson et al., 2003b, 2006b). Total chlorophyll (Chl) content was defined as the product of leaf Chl content and LAI (Gitelson et al., 2005; Ciganda et al., 2009). Close relationships between GPP and total Chl content have been documented in three

contrasting crop types: maize, soybean and wheat (Gitelson et al., 2003b; Gitelson et al., 2006b; Wu et al., 2009).

Thus, total Chl content relates both to GPP and to leaf nitrogen content, which, in turn, relates directly to photosynthesis. So, the remote estimation of GPP in crops can be based on total Chl content retrieval from remotely sensed data.

2.2.2 Advantages of using total Chl content for GPP estimation

The approach for estimating GPP via total Chl content has advantages when used in both CPM and PEM models. In CPM models, the green LAI is used as a measure of the amount of radiation absorbed by the plants. However, a potential bias will be introduced when measuring the green LAI, because it is somewhat subjective to decide whether a leaf is green or non-green when crops are at the reproductive stage (Ciganda et al., 2008). In practice, mature dark green leaves with high Chl content during the green-up stage and leaves with much lower Chl content during the reproductive stage are both designated as 'green' leaves (e.g., Law et al., 2008) although they may have very different photosynthesis ability. For the same green LAI, the Chl content in a leaf taken in the green-up stage might be more than two times higher than the Chl content in a leaf taken in the reproductive stage (Fig. 2.1). Thus, the total Chl content is a much more objective parameter than green LAI in quantifying the amount of absorbed radiation. Therefore, the use of total Chl content instead of green LAI can decrease uncertainties in CPM models due to the bias involved in determining green LAI.

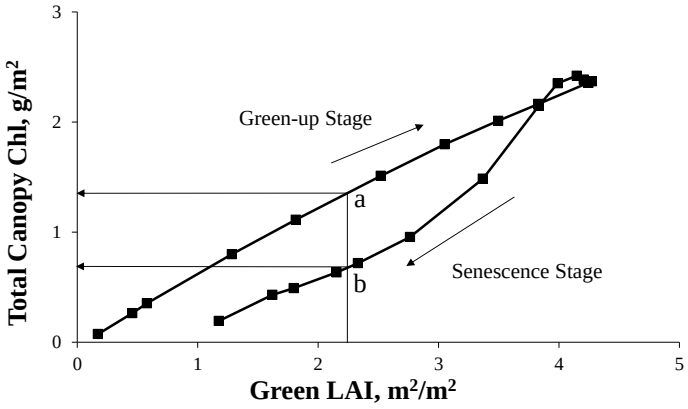

Figure 2.1 Relationship between total chlorophyll content and green LAI. Mature dark green leaves with high chlorophyll content in green-up stage (point a) and leaves with much lower chlorophyll in reproductive stage (point b) are both designated as 'green' leaves. Thus, for the same green LAI, total chlorophyll content may be significantly different.

Total Chl content is a main factor that influences the amount of PAR absorbed by photosynthetically active vegetation. It relates closely to $fAPAR_{green}$, which is used in PEM models (Fig. 2.2). But, as total Chl content exceeds 2.3 g/m^2, $fAPAR_{green}$ becomes almost invariant. Osborne and Raven (1986) noted that although proportional changes in light absorption will not occur at high Chl content, they may be important in situations where low incident radiation severely limit photosynthesis, as may occur within crop canopies or in deep shade, or for shaded leaves of single plants. Importantly, contrary to the saturation evident in the $fAPAR_{green}$ vs. total Chl content relationship, the GPP does remain sensitive to total Chl content even when it exceeds 2.3 g/m^2 (in Fig. 2.3 it corresponds to $Chl \times PAR_{in}$ above 23 $g/m^2 \times MJ/m^2/d$).

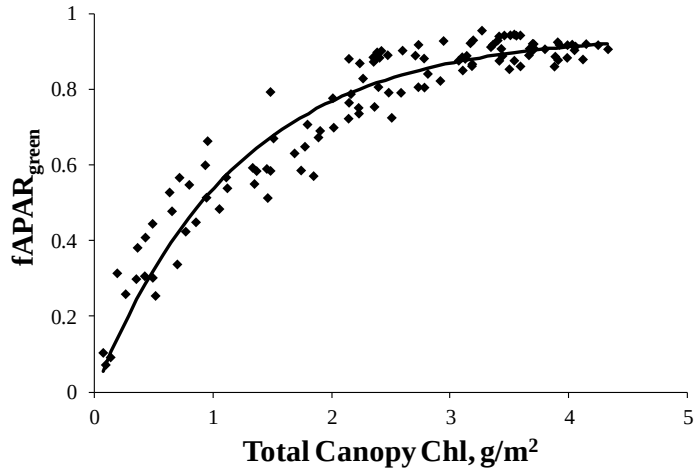

Figure 2.2 Fraction of PAR absorbed by photosynthetically active vegetation ($fAPAR_{green}$) plotted versus total maize canopy chlorophyll content. When chlorophyll content exceeds 2.3 g/m^2, $fAPAR_{green}$ virtually does not change with further increase in chlorophyll content.

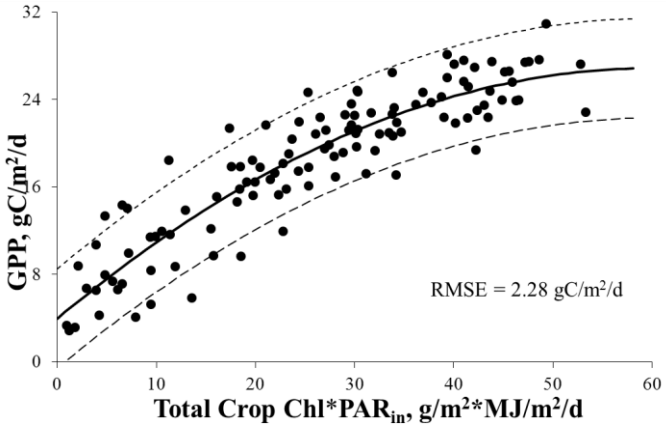

Figure 2.3 Gross primary production of maize plotted versus the product of total chlorophyll content and PAR_{in}.

This behavior of the relationship between GPP and total Chl content may be explained by the increase in LUE that follows an increase in total Chl content. LUE does

indeed relate to the Chl content of a crop. The relationship LUE vs. total Chl content, shown in Fig. 2.4, is based on the data collected in both irrigated and rainfed sites for different maize hybrids, phenological stages, environmental conditions, field management procedures, and growing situations. The relationship is positive and statistically significant (R^2 = 0.46, P-value = 0.0078). One of the reasons for the close relationship LUE vs. total Chl content is total Chl content directly relates to the electron transport apparatus, which governs LUE to plant stress (Terry, 1980; Terry 1983).

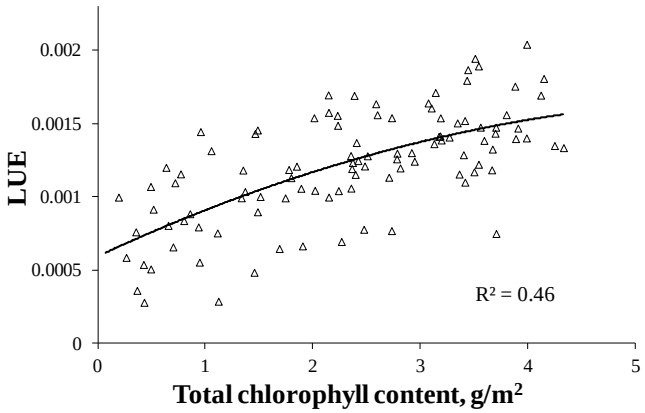

Figure 2.4 Light use efficiency, calculated as LUE = GPP/(PAR_{in}×$fAPAR_{green}$), plotted versus total chlorophyll content in maize.

Thus, while the relationship $fAPAR_{green}$ vs. total Chl content saturates at Chl contents above 2.3 g/m^2 and the amount of radiation absorbed by the crop remains almost invariant at moderate-to-high levels of Chl content (Fig. 2.2), LUE increases (Fig. 2.4); it results in an increase in GPP (Fig. 2.3). Our finding supports also the results obtained in several recent studies. Dawson et al. (2003) showed that the variation in foliar Chl content may account for some of the seasonal variability in LUE. Houborg et al. (2010)

demonstrated that variations in leaf Chl content were well-correlated with temporal changes in LUE. Kergoat et al. (2008) found that foliar nitrogen of the dominant plant species, which closely related total Chl content, explained 71% of the variation in LUE.

Therefore, two key physiological properties included in Eq. 2.2, light capture and the efficiency of the use of absorbed light, relate closely to total canopy Chl content, which subsumes a broad range of processes and can be applied as an integrative diagnostic tool. It means that total Chl content is relevant for estimating GPP in PEMs and CPMs. As a result, a procedure was suggested to remotely assess GPP in crops (Eq. 2.3) employing total crop Chl content (Gitelson et al., 2006b):

$$GPP \propto Chl \times PAR_{in} \quad (2.3)$$

2.3 Remote estimation of total chlorophyll content

Several remote sensing techniques have been proposed to estimate vegetation Chl content by relating it to vegetation indices (VI), which are calculated based on mathematical combinations of ratios, differences and sums of spectral reflectance data that can be remotely sensed. Table 2.1 shows different VI developed to remotely assess the vegetation Chl content. Generally, there are two different approaches to the remote estimation of Chl content in crops. One of them is to assess the *leaf Chl content* by such VI as MCARI, TCARI or combined index such as TCARI/OSAVI (Haboudane et al., 2002). The other approach is to assess the *total canopy Chl content* by such VI as Chl Indices (CI_{green} and $CI_{red\ edge}$) and MTCI, or to estimate *green LAI*, which closely relates to total crop canopy Chl content (Ciganda et al., 2008), by SR, NDVI, EVI or EVI2, WDRVI, and TVI-like indices.

Table 2.1. Summary of Vegetation Indices (VI) used for estimating vegetation total chlorophyll content. ρ_{NIR}, $\rho_{red\ edge}$, ρ_{red}, ρ_{green}, ρ_{800}, ρ_{750}, ρ_{670}, ρ_{550} are reflectance values in spectral bands of NIR, red edge, red, green region and 800 nm, 750 nm, 670 nm, 550 nm respectively.

Vegetation Index	Formula	Reference
Simple Ratio (SR)	ρ_{NIR}/ρ_{red}	Jordan, 1969
Normalized Difference Vegetation Index (NDVI)	$(\rho_{NIR} - \rho_{red}) / (\rho_{NIR} + \rho_{red})$	Rouse et al., 1974
OSAVI	$(1+1.16) \times (\rho_{NIR} - \rho_{red}) / (\rho_{NIR} + \rho_{red} + 0.16)$	Rondeaux et al., 1996
Enhanced Vegetation Index 2 (EVI2)	$2.5 \times (\rho_{NIR} - \rho_{red}) / (1 + \rho_{NIR} + 2.4 \times \rho_{red})$	Jiang et al., 2008
Triangular Vegetation Index (TVI)	$0.5\times [120\times (\rho_{750} - \rho_{550}) - 200\times(\rho_{670} - \rho_{550})]$	Broge & Leblanc, 2000
Modified TVI 1(MTVI1)	$1.2\times [1.2\times (\rho_{800} - \rho_{550}) - 2.5\times (\rho_{670} - \rho_{550})]$	Haboudane et al., 2004
Modified TVI 2 (MTVI2)	$1.5\times [1.2(\rho_{800} - \rho_{550}) - 2.5\times (\rho_{670} - \rho_{550})] / \text{sqrt}((2\rho_{800}+1)^2 - (6\rho_{800} - 5\text{sqrt}(\rho_{670})) - 0.5)$	Haboudane et al., 2004
Visible Atmospherically Resistant Index (VARI)	$(\rho_{green} - \rho_{red}) / (\rho_{green} + \rho_{red})$	Gitelson et al, 2002
Wide Dynamic Range Vegetation Index (WDRVI)*	$(\alpha \times \rho_{NIR} - \rho_{red}) / (\alpha \times \rho_{NIR} + \rho_{red}),\ 0 < \alpha < 1$ $(\alpha \times \rho_{NIR} - \rho_{red}) / (\alpha \times \rho_{NIR} + \rho_{red}) + (1 - \alpha) /(1+ \alpha)$	Gitelson, 2004 Peng & Gitelson, 2011b
Green Wide Dynamic Range Vegetation Index (Green WDRVI)	$(\alpha \times \rho_{NIR} - \rho_{green}) / (\alpha \times \rho_{NIR} + \rho_{green}) + (1 - \alpha) /(1+ \alpha),\ 0 < \alpha < 1$	Gitelson et al., 2012
MCARI	$[(\rho_{700} - \rho_{670}) - 0.2(\rho_{700} - \rho_{550})] \times (\rho_{700}/ \rho_{670})$	Daughtry et al., 2000
TCARI	$3[(\rho_{700} - \rho_{670}) - 0.2(\rho_{700} - \rho_{550}) \times (\rho_{700} / \rho_{670})]$	Haboudane et al., 2002
Red edge NDVI	$(\rho_{NIR} - \rho_{red\ edge}) / (\rho_{NIR} + \rho_{red\ edge})$	Gitelson & Merzlyak,1994, 1997
MERIS Terrestrial Chlorophyll Index (MTCI)	$(\rho_{NIR} - \rho_{red\ edge}) / (\rho_{red\ edge} - \rho_{red})$	Dash & Curran, 2004
Green Chlorophyll Index (CI_{green})	$\rho_{NIR} / \rho_{green} - 1$	Gitelson et al., 2003a, 2005
Red edge Chlorophyll Index ($CI_{red\ edge}$)	$\rho_{NIR} / \rho_{red\ edge} - 1$	Gitelson et al., 2003a, 2005

* In original formulation of WDRVI (Gitelson, 2004), it may be negative for low to moderate vegetation density. Here WDRVI was calculated as $(\alpha \times \rho_{NIR} - \rho_{red}) / (\alpha \times \rho_{NIR} + \rho_{red}) + (1 - \alpha)/(1+ \alpha)$, which ranged from 0 to $(1 - \alpha)/(1+ \alpha)$.

The most widely used NDVI was found to be a good indicator of low-to-moderate vegetation Chl content; however, saturation of red reflectance and much higher NIR

reflectance compared to red reflectance ($\rho_{NIR} >> \rho_{red}$) at intermediate to high Chl content (e.g., Kanemasu, 1974; Buschmann and Nagel, 1993; Gitelson, 2004) limit the applicability of NDVI for estimating vegetation Chl content above 1 g/m^2 (Gitelson et al., 2005). WDRVI (Gitelson, 2004) is a non-linear transformation of NDVI, which is much more sensitive than NDVI to moderate to high vegetation Chl content, by introducing a weighting coefficient α to attenuate the contribution of the NIR reflectance, and to make NIR reflectance comparable to red reflectance at moderate-to-high green biomass (Gitelson, 2004; Vina et al., 2004).

It has been shown that reflectance in the green or the red edge regions is sensitive to a wide range of vegetation Chl content (Thomas and Gaussman, 1977; Chappelle et al., 1992; Buschmann and Nagel, 1993; Yoder and Waring, 1994; Lichtenthaler et al., 1996; Gitelson et al., 1996). Several vegetation indices based on these spectral regions have been developed and used successfully to estimate Chl content (e.g., Broge and Leblanc, 2000; Dash and Curran, 2004; Gitelson and Merzlyak, 1994; Gitelson et al., 2005).

Huete et al. (1997) introduced the Enhanced Vegetation Index (EVI), which has a higher sensitivity to moderate-to-high vegetation biomass and is widely used as a product of the MODIS (MODerate resolution Imaging Spectroradiometer) system. EVI and its alternative form EVI2 were shown to be much more accurate than NDVI in estimating GPP for different vegetation types, including crops (e.g., Sims et al., 2006; Xiao et al., 2004).

Recently, a conceptual model that relates reflectance with pigment content (Chl, carotenoids, and anthocyanins) at leaf and canopy level (Gitelson et al., 2003a) was developed in the form:

$$\text{Pigment content} \propto [\rho(\lambda_1)^{-1} - \rho(\lambda_2)^{-1}] \times \rho(\lambda_3) \quad (2.4)$$

where $\rho(\lambda_1)$, $\rho(\lambda_2)$ and $\rho(\lambda_3)$ are reflectance values at wavelength λ_1, λ_2 and λ_3 respectively.

Special cases of the conceptual model for estimating particular pigment contents are achieved by appropriately choosing the locations of the wavelengths in the model, based on the optical characteristics of the object containing the pigment of interest. For estimating vegetation Chl content, the optimal location for λ_1 was either in the green (540–560 nm) or red edge (700–730 nm) region; $\lambda_2 = \lambda_3$ was optimally located in the NIR region beyond 750 nm (Gitelson et al., 2005). Thus, the Chl Indices, CI, for estimating total canopy Chl content are in the form:

$$CI_{green} = \rho_{NIR} / \rho_{green} - 1 \quad (2.5)$$

$$CI_{red\ edge} = \rho_{NIR} / \rho_{red\ edge} - 1 \quad (2.6)$$

Chapter 3: Materials and methods

3.1 Study area

Data from seven AmeriFlux sites were used in our investigation (Fig. 3.1, Table 3.1), three of which are located at the University of Nebraska-Lincoln Agricultural Research and Development Center near Mead, Nebraska (NE), USA (public.ornl.gov/ameriflux/Site_Info/siteInfo.cfm?KEYID=us.mead_maize.01; public.ornl.gov/ameriflux/Site_Info/siteInfo.cfm?KEYID=us.mead_maize_soybean_irrigated.01; public.ornl.gov/ameriflux/Site_Info/siteInfo.cfm?KEYID=us.mead_maize_soybean_rainfed.01). Those three sites are all approximately 60-ha fields within 1.6 km of each other. Site 1 is planted in continuous maize equipped with a center pivot irrigation system. Site 2 and 3 are both planted in maize-soybean rotation, but the former is irrigated in the same way as site 1, while site 3 relies entirely on rainfall for moisture. Crop management details, yield and maximum GPP for these three Nebraska sites during 2001 through 2008 were given in Table 3.2.

Site 4, near Rosemount, Minnesota (MN), is 18.4 ha in size (public.ornl.gov/ameriflux/Site_Info/siteInfo.cfm?KEYID=us.rosemount.01). Sites 5 and 6 are 60-ha fields, in close proximity, near Ames, Iowa (IA) (public.ornl.gov/ameriflux/Site_Info/siteInfo.cfm?KEYID=us.ames_tl10.01; public.ornl.gov/ameriflux/Site_Info/siteInfo.cfm?KEYID=us.ames_tl11.01). Site 7 is located at Bondville, Illinois (IL) (public.ornl.gov/ameriflux/Site_Info/siteInfo.cfm?KEYID=us.bondville.01). The rainfed study sites in MN, IA and IL are all planted in rainfed maize-soybean rotation, and the

planting density was 86000 plants per ha for maize and 340600 plants per ha for soybean. More details about the crop management and field history of these study sites are available in Hatfield et al., (1999), Baker and Griffis, (2005), Hollinger et al., (2005) and Verma et al., (2005).

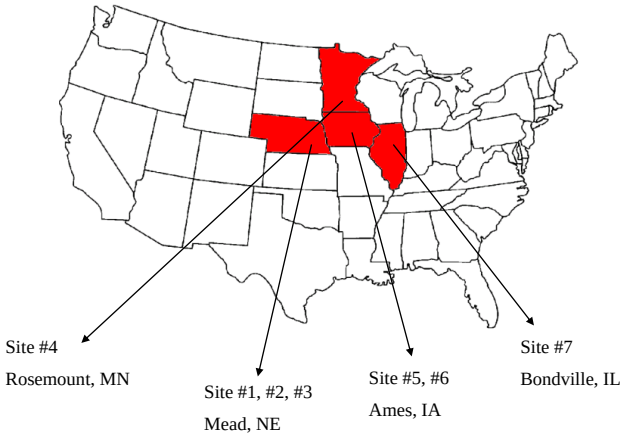

Figure 3.1 The general location of the seven study sites in Minnesota, Nebraska, Iowa and Illinois.

Table 3.1. Details regarding locations of seven study sites in our investigation. ICM: irrigated continuous maize; IMS: irrigated maize-soybean rotation, with maize planted in odd years; RMS: rainfed maize-soybean rotation, with maize planted in odd years; RSM: rainfed maize-soybean rotation, with soybean planted in odd year.

Ameriflux ID	Site Location	Latitude	Longitude	Elevation (m)	Vegetation type	Study period
1. US-Ne1	Mead, NE	41°09′54.2″N	96°28′35.9″W	361	ICM	2001-2008
2. US-Ne2	Mead, NE	41°09′53.5″N	96°28′12.3″W	362	IMS	2001-2008
3. US-Ne3	Mead, NE	41°10′46.8″N	96°26′22.7″W	363	RMS	2001-2008
4. US-Br1	Ames, IA	41°58′29.6″N	93°41′25.4″W	275	RMS	2005-2007
5. US-Br3	Ames, IA	41°58′28.9″N	93°41′37.0″W	314	RSM	2005-2007
6. US-Bo1	Bondville, IL	40°0′22.3″N	88°17′25.4″W	219	RMS	2001-2003
7. US-Ro1	Rosemount, MN	44°42′51.5″N	93°05′23.4″W	260	RMS	2005-2007

Table 3.2. Crop management details, yield and maximum GPP for three study sites in Mead, Nebraska during 2001–2008.

Site/year	Crop hybrid	Density (plants/ha)	Tillage operation	Applied N (kg N/ha)	Max GPP ($gC/m^2/d$)	Yield (Mg/ha)
Site 1 Irrigated continuous maize						
2001	Maize Pioneer 33P67	82000	Intensive tillage	196	31.1	13.51
2002	Maize Pioneer 33P67	81000	No-till	214	28.8	12.97
2003	Maize Pioneer 33B51	77000	No-till	233	27.3	12.12
2004	Maize Pioneer 33B51	84012	No-till	293	30.4	12.24
2005	Maize DeKalb 63-75	82374	No-till	246	26.7	12.02
2006	Maize Pioneer 33B53	84012	Conservation-plow	210	26.2	10.46
2007	Maize Pioneer 31N30	74000	Conservation-plow	272	30.6	12.79
2008	Maize Pioneer 31N30	84000	Conservation-plow	123	26.9	11.99
Site 2 Irrigated maize-soybean rotation						
2001	Maize Pioneer 33P67	81000	Intensive tillage	196	33.5	13.41
2002	Soybean Asgrow 2703	370644	No-till	0	18.7	
2003	Maize Pioneer 33B51	78000	No-till	169	28.2	14.00
2004	Soybean Pioneer 93B09	370644	No-till	0	15.3	
2005	Maize Pioneer 33B51	81000	No-till	170	27.2	13.24
2006	Soybean Pioneer 93M11	370644	No-till	0	16.1	
2007	Maize Pioneer 31N28	75000	No-till	183	27.6	13.21
2008	Soybean Pioneer 93M11	370644	No-till	0	15.3	
Site 3 Rainfed maize-soybean rotation						
2001	Maize Pioneer 33B51	52600	Intensive tillage	128	28.9	8.72
2002	Soybean Asgrow 2703	370644	No-till	0	15.3	
2003	Maize Pioneer 33B51	57600	No-till	90	25.2	7.72
2004	Soybean Pioneer 93B09	370644	No-till	0	14.7	
2005	Maize Pioneer 33G68	56300	No-till	118	22.5	9.10
2006	Soybean Pioneer 93M11	370644	No-till	0	16.2	
2007	Maize Pioneer 33H26	52000	No-till	125	24.3	10.23
2008	Soybean Pioneer 93M11	370644	No-till	0	16.8	

3.2 GPP from eddy covariance flux measurements

Each study site is equipped with an eddy covariance tower and meteorological sensors, with which the continuous measurements of CO_2 fluxes, water vapor and energy fluxes every hour. Daytime net ecosystem exchange (NEE) values were computed by integrating the hourly CO_2 fluxes collected during a day when PAR_{in} exceeded $1\mu mol/m^2/s$. Daytime estimates of ecosystem respiration (Re) were obtained from the night CO_2 exchange-temperature relationship (e.g., Xu and Baldocchi, 2003). The GPP was then obtained by subtracting Re from NEE as: GPP = NEE - Re. GPP values are

presented in the unit of $gC/m^2/d$, and sign convention used here is such that CO_2 flux to the surface is positive so that GPP is always positive and Re is always negative (Verma et al., 2005). This approach has been widely used in the context of tower flux measurements and is considered to provide reasonable estimates at the landscape level (details in Verma et al., 2005; Suyker et al., 2005). The GPP data used in this study were collected and processed by Dr. S.B. Verma's group for NE sites, by Dr. T. Meyers's group for IL sites, by Dr. J.M. Baker's group for MN sites, and by Dr. J.L. Hatfield's group for IA sites.

3.3 Ground-observed incoming PAR

Photosynthetically active radiation (PAR) is the solar radiation in spectral range of 400 - 700 nm that photosynthetic organisms are able to use in the process of photosynthesis. In this study, point quantum sensors (LI-190, LI-COR Inc., Lincoln, Nebraska) were placed in each study site, 6 m above the surface pointing toward the sky, to measure hourly incoming PAR (PAR_{in}). Daytime PAR_{in} values were computed by integrating the hourly measurements during a day when PAR_{in} exceeded $1\mu mol/m^2/s$. Daily PAR_{in} values were presented in $MJ /m^2/d$ (Turner et al., 2003). PAR data used in this study were collected by Dr. S.B. Verma's group for NE sites, by Dr. T. Meyers's group for IL sites, by Dr. J.M. Baker's group for MN sites, and by Dr. J.L. Hatfield's group for IA sites.

The temporal behavior of PAR_{in} during the growing season includes two types of variation: low- and high-frequency variation (Fig. 3.2). The former is due to seasonally decreased PAR_{in} intensity; total hours of sunlight in the Northern Hemisphere gradually decrease after the summer solstice (e.g. such decrease occurs around June 21: day of

year, DOY, 172, for Nebraska). For example, the monthly-average incoming PAR_{in} intensity in the Midwestern U.S. declined by 31% from July to September (Sakamoto et al., 2011b). There is also high frequency PAR_{in} variation, which corresponds to short-period changes in atmospheric transmissivity due to clouds or aerosols (Peng et al., 2011).

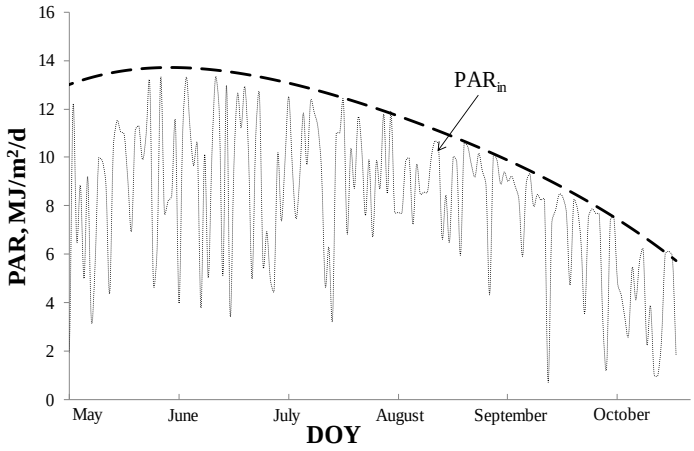

Figure 3.2 Temporal behavior of PAR_{in} during the growing season in Mead, Nebraska. High frequency of PAR_{in} variation is due to short-period changes in atmospheric transmissivity and low frequency of PAR_{in} variation (shown as the dashed line) is due to seasonally decreased PAR_{in} intensity.

3.4 Destructive determination of leaf area index

Within each of three Nebraska sites, six small plot areas (20 m × 20 m) were established, called as Intensive Measurement Zones (IMZ). These IMZs represented all major occurrences of soil and crop production zones within each field (Verma et al., 2005).

Leaf area index (LAI) was estimated by Dr. T. Arkebauer's group from destructive samples at 10 – 14 day intervals during the growing season from 2001 through 2008 for the Nebraska sites. On each sampling date, plants from a 1m length of either of two rows within each IMZ were collected and the total number of plants recorded. Collection rows were alternated on successive dates to minimize edge effects on subsequent plant growth. Plants were kept on ice and transported to the laboratory. In the lab, plants were separated into green leaves, dead leaves, and litter components. All leaves were run through an area meter (Model LI-3100, Li-Cor, Inc., Lincoln, Nebraska) and the leaf area per plant was determined. For each IMZ, the leaf area per plant was multiplied by the plant population to obtain a total LAI. Total LAI for the six IMZs were then averaged as a site-level value (details in Vina, 2004). Green leaves were measured in the same way to obtain the green LAI. Since the LAI values changes gradually during the growing season, daily total LAI and green LAI values were cubic spline interpolated based on measurements on sampling dates for each site in each year using MATLAB (V. 7.9.0.529,The MathWorks, Massachusetts, USA).

3.5 Canopy chlorophyll content

During 2001 through 2004, spectral reflectance measurements of the collar or ear leaves in maize and soybean were collected by Ocean Optics radiometer in three Nebraska sites biweekly during growing seasons. Around 70 maize and 15 soybean leaves were punched in the lab and leaf Chl content was determined for each leaf analytically (details in Vina, 2004; Gitelson et al., 2005). A linear relationship of leaf Chl content vs. red edge Chl index calculated from leaf reflectance (Gitelson et al., 2005) was

then established. With this calibrated algorithm, leaf Chl content was retrieved for all sample leaves with scanned spectral reflectance using red edge Chl index. And such method for non-destructively estimation of leaf Chl content was shown to be very accurate (Gitelson et al., 2005). Total canopy Chl content was estimated as:

$$Chl_{canopy} = Chl_{leaf} \times \text{green LAI} \quad (3.1)$$

where Chl_{canopy} is canopy Chl content and Chl_{leaf} is leaf Chl content of the collar or ear leaves in the plant (Gitelson et al., 2005, Ciganda et al., 2009).

In 2005, three plants from each field were sampled weekly during the growing season (128 plants in total). In the laboratory, each leaf of the plant was visually examined to identify and separate sections that were different in color. The Chl content of each section with the homogeneous "greenness" was determined, as well as the area of each section measured by a leaf area meter (Model LI-3100, Li-Cor, Inc., Lincoln, Nebraska). And the total amount of Chl content in a leaf section was then determined as a product of section Chl content and section area. Total canopy Chl content of each plant was calculated as the sum of Chl amount of all leaf sections normalized to ground area (details in Ciganda et al., 2009). The canopy Chl content data used in this study was measured by Dr. A.A. Gitelson's group.

3.6 Fraction of absorbed photosynthetically active radiation by the canopy

PAR reflected by the canopy and soil (PAR_{out}) was measured with Li-Cor point quantum sensors aimed downward, and placed at 6 m above the ground. PAR transmitted through the canopy (PAR_{transm}) was measured with Li-Cor line quantum sensors placed at about 2 cm above the ground, pointing upward; PAR reflected by the soil (PAR_{soil}) was

measured with Li-Cor line quantum sensors placed about 12 cm above the ground, pointing downward (details in Hanan et al., 2002; Burba 2005). Absorbed PAR (APAR) was calculated as (Goward and Huemmerich, 1992):

$$APAR = PAR_{in} - PAR_{out} - PAR_{transm} + PAR_{soil} \quad (3.2)$$

All the daytime radiation values were computed by integrating the hourly measurements during a day when PAR_{in} exceeded 1μmol/m^2/s, and fAPAR was then calculated as $APAR/PAR_{in}$. fAPAR measurements used in this study were collected by Dr. S.B. Verma's group in Nebraska sites.

During the vegetative stage, fAPAR increased coinciding with the increase of canopy Chl content. However, during the reproductive stage fAPAR remained insensitive to decreases in canopy Chl. That is because in this stage both photosynthetic and non-photosynthetic components intercepting PAR, which was progressively less used for photosynthesis (Vina and Gitelson, 2005). Therefore, to obtain a measure of the fAPAR absorbed only by the photosynthetic component of the vegetation, green fAPAR ($fAPAR_{green}$) was calculated as (see Hall et al., 1992; Hanan et al., 2002):

$$fAPAR_{green} = fAPAR \times (\text{green LAI} / \text{total LAI}) \quad (3.3)$$

3.7 Canopy reflectance collected at close range

In three Nebraska sites during 2001 through 2008, canopy reflectance measurements were made by the group of Center for Advanced Land Management Information Technologies (CALMIT) using hyperspectral radiometers mounted on "Goliath", an all-terrain sensor platform (Rundquist et al., 2004). A dual-fiber optic system, with two inter-calibrated Ocean Optics USB2000 radiometers, was used to collect radiometric data in

the range 400-1100 nm with a spectral resolution of about 1.5 nm. Radiometer 1, equipped with a 25° field-of-view optical fiber was pointed downward to measure the upwelling radiance of the crop ($L_{\lambda crop}$). The position of the radiometer above the top of canopy was kept constant (around 5.4 m) throughout the growing season, yielding a sampling area with a diameter of around 2.4 m. Radiometer 2, equipped with an optical fiber and a cosine diffuser (yielding a hemispherical field of view), was pointed upward to simultaneously measure incident downwelling irradiance ($E_{\lambda inc}$). In order to match the transfer functions of both radiometers, inter-calibration was accomplished by measuring the upwelling radiance ($L_{\lambda cal}$) of a white Spectralon® (Labshere, Inc., North Sutton, NH) reflectance standard simultaneously with incident downwelling irradiance ($E_{\lambda cal}$) - Vina et al., 2011. Percent reflectance ρ_λ was then computed as:

$$\rho_\lambda = \frac{L_{\lambda crop}}{E_{\lambda inc}} \times \frac{E_{\lambda cal}}{L_{\lambda cal}} \times 100 \times \rho_{\lambda cal} \quad (3.4)$$

where $\rho_{\lambda cal}$ is the reflectance of the Spectralon panel linearly interpolated to match the band centers of the radiometers. In order to check whether the transfer functions of both radiometers were nearly constant through time and minimally affected by changes in environmental conditions, the two radiometers were tested under field conditions (with changing illumination angles), and it was found that over a four-hour period (10:20-14:20) the coefficient of variation of the ratio of the transfer functions of the radiometers did not exceed 5% (Vina et al., 2011).

Radiometric data were collected close to solar noon (between 11:00 and 13:00 local time), when changes in solar zenith angle were minimal. For each measurement site, six randomly selected plots were established along the pivot roads of site 1 and site 2 and along an entrance road of site 3 (Fig. 3.3), each with six randomly selected sampling

points (details in Vina, 2004). Thus, a total of 36 points within these areas were sampled per site at each data acquisition. Measurements took about 5 minutes per plot and about 30 minutes per field. The two radiometers were inter-calibrated immediately before and immediately after measurement in each field. Reflectance measurements were carried out during the growing seasons from 2001 through 2008. This resulted in a total of 314 reflectance spectra for maize (47 in 2001, 30 in 2002, 92 in 2003, 30 in 2004, 53 in 2005, 13 in 2006, 40 in 2007 and 9 in 2008) and 145 spectra for soybean (54 in 2002, 49 in 2004, 26 in 2006 and 16 in 2008), which were representative of wide dynamic ranges of GPP variation found in maize and soybean.

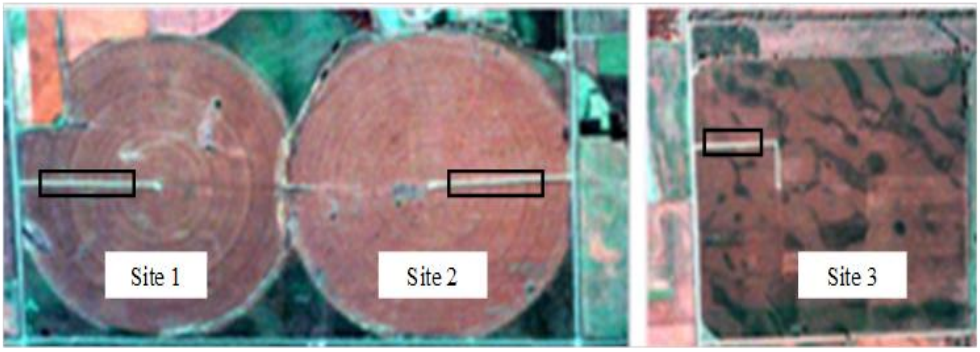

Figure 3.3 Canopy spectral measurement location for site 1, site 2 and site 3 in Mead, Nebraska shown on an airborne AISA image. A total of 36 points within "Goliath" sampling areas (black rectangles) were sampled per site at each data acquisition, and their median value was used as the site reflectance.

In order to relate spectral reflectance measured in "Goliath" sampling areas with eddy covariance measurements of CO_2 fluxes, which were considered to be representative of the whole field, we need to check whether the reflectance in "Goliath" sampling areas were representative of the whole field. Field heterogeneity was tested

(Gitelson et al., 2003c; Vina et al., 2011) using six AISA images acquired on June 21, June 27, July 12, July 15, September 7 and September 17, 2002 and two HYPERION images acquired on August 13 and August 29, 2001, which were representative of a wide dynamic range of crop spectra variations during the growing season. AISA is an aircraft-mounted hyperspectral imaging spectroradiometer, with 35 spectral bands from 480 – 860nm and a spatial resolution of 3 m per pixel. HYPERION is a hyperspectral imager onboard NASA's Earth Observing – 1 satellite, with 220 spectral bands from 400 – 2500 nm and a spatial resolution of 30 m per pixel. Using the two-sample t-test, pixel digital values were compared between pixels located in six IMZs in the field and those located in the "Goliath" sampling area for all AISA and HYPERION images, and no statistically significant differences were obtained for most cases (Gitelson et al., 2003c; Vina et al., 2011). Since these IMZs represent all major occurrences of soil and crop production zones within each site (Verma et al., 2005), the conducted reflectance measurements were considered representative of the reflectance for the whole field. Therefore, the median value of 36 spectral scans within the "Goliath" sampling area per site was used as the site reflectance for each data acquisition.

3.8 Shortwave radiation

The wavelength range of shortwave radiation (SW) is from 300 – 4000 nm, including the specific bands of water vapor absorption and relatively narrower range of PAR (400 – 700 nm). In this study, the daily SW data of the reanalysis dataset (North American Land Data Assimilation System, NLDAS-2) was used as a proxy of PAR_{in} (Sakamoto et al., 2011b). The footprint of one SW pixel (spatial resolution: 11 km)

covers all three Nebraska sites. NLDAS-2 land-surface forcing files are derived from the analysis fields of the National Centers for Environmental Prediction (NCEP) North American Regional Reanalysis (Fang, 2009).

To assess the uncertainty, related to the use of SW as a proxy of PAR_{in}, we compared the NLDAS-2 estimates of SW with ground-observed daily PAR_{in} data for three Nebraska sites during 2001 through 2008. There is a strong linear relationship between SW and PAR_{in} with determination coefficients (R^2) more than 0.68 and coefficients of variation (CV) below 21% (Fig. 3.4). Thus, it seemed reasonable to substitute SW for PAR_{in} observations to help detect the high frequency variation of incoming light intensity (Sakamoto et al., 2011b). The SW data used in this study was processed by Dr. T. Sakamoto.

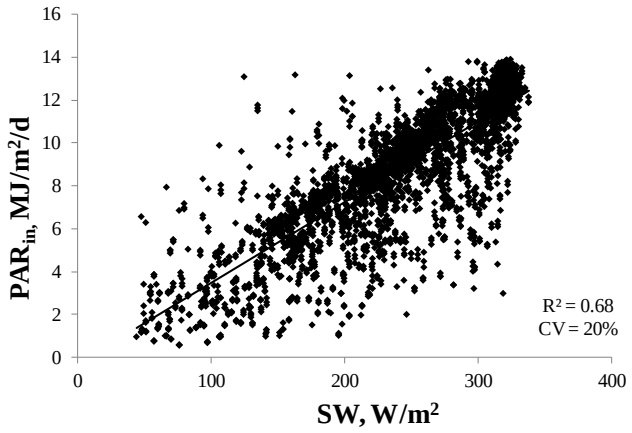

Figure 3.4 Comparison between the shortwave radiation (SW) from NLDAS-2 and the daily ground-observed PAR_{in} with data for three Nebraska sites during 2001 through 2008.

3.9 Potential PAR

In this study, we attempted to use the maximal value of PAR_{in} that may occur when the concentrations of atmospheric gases and aerosols are minimal. We term this variable "potential incident photosynthetically active radiation" ($PAR_{potential}$) – dashed line in Fig. 3.2. $PAR_{potential}$ represents the seasonal changes in hours of sunshine (i.e. day length) but does not account for high frequency variation of incoming radiation related to daily weather conditions. It may be calculated based solely on astronomy data at a given location (Weiss & Norman, 2003). For example, it may be calculated using the 6S radiative transfer code (Vermote et al, 1997a; Kotchenova and Vermote, 2007) for a "clean" (non- absorbing) aerosol model with optical thickness of 0.05 at 550 nm and water vapor below 1 g/m2. The solar irradiance at the top of the atmosphere (TOA), geographic coordinates and solar angle for a given location should be used as input data (Vermote, personal communication). $PAR_{potential}$, as calculated for several sun angles, would be used to define a total daily value. Another way to find $PAR_{potential}$ is using a look-up table (LUT)-based algorithm, providing PAR_{in} as a function of solar zenith angle, column water vapor and optical thickness for several different representative aerosol models (Lyapustin, personal communication). LUTs were generated using the Interpolation and Profile Correction method (Lyapustin, 2003). For our purpose, $PAR_{potential}$ will be obtained as a look-up table value for the background aerosol and a typical column water vapor.

In this study, we calculated $PAR_{potential}$ using measured PAR_{in} values. Since the daylight duration is mainly determined by the day of a year (DOY) and geographic location, we created profiles of $PAR_{potential}$ as functions of DOY for site locations in

Nebraska, Minnesota, Iowa and Illinois, based on daytime PAR_{in} obtained during study periods. For each DOY, a maximal PAR_{in} value was found in the 8-day-PAR_{in} window centered on that particular DOY. This procedure was applied to the entire growing season of a year using the 8-day moving window. The best-fit functions of the relationships between maximal PAR_{in} and DOY were found for each year and the variation among the years was very small (coefficient of variation below 3.5%) – Fig. 3.5. Thus, the $PAR_{potential}$ vs. DOY function was defined as the maximum within the relationship between maximal PAR_{in} and DOY for each year.

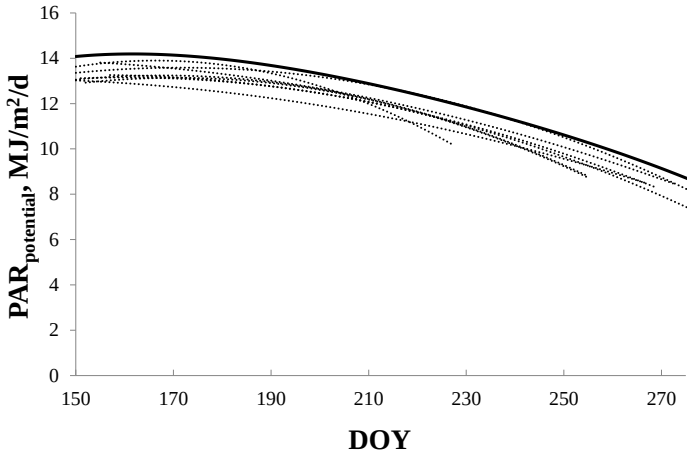

Figure 3.5 The best-fit functions of the relationships between maximal PAR_{in} and DOY for each year during 2001 through 2008 for site 1 in Nebraska (dotted lines). The variation among the years was very small (coefficient of variation below 3.5%). Thus, the $PAR_{potential}$ vs. DOY function was defined as the maximum within the relationship between maximal PAR_{in} and DOY for each year (the solid line).

3.10 Landsat data

Both Landsat-5 TM and Landsat-7 ETM+ images were used in order to maximize cloud-free imaging opportunities. The details about the images used in this study are

given in Table 3.3. The Landsat data used as input in this study were standard L1t files (georegistered, orthorectified) from the US Geological Survey, processed by Dr. J.G. Masek's group at GSFC/NASA. The geodetic accuracy of the L1t product is typically within 30m (Lee et al., 2004). The image digital numbers were converted to top-of-atmosphere (TOA) reflectances, and then atmospherically corrected to surface reflectance using the Landsat Ecosystem Disturbance Adaptive Processing System (LEDAPS) at NASA GSFC (Masek et al., 2006). The atmospheric correction procedure corrected for gaseous absorption, Rayleigh scattering, and Mie (aerosol) scattering using the MODIS/6S radiative transfer model (Vermote et al, 1997b). Ozone concentrations are derived from Total Ozone Mapping Spectrometer (TOMS) data aboard the Nimbus-7, Meteor-3, and Earth Probe platforms. Column water vapor was taken from NOAA National Centers for Environmental Prediction (NCEP) re-analysis data available at a resolution of $2.5^{o} \times 2.5^{o}$.

Table 3.3. Details regarding Landsat data acquisitions over seven study sites used in this analysis.

Site #	Site Location (Ameriflux ID)	Image information	Study period	Total number of images
1	Mead, NE	W2P028R031	01 - 08	60
2	Mead, NE	W2P028R031	01 - 08	59
3	Mead, NE	W2P028R031	01 - 08	56
4	Ames, IA	W2P026R031, W2P027R031	05 - 07	32
5	Ames, IA	W2P026R031, W2P027R031	05 - 07	34
6	Bondville, IL	W2P022R032, W2P023R032	01 - 03	35
7	Rosemount, MN	W2P027R029	05 - 07	16

Aerosol optical thickness was derived for each image using the dark, dense vegetation approach of Kaufman et al (1997). Based on the physical correlation between Chl absorption and absorption by liquid water in vegetation, this method postulates a linear relationship between shortwave-infrared (2.2 μm) surface reflectance (nearly unaffected by the atmosphere) and surface reflectance in the visible bands. By using the relationship to calculate surface reflectance for the visible bands, and comparing the result to the TOA reflectance, aerosol optical depth may be estimated.

LEDAPS surface reflectance products have been compared to *in situ* data from the Aerosol Robotic Network (AERONET) and to daily 500 meter resolution surface reflectance products from the MODIS sensor aboard the NASA Terra spacecraft (Masek et al., 2006; Feng et al., 2011). The uncertainties associated with the calculated reflectance values appear to be within the uncertainty of the MODIS surface reflectance product (the greater of 0.5% absolute reflectance or 5% of the recorded reflectance value) for normal aerosol loadings (τ_{550nm}<0.5).

For each study site, we defined a maximum rectangle in the center of a Landsat image that fitted the field. The rectangle included 552 pixels (690 m × 720 m) for site 1 Nebraska, 506 pixels (690 m × 660 m) for site 2 Nebraska, 576 pixels (720 m × 720 m) for site 3 Nebraska, 276 pixels (360 m × 690 m) for site 4 IA, 325 (390 m × 750 m) pixels for site 5 IA, 132 pixels (330 m × 360 m) for site 6 IL, and 272 pixels (480 m × 510 m) for site 7 MN. We applied the same rectangle to all images to extract the pixels of interest, and the reflectance values for study sites were calculated by averaging all the per-pixel values within the rectangle.

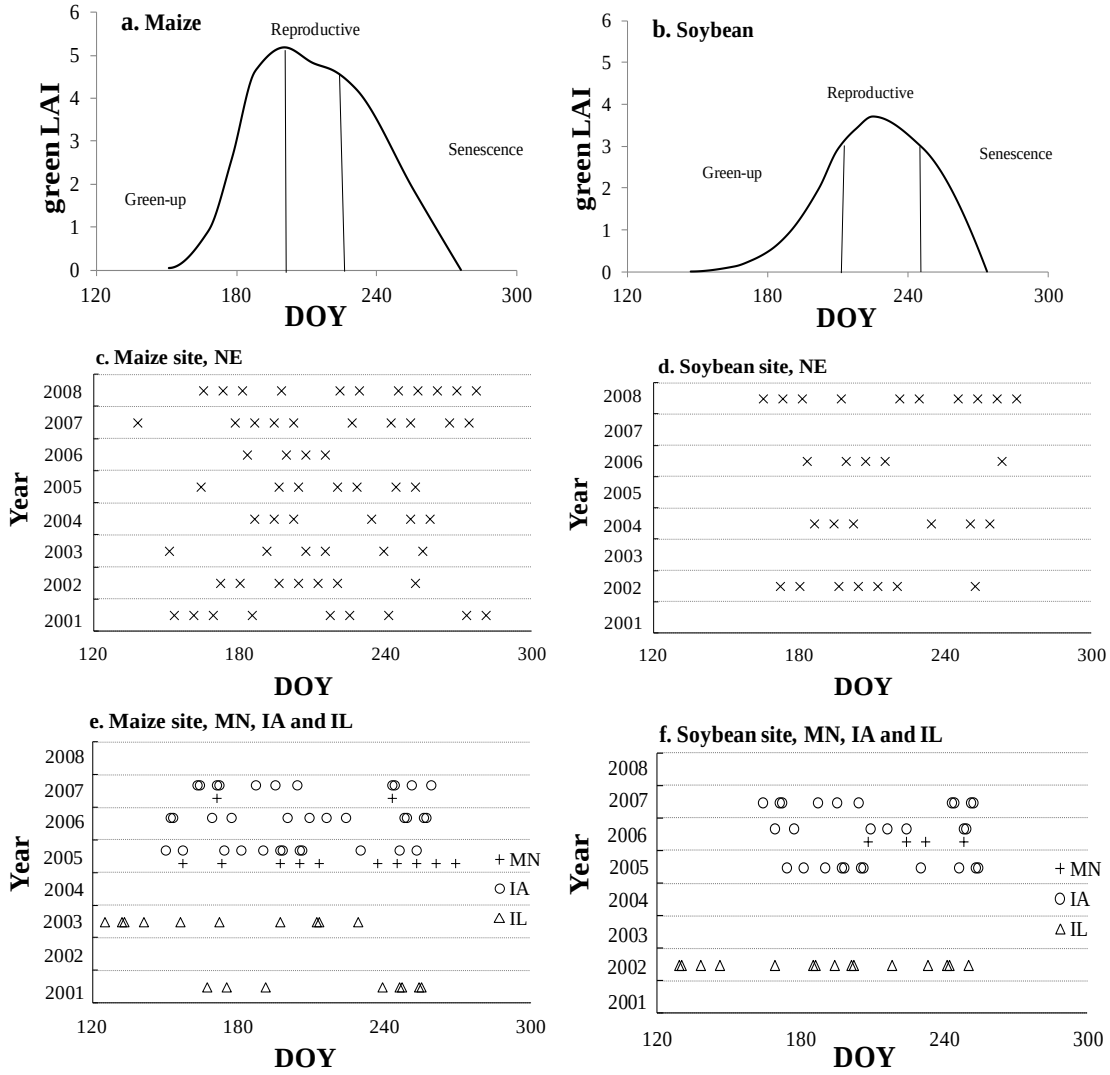

Figure 3.6 Phenology of green LAI in (a) maize and (b) soybean, and dates of Landsat data acquisition over (c) maize sites in Nebraska, (d) soybean sites in Nebraska, (e) maize sites in Minnesota, Iowa and Illinois and (f) soybean site Minnesota, Iowa and Illinois.

A total of 290 Landsat-retrieved site spectral reflectance were paired with corresponding daytime GPP observations during our study period (Fig. 3.6). Figure 3.6a and 3.6b showed the dynamics of green LAI in maize and soybean during the growing

season. In general, maize has a longer growth period than soybean, and the maximum green LAI of maize is about 25% higher than for soybean.

For maize data, we compiled a total of 120 images for NE sites, 12 for MN sites, 38 for IA sites and 20 for IL sites. Compared to maize data, the number of images for soybean fields was limited. In total, we had 55 images for NE sites, 4 for MN sites, 28 for IA sites, 15 for IL sites. The data from three NE study sites, which were representative of all phenological stages found in maize and soybean (Fig. 3.6c and 3.6d), were used for model development and calibration, while the limited number of images taken over MN, IA and IL sites, were employed for model validation (Fig. 3.6e and 3.6f).

3.11 MODIS data

An 8-day time series of 250m and 500m MODIS surface reflectance data (MOD09Q1 and MOD09A1, collection 5, tile: h10v04) acquired from 2001 through 2008 were used in this study. Such surface reflectance (MOD09 product) is atmospherically corrected to reduce the effects of gaseous absorption and aerosol scattering (Vermote et al., 2002). And 8-day CV-MVC technique is also applied to avoid low quality observation values caused by poor observation conditions resulting from cloud cover and extremely large off-nadir observation angles. The specific data layers used were the 250m red (Band 1) and NIR (Band 2) reflectance data from the MOD09Q1 product and the 500 m blue reflectance (Band 3) and the observation date (DOY) from the MOD09A1 product (Sakamoto et al., 2011b). The blue reflectance was resampled from 500 m to 250 m resolution using the nearest-neighbor method (Sakamoto et al., 2011b). In each MODIS image, pixels for the three Nebraska study sites were extracted for analysis. The

actual ground area sampled for each MODIS pixel can vary depending on the sensor view angle on the date at which that location is observed in the 8-day composite image. Therefore, it is inevitable that the surrounding land cover types can affect the spectral response of the target MODIS pixel with the greatest affects occurring for off-nadir observations. The MODIS data used in this study was processed by Dr. T. Sakamoto.

3.12 Chlorophyll-related vegetation indices

In this study, several widely used Chl-related vegetation indices were tested for GPP estimation with remotely sensed data at close range, collected 6 m above the canopy, as well as Landsat and MODIS 250 data.

For hyperspectral reflectance collected at close range, the site spectra were resampled to spectral bands of MODIS (green: 545 - 565 nm, red: 620 - 670 nm, and NIR: 841 - 876 nm) using MODIS spectral response function and SR, NDVI, EVI2, VARI, WDRVI and CI_{green} were calculated (Table 2.1). The reflectance spectra were also resampled to the spectral bands of MERIS (green: 555 - 565 nm, red: 660 - 670 nm, red edge: 703 – 712 nm and NIR: 750 - 760 nm) using a MERIS spectral response function and MCARI, TVI, MTVI1, MTVI2, MTCI, Red edge NDVI and $CI_{red\ edge}$ were calculated (Table 2.1). PRI (Gamon et al., 1992) was also calculated in the form: $PRI = (\rho_{531} - \rho_{570}) / (\rho_{531} + \rho_{570})$, where ρ_{531} and ρ_{570} are reflectances at 530 nm and 570 nm, respectively. It was used as a surrogate of LUE in the model.

For Landsat data, four spectral bands with 30m spatial resolution were used in this study: blue (band 1: 450 – 520 nm), green (band 2: 520 – 600 nm), red (band 3: 630 – 690 nm), and near-infrared (band 4: 750 – 900 nm). SR, NDVI, green NDVI, EVI2,

green WDRVI and CI_{green} were tested for GPP estimation (Table 3.4). These VIs were calculated from Landsat surface reflectance data, as well as Landsat TOA reflectance data.

Table 3.4. Vegetation Indices (VI) tested in this study with Landsat data.

Vegetation Index	Formula in equivalent bands in Landsat
Simple Ratio (SR)	Band 4/ Band 3
Normalized Difference Vegetation Index (NDVI)	(Band 4 – Band 3) / (Band 4 + Band3)
Green NDVI	(Band 4 – Band 2) / (Band 4 + Band 2)
Enhanced Vegetation Index 2 (EVI2)	2.5 × (Band 4 – Band 3) / (1 + Band 4 + 2.4 × Band 3)
Green Wide Dynamic Range Vegetation Index (Green WDRVI)*	(α × Band 4 – Band 2) / (α × Band 4 + Band 2) + (1 – α) /(1+ α), 0 < α < 1
Green Chlorophyll Index (CI_{green})	Band 4 / Band 2 – 1

* The weight coefficient α (0 < α < 1) is to attenuate the contribution of ρ_{NIR} at moderate-to-high green biomass, and to make it comparable to that of ρ_{red}. Based on the dynamic range of the Landsat reflectance used in this analysis, we used α = 0.3.

For MODIS data, we used MODIS NDVI and EVI products (MOD 13 – Gridded Vegetation Indices) retrieved from MODIS 250 m surface reflectance data (MOD09Q1 and MOD09A1). MODIS WDRVI was calculated based on MODIS NDVI product as:

$$WDRVI = \frac{\alpha-1 \ +(\alpha+1)\times NDVI}{\alpha+1 \ +(\alpha-1)\times NDVI} + \frac{1-\alpha}{1+\alpha}, 0 < \alpha < 1 \quad (3.5)$$

Even though the surface reflectance used to calculate VI were atmospherically corrected, the observed VI time-series is liable to include various residual noise components resulting in an erratic time series behavior and many sharp declines in VI values, because of the moderate spatial resolution (250 m) and wide view angle ($\pm 55^{o}$) of MODIS. The irregular temporal features in the VI time series data are caused by persistent and residual, sub-pixel cloud cover, bidirectional reflectance distribution function effects, and

mixed-pixel effects. Therefore, a wavelet based filter was applied for removing the high-frequency noise components to produce a daily and smoothed VI profile based on the linear interpolation of unequally-spaced observations of MODIS 8-day composite products (Sakamoto et al., 2010, 2011b).

3.13 Statistic metrics

Several statistical metrics were used in this study to evaluate the accuracy of the established relationship for GPP estimation. The root mean square error (RMSE) is frequently used to measure the differences between values predicted by a model or an estimator (θ) and the values actually observed (θ):

$$RMSE = \sqrt{\frac{\sum_{i=1}^{n}(\theta-\theta)^2}{n-1}} \tag{3.6}$$

In order to compare the estimation errors for data sets with different dynamic ranges of variables, the coefficient of variation (CV) is defined as the ratio of the RMSE to the mean value of samples:

$$CV = \frac{\mathrm{RMSE}}{\frac{1}{n}\left(\sum_{i=1}^{n}\theta\right)} \tag{3.7}$$

The coefficient of determination (R^2) provides a measure of how well future outcomes are likely to be predicted by the model:

$$R^2 = 1 - \frac{\sum_{i=1}^{n}(\theta-\theta)^2}{\sum_{i=1}^{n}\left(\theta-\frac{1}{n}\sum_{i=1}^{n}\theta\right)^2} \tag{3.8}$$

The Standard Error (SE) provides the measure of the scatter of samples from the best-fit-function:

$$SE = \sqrt{\frac{\sum_{i=1}^{n}(\theta-\theta_{est})^2}{n}} \tag{3.9}$$

where θ_{est} is estimated value can be obtained from the best-fit-function, and n is the number of samples.

To assess the accuracy of estimating GPP by different VI, the Noise Equivalent (NEΔGPP) of each VI was compared. It was calculated as (Vina & Gitelson, 2005):

$$NE\Delta GPP = \frac{\text{RMSE}\{\text{VI vs.GPP}\}}{\text{d(VI)/d(GPP)}} \quad (3.10)$$

where d(VI)/d(GPP) is the first derivative of the best fit function of the relationship VI vs. GPP with respect to GPP, and RMSE{VI vs. GPP} is root mean square error of the best fit function of this relationship.

The noise equivalent (NEΔGPP) is a measure of how accurate a VI responds to a change of GPP across its entire dynamic range. The widely used statistical metrics such as R^2 and RMSE represent only the overall dispersion of the points from the best fit regression lines. They constitute measures of how good the regression model is at capturing the relationship between GPP and VI. However, when the best fit function is nonlinear, the R^2 as well as RMSE values might be misleading. The relationships with very different shapes may have similar R^2 and RMSE values. NEΔGPP has the advantage of considering both the slope and scattering of the points from the best fit function, allowing calculating direct comparisons among different indices with different scales and dynamic ranges (Vina & Gitelson, 2005).

3.14 K-fold Cross-validation

When using a k-fold cross validation procedure (Fielding & Bell, 1997; Kohavi, 1995) to establish the algorithm of estimating crop GPP by vegetation indices, the original samples are randomly split into k mutually exclusive sets (k=number of total

samples/n, n=10 in this study) and they are trained and tested k times. For each time, k-1 sets are used iteratively as training data for calibrating the coefficients ($Coef_i$) of the relationship, and the remaining single set is retained as the validation dataset to test the model and obtain R^2_i and $RMSE_i$ for the established algorithm. This procedure is then repeated k times, with each of the k sets used exactly once as the validation data. The results from k iterations then can be averaged to produce a single estimation:

$$Coef = \frac{1}{k} \sum_{i=1}^{k} Coef_i \qquad R^2 = \frac{1}{k} \sum_{i=1}^{k} R_i^2 \qquad RMSE = \frac{1}{k} \sum_{i=1}^{k} RMSE_i \qquad (3.9)$$

This method reduces the dependence on a single random partition into calibration and validation datasets. By repeating the training procedure k times, all observations are used for both calibration and validation, with each observation used for validation one time.

Chapter 4: GPP estimation at close range

This chapter is based on three published papers:

1. Peng, Y. & Gitelson, A.A. (2011) Remote estimation of gross primary productivity in soybean and maize based on total crop chlorophyll content. Remote Sensing of Environment, 117, 440-448.

2. Peng, Y. & Gitelson, A.A. (2011) Application of chlorophyll-related vegetation indices for remote estimation of maize productivity. Agricultural and Forest Meteorology, 151, 1267 – 1276.

3. Peng, Y., Gitelson, A.A., Keydan, G., Rundquist, D.C. & Moses, W. (2011) Remote estimation of gross primary production in maize and support for a new paradigm based on total crop chlorophyll content. Remote Sensing of Environment, 115, 978-989.

4.1 Introduction

With the rapid development of field spectroscopy, scientists have explored a variety of ways of deploying radiometers or spectroradiometers in field settings for collecting spectra of the targets of interest. The approaches include holding a portable sensor with the human hand (e.g., Stark and Gitelson, 2000), attaching the instruments to a platform at a fixed height above the ground (e.g., Sakamoto et al., 2012), or mounting them on a variety of motorized booms (e.g., Rundquist et al., 1995). Spectral reflectance collected by such field-based sensors has been successfully used for monitoring the vegetation dynamics. For example, VI retrieved from the canopy hyperspectral reflectance collected by “Goliath”, a motorized and all-terrain platform were widely used to accurately

estimate canopy Chl content (Gitelson et al., 2005), LAI (Vina et al., 2011), fAPAR (Vina and Gitelson, 2005) and vegetation fraction (Gitelson et al., 2002); Sakamoto et al. (2010a, 2011a) devised a low-cost camera observation system to estimate seasonal changes in the biophysical parameters of rice, barley and maize. Since the change in crop production accompanies with changes in vegetation biophysical characteristics, the spectral information collected by such field-based sensors is a viable tool for estimating crop GPP.

The advantages of spectral data collected with a field instrument are: (1) it is a flexible technique with which the researcher can select the time of data collection and fields of view; (2) the researcher can decide what spectral channels to use in attempting to identify or diagnose a particular target; (3) the collected spectral data in a field can be used to calibrate aircraft and/or satellite sensors; and (4) the field-based results can provide a conceptual background for using real satellite data.

In this chapter, we used the *in situ* reflectance collected at close range by "Goliath" platform, with which canopy spectra were obtained in a stable and consistent manner (Rundquist et al., 2004). The overall goal of this chapter is to develop quantitative techniques to accurately estimate GPP in maize-soybean croplands based on spectral reflectance collected at close range.

4.2. Methodology of VI-PAR_{in}-based model

As we discussed above (Chapter 2.2), total canopy Chl content is a good proxy of crop GPP. Fig. 4.1 documents the fact that the GPP followed the seasonal change in total Chl content based on 5-years of observations. Therefore, to remotely estimate GPP in

crops, one needs to retrieve an accurate measure of total Chl content from remotely sensed data.

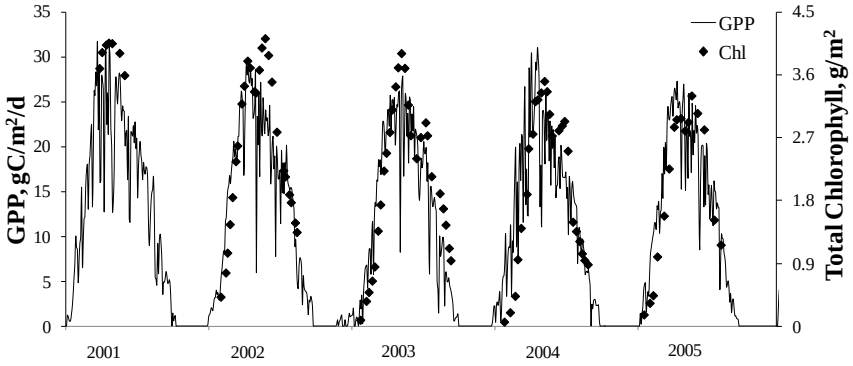

Figure 4.1 Temporal behavior of total canopy chlorophyll content and GPP in maize during the growing seasons 2001 through 2005.

Fig. 4.2 compares the performances of several widely used VI for estimating total Chl content with *in situ* reflectance transformed to simulate the spectral bands of MODIS and MERIS. NDVI was very sensitive to Chl content below 1.5 g/m^2 and lost sensitivity to Chl content above 2 g/m^2. EVI2 and WDRVI with α=0.1 were much more sensitive than NDVI to moderate to high Chl contents, but exhibited non-linear relationships. SR, CI_{green} and $CI_{red\ edge}$ were linearly related to Chl content, remaining sensitive to the wide range of Chl content. However, the points in the relationship of SR vs. Chl content were more scattered than that of CI_{green} and $CI_{red\ edge}$, due to the very low values of red reflectance (not exceeding 2-3%) of crops with moderate to high Chl content. A low value of the red reflectance in the denominator makes SR quite noisy.

The temporal behavior of GPP during the growing season includes two types of variation. Low frequency variation of GPP mainly follows changes of crop growing cycles, which closely relates to total Chl content, thus, to Chl-related VI. Fig. 4.3 shows

several examples of the temporal behavior of VI and GPP, illustrating their similar temporal pattern during eight growing seasons.

Another type of GPP variation occurs at much higher frequency, which corresponds to high frequency variations of PAR_{in} as a result of short-period changes in atmospheric transmissivity due to clouds or aerosols (see chapter 3.3). Under overcast conditions, associated with low values of PAR_{in}, the crop absorbed less incoming light, thus resulting in lower production. Moreover, there is a significant decline in PAR_{in} intensity in the late season (see chapter 3.3, Fig. 3.2), which is due to the gradual decrease in total hours of sunlight in the Northern Hemisphere after the summer solstice. Thus, with the same greenness/Chl content, crop produces lower production in late stages of the season (Peng et al., 2011; Sakamoto et al., 2011).

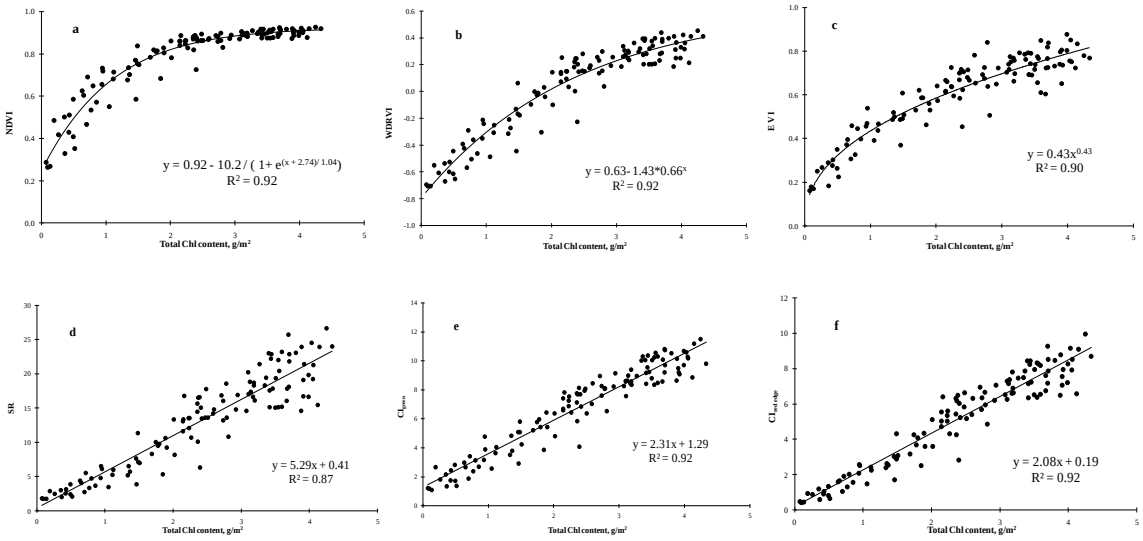

Figure 4.2 Relationship between total chlorophyll content and (a) NDVI, (b) WDRVI, (c) EVI2, (d) SR, (e) CI_{green} and (f) $CI_{red\ edge}$.

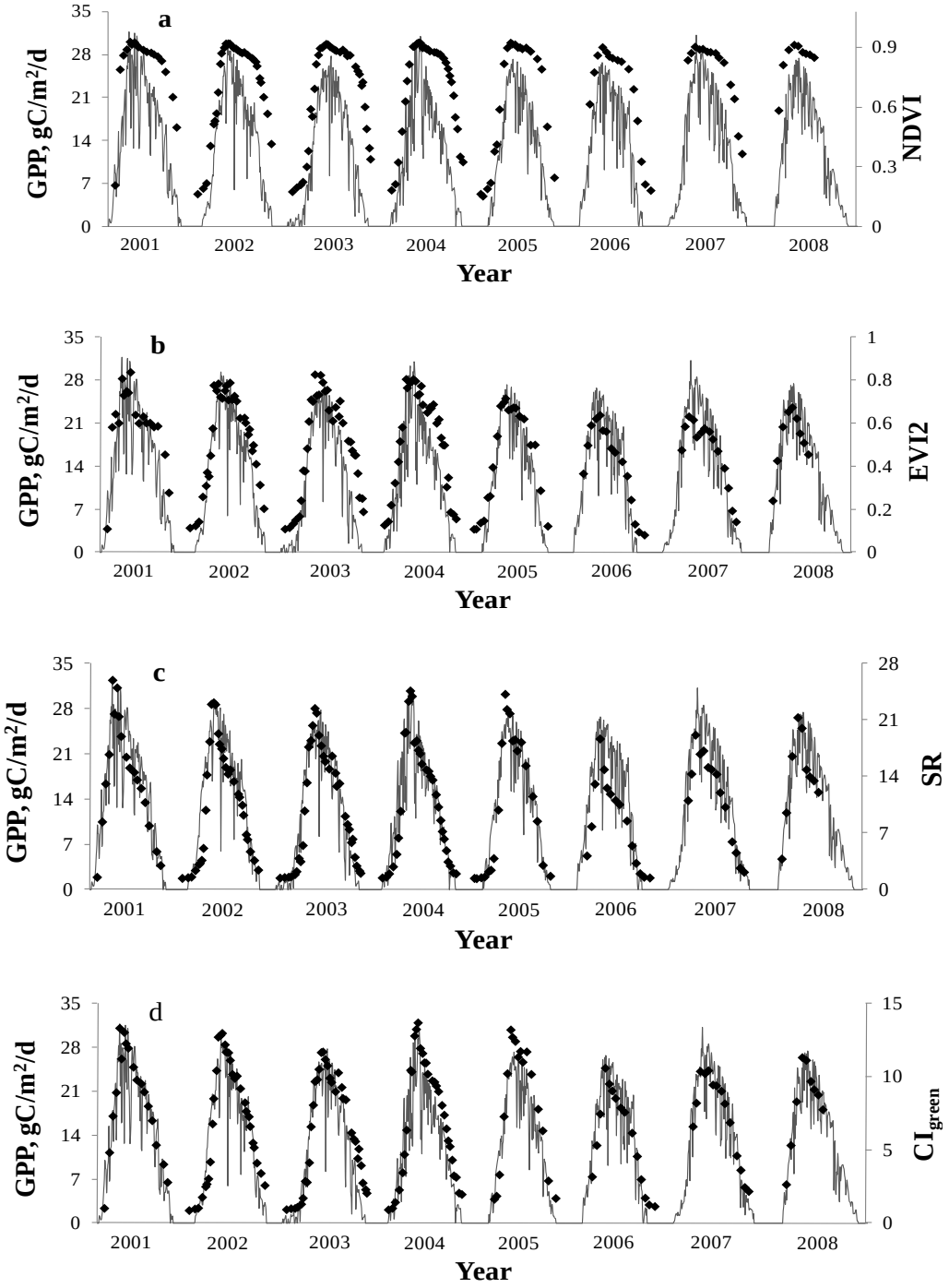

Figure 4.3 Temporal behavior of GPP and (a) NDVI, (b) EVI2, (c) SR, (d) CI_{green} in maize during the growing seasons 2001 through 2008. The solid lines are the daily GPP; the diamonds represent the VIs at sampling dates.

Fig. 4.4 shows that the CI_{green} index was closely related to crop GPP in accord with the growing season cycle. However, it did not capture GPP variations that were caused by changes in the high frequency of PAR_{in} variation, which do not produce an immediate direct change in total Chl content. Also, it did not take into account low frequency variation of PAR_{in}, which occurs late in the season. In reproductive stage, as PAR_{in} declined, discrepancies between CI_{green} and GPP increased (Fig. 4.4).

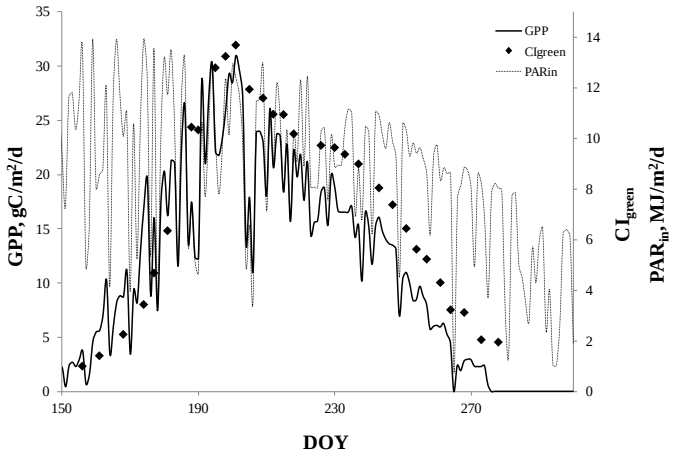

Figure 4.4 Temporal change in GPP, CI_{green} and PAR_{in} for maize in the growing season of 2004.

Therefore, in accord with Eq. 2.3 during the growing season, crop GPP is affected by variation in total Chl content, as well as low and high frequency variations of PAR_{in}. Since Chl-related VIs can be used as proxies of total Chl content, the model for the remote estimation of GPP in crops has the form (Gitelson et al., 2006b):

$$GPP \propto VI \times PAR_{in} \quad (4.1)$$

The product of VI and the PAR_{in}, relates more closely to GPP than does VI alone (Fig. 4.5) because it accounts for the modulation of GPP by changes in radiation conditions.

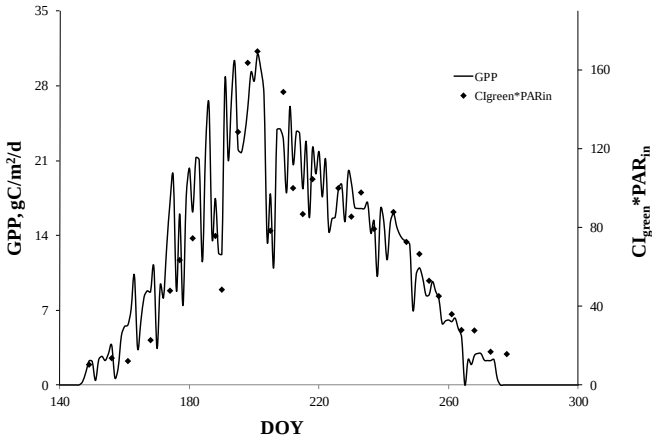

Figure 4.5 Temporal change in GPP and the product of CI_{green} and PAR_{in} for maize in the growing season of 2004.

Based on above methodology, we attempted in this chapter: 1) to test and compare the performance of several widely used Chl-related VI for GPP estimation in crops using Eq. 4.1; (2) to assess the accuracy and uncertainties of the model Eq. 4.1, as well as the algorithms for GPP estimation in fields that are different in crop management practices, field history and climatic conditions; and (3) to explore the possibility of using a unified algorithm for GPP estimation in two contrasting crop types as soybean and maize.

4.3 Results and discussion

During the growing seasons from 2001 through 2008, data from 24 maize and soybean site-years were collected. The crop hybrids, growth situations, irrigation practices, crop managements and climatic conditions were different from field to field (Table 3.2).

4.3.1 GPP estimating in rainfed and irrigated maize

Maize grown in site 1 and site 2 was under scheduled irrigation management, which provides about 40-50% of the total water received by crop. In rainfed site 3, the rainfall is the only source of water for the cropland use. Therefore, the soil moisture in the rainfed site could be very different from irrigated sites, especially in drought years with little precipitation. It was reported that 2003 and 2005 were especially dry with annual precipitation 25.6 in and 23.9 in compared to the 40.4 in in 2007, a "normal" year. Water stress occurred under low soil moisture conditions, which severely affected grain yield. For example, during dry periods in 2003, soil moisture at 10 cm depth in the rainfed site dropped more than 40% compared to that in irrigated sites. The difference in daily GPP between irrigated and rainfed sites increased during the dry periods and reached a peak value of 9.3 $gC/m^2/d$, which corresponded to 40% of the maximal daily GPP value (Suyker and Verma, 2010). As a result, the ratio of grain yield in the irrigated site to that in rainfed site was above 1.8 in 2003, while in a "normal" year with higher precipitation (e.g., 2007), it was below 1.3 (Suyker and Verma, 2010). It shows how different were physiological conditions of crops in irrigated and rainfed sites, thus, providing very wide range of GPP variation.

The close proximity of the study sites containing rainfed and irrigated maize allowed examination of the impact of water deficiency on the accuracy of GPP estimation by the model Eq. 4.1 that relies on Chl content. The temporal behavior of GPP in irrigated and rainfed sites is shown in Fig. 4.6a during a dry year (2003), while Fig. 4.6b presents estimates of GPP by $CI_{red\ edge} \times PAR_{in}$. It can be seen that the model Eq. 4.1 was sensitive not only to the difference in GPP between irrigated and rainfed sites in the very

beginning of the dry period (around DOY 210 when early stages of stress occurred) but also to small differences between GPP in the two irrigated maize fields (site 1 and site 2). It shows that Chl-related VI was sensitive to variation of crop physiological status, affected by the environmental conditions (e.g., decrease in soil moisture, increase in temperature.

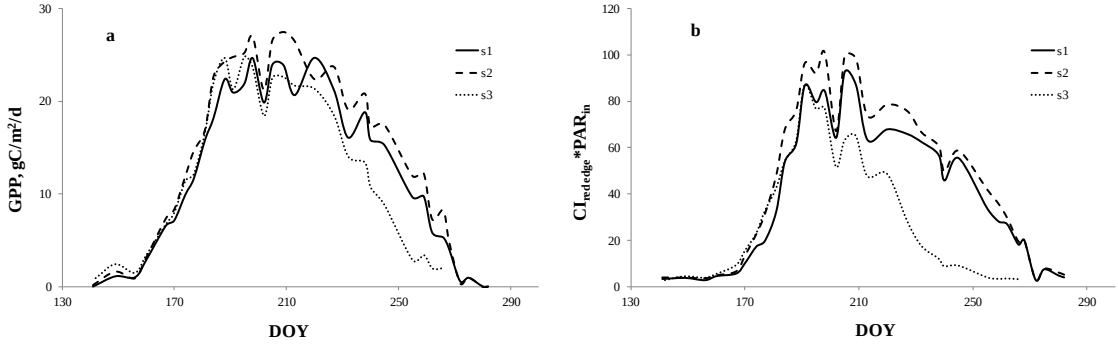

Figure 4.6 (a) GPP and (b) $CI_{red\ edge} \times PAR_{in}$ at three sites in 2003. Sites 1 and 2 were irrigated and site 3 relied entirely on rainfall. The model Eq. 4.1 was sensitive not only to the difference in GPP between irrigated and rainfed sites but also to small differences between GPP in two irrigated maze fields (site 1 and site 2).

In addition to different water managements of irrigated and rainfed sites, in order to account for differences in water-limited attainable yield, the density of planting in the rainfed site was lower than in irrigated sites (Fig. 4.7). The maximal values of LAI, biomass and GPP were different between irrigated and rainfed maize (Table 3.2).

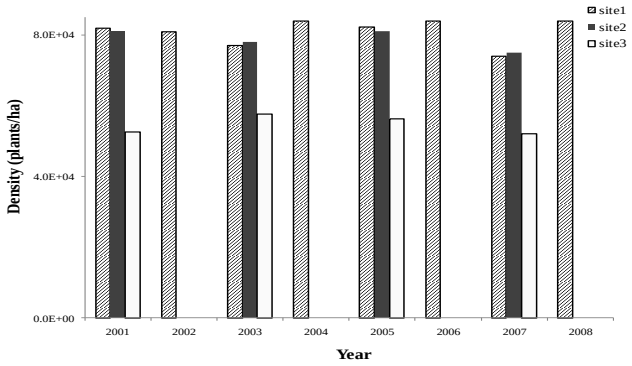

Figure 4.7 Density of maize planting in the three sites from 2001 through 2008.

We established the relationships of GPP vs. VI $\times$ PAR_{in} for irrigated maize (12 site-years: site 1 from 2001 through 2008; site 2 in 2001, 2003, 2005 and 2007) and for rainfed maize (4 site-years: site 3 in 2001, 2003, 2005 and 2007) separately, and then compared the determination coefficients (R^2), standard errors (SE) and coefficients of variation (CV) of the two relationships for fifteen VIs; twelve of them presented in Table 4.1. R^2 of the relationships GPP vs. TCARI×PAR_{in} was 0.40 for irrigated maize and 0.62 for rainfed maize; R^2 was even lower for TCARI/OSAVI (0.11 for irrigated maize and 0.22 for rainfed maize). These VIs were suggested for leaf Chl estimation and, not surprisingly, they do not track total crop Chl.

For all VIs, presented in Table 4.1, except MCARI, the relationships with GPP for both irrigated and rainfed maize were quite accurate for GPP estimation with CV below 25% in irrigated sites and 23% in rainfed sites. As was discussed in chapter 2.3, NDVI is sensitive to low total Chl content, but tends to be saturated at moderate to high total Chl content (Fig. 4.2). Since total Chl content is a main driver of GPP, NDVI was a good indicator of low-to-moderate GPP but was insensitive to moderate to high value of GPP. VARI, EVI2 and WDRVI were more sensitive than NDVI to moderate-to-high GPP, but

these normalize difference indices were still less sensitive to high Chl content. The SR, CIs and MTCI remain sensitive to the wide range of Chl content as well as GPP (Gitelson et al., 2003a, 2003b; Dash and Curran, 2004; Peng et al., 2011).

Table 4.1. Determination coefficients (R^2), standard errors (SE) and coefficients of variation (CV) of quadratic polynomial relationships between daytime GPP and the product of vegetation index and incident PAR ($VI \times PAR_{in}$) for 12 vegetation indices in irrigated maize (12 fields) and rainfed maize (4 fields). Maximum GPP produced by maize was 34.17 $gC/m^2/d$ in irrigated sites, while 29.47 $gC/m^2/d$ in the rainfed sites.

		MCARI	NDVI	MTVI1	TVI	VARI	EVI2
R^2	Irrigated	0.63	0.78	0.80	0.80	0.81	0.81
	Rainfed	0.82	0.84	0.90	0.90	0.88	0.87
SE $gC/m^2/d$	Irrigated	4.94	3.85	3.64	3.60	3.57	3.48
	Rainfed	3.23	3.14	2.43	2.45	2.68	2.60
CV (%)	Irrigated	31.3	24.4	23.1	22.8	22.6	22.0
	Rainfed	23.6	22.9	17.7	17.9	19.6	19.0
		MTVI2	WDRVI	MTCI	SR	CI_{green}	$CI_{red\ edge}$
R^2	Irrigated	0.85	0.87	0.92	0.88	0.91	0.91
	Rainfed	0.92	0.91	0.80	0.88	0.89	0.89
SE $gC/m^2/d$	Irrigated	3.17	2.98	2.25	2.59	2.56	2.41
	Rainfed	2.14	2.27	3.39	2.33	2.28	2.26
CV (%)	Irrigated	20.1	18.8	14.2	16.4	16.2	15.2
	Rainfed	15.7	16.5	24.8	17.0	16.6	16.5

The maximum GPP, produced by irrigated maize, was approximately 15% higher than for rainfed maize (Table 3.2). So, the models based on NDVI- and TVI-like indices for GPP estimation are more accurate for rainfed than for irrigated maize, because they are more capable of estimating low-to-moderate GPP, but less sensitive to high GPP, which is more often in irrigated sites. The SR and CIs, which are sensitive to the wide range of Chl content and GPP, are able to estimate GPP in rainfed maize as accurately as

in irrigated maize. As shown in Table 4.1, the different water supply, dynamic ranges of LAI, biomass and GPP did not result in significant differences in R^2, SE and CV of the relationships based on SR and CIs in irrigated and rainfed fields. It shows that the model Eq. 4.1 that relies on total crop Chl content and PAR_{in} can be applied to estimate GPP accurately not only in maize under best management practices (irrigated maize) but also the maize grown in water-limited conditions (rainfed maize).

While the model Eq. 4.1 was accurate in estimating GPP in both rainfed and irrigated maize, the algorithms, developed for irrigated and rainfed maize, were statistically significantly different for all the VIs except NDVI (p-value was 0.84 for NDVI, less than 0.01 for EVI2, VARI, MTCI and WDRVI, and less than 0.0001 for CI_{green}, $CI_{red\ edge}$ and SR). A rather wide scattering of points in the relationship of NDVI × PAR_{in} vs. GPP made it impossible to distinguish between rainfed and irrigated sites. For other VI tested, the slope of the relationship of VI × PAR_{in} vs. GPP for the irrigated fields was consistently higher than for those for rainfed fields (Fig. 4.8 for CI_{green} and $CI_{red\ edge}$).

The main reason for such a difference might be that the density of planting in the rainfed site was at least 25% lower than in irrigated sites (Fig.4.7). For the same product VI× PAR_{in}, maize in the rainfed site had higher GPP than that in more densely planted irrigated site. The plant density affected the light climate inside the canopy, so fAPAR value. The light penetrates deeper into the sparsely distributed plants and can be absorbed for photosynthesis more efficiently than for dense crops. In more densely planted fields, light absorption by leaves below the top layer would be somewhat limited by the shadow by nearby plants. In other words, maize planted at a lower density can produce more GPP

per total Chl content than maize planted at a higher density, due to the higher efficiency of light absorption in sparse vegetation than in dense vegetation. So, specific absorption (fAPAR/total Chl content) is higher in sparse vegetation than in dense vegetation. This is accord with Borras et al. (2003) finding that increased maize plant population decreases the light penetration within the canopy, and also affects light composition received by leaves and the vertical profile of leaf N content of crops, thus decreasing grain protein concentrations.

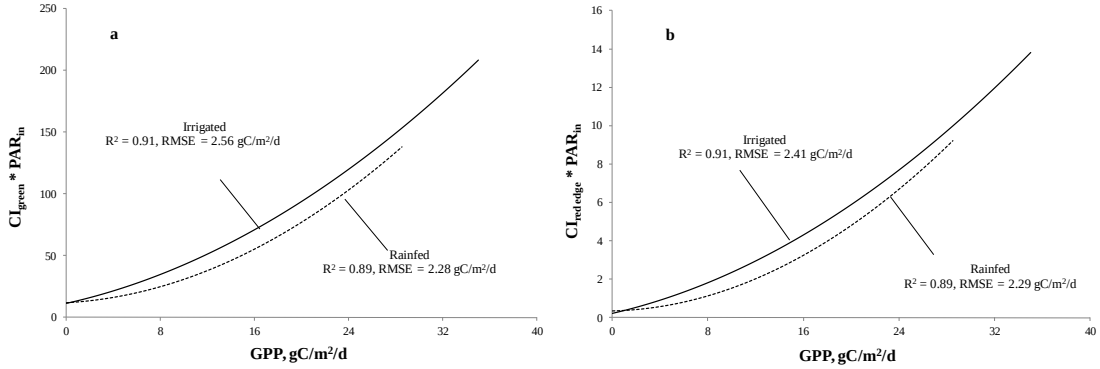

Figure 4.8 Best fit functions of the relationships between daytime gross primary production and (a) $CI_{green} \times PAR_{in}$ and (b) $CI_{red\ edge} \times PAR_{in}$. Solid line: 12 irrigated sites with higher density in 2001 through 2008, dotted line: 4 rainfed sites with lower density in 2002, 2004, 2006 and 2008.

4.3.2 GPP estimation in different maize fields

In addition to the difference in water supply, the maize hybrids, field histories and crop managements were different for the maize sites during 8 years of observation. (Table 3.2). Eight different cultivars of maize were grown in the 16 site-years, density of planting ranged from 52000 to 84012 plants/ha, and nitrogen applied ranged from 90 to

293 kg N/ha among the fields. Site 1 is irrigated continuous maize system, site 2 is irrigated maize-soybean rotation system, and site 3 is rainfed maize-soybean rotation system. Furthermore, the climatic conditions were also quite different among 8 years. For example, the growing seasons of 2001 and 2002 were slightly warmer than 2003. There were obvious dry periods during reproductive stages in 2001 and 2003 and during vegetative stages in 2005. However, 2006, 2007 and 2008 were relatively wet years with no significant dry period (Suyker and Verma 2010). In accord with that, the dynamic ranges of LAI, GPP and yield produced by maize were different in the 16 site-years. For example, the maximum LAI was 6.2 m^2/m^2 in the wet year (site 1 in 2001), while only 4.3 m^2/m^2 in the dry year (site 3 in 2003). All these differences existing among years and fields might affect relationships between GPP and $VI \times PAR_{in}$.

To study how the model Eq. 4.1 works in estimating GPP by different VIs in each field from 2001 through 2008 (16 site-years all together), we established quadratic polynomial relationships between daytime GPP and the product $VI \times PAR_{in}$ for six vegetation indices (SR, NDVI, EVI2, WDRVI, CI_{green}, and $CI_{red\ edge}$).

Table 4.2 summarizes the standard errors (SE) and the coefficients of variation (CV = SE/mean GPP) of these relationships as well as minimum, maximum, and median GPP values in each field and year. Daytime GPP measured during the growing season varied widely, ranging around from 0 to 35 $gC/m^2/d$. The last row in Table 4.2 shows mean values of the coefficient of variation for each index, which are quite informative for comparing the performances among indices regardless of the different dynamic ranges of GPP.

Table 4.2 Standard errors (SE) and coefficients of variation (CV = SE/mean GPP) of quadratic polynomial relationships between daytime GPP and the product of vegetation index (VI) and incident PAR ($VI \times PAR_{in}$) for five vegetation indices: NDVI, WDRVI, EVI2, SR, CI_{green}, and $CI_{red\ edge}$. Maize hybrids and crop management practices in each field are shown in Table 3.2.

		GPP (gC/m2/d)			Standard Error (gC/m2/d)						CV (%)					
Year	Site	Max	Median	Mean	NDVI	WDRVI	EVI2	SR	CI_{green}	$CI_{red\ edge}$	NDVI	WDRVI	EVI2	SR	CI_{green}	$CI_{red\ edge}$
2001	1	31.7	16.23	15.11	4.74	2.26	4.00	2.23	2.1	2.03	31.4	15.0	26.5	14.8	13.9	13.4
2001	2	34.17	15.13	13.93	4.57	2.45	3.93	2.02	2.11	1.92	32.8	17.6	28.2	14.5	15.2	13.8
2001	3	29.47	14.53	12.98	4.16	3.08	1.73	2.79	2.73	2.44	32.0	23.8	13.3	21.5	21.0	18.8
2002	1	29.29	16.18	14.54	2.85	3.42	1.97	2.81	2.46	2.38	19.6	23.5	13.6	19.3	16.9	16.4
2003	1	27.76	13.28	12.49	3.35	3.61	2.69	2.54	2.66	2.38	26.8	28.9	21.5	20.3	21.3	19.1
2003	2	28.69	15.15	13.81	3.6	3.35	2.99	2.23	2.48	2.04	26.1	24.3	21.7	16.2	18.0	14.8
2003	3	25.62	7.56	10.44	2.65	2.21	2.29	2.30	2.10	2.42	25.4	21.2	21.9	22.0	20.1	23.2
2004	1	30.98	13.5	13.15	3.67	2.95	2.30	2.30	2.43	2.06	27.9	22.4	17.5	17.5	18.5	15.7
2005	1	27.24	13.75	13.96	2.82	2.89	1.90	2.08	1.88	1.82	20.2	20.7	13.6	14.9	13.5	13.0
2005	2	27.74	14.57	14.59	3.42	2.88	2.29	2.38	2.13	1.96	23.5	19.7	15.7	16.3	14.6	13.4
2005	3	22.88	13.31	12.7	3.19	2.48	2.53	1.77	1.65	1.41	25.1	19.5	19.9	13.9	13.0	11.1
2006	1	26.7	16.84	14.75	2.67	2.02	2.39	1.15	1.18	0.97	18.1	13.7	16.2	7.8	8.0	6.6
2007	1	31.17	13.68	13.73	3.5	1.17	2.51	1.57	1.76	1.25	25.5	8.5	18.3	11.4	12.8	9.1
2007	2	28.07	14.06	13.17	3.25	2.38	2.31	1.20	1.28	1.19	24.7	18.1	17.5	9.1	9.7	9.0
2007	3	24.75	11.74	11.55	2.32	2.58	1.85	1.60	1.68	1.39	20.1	22.3	16.0	13.9	14.6	12.0
2008	1	27.42	15.24	13.68	4.72	1.79	1.76	1.89	1.01	1.04	34.5	13.1	12.9	13.8	7.4	7.6
Mean											**25.9**	**25.9**	**19.5**	**18.4**	**15.5**	**14.9**

Overall, CI and SR were the most accurate in GPP estimation except for site 3 in 2001 and site 1 in 2002 where EVI2 performed the best. NDVI was consistently less accurate as a GPP predictor for each field with the mean CV > 25% due to its saturation for moderate to high GPP. The same pattern of VI performance was found for the estimation of total crop Chl content (Fig. 4.2). Therefore, the indices that are the most accurate in estimating crop Chl content are likely to work the best for GPP estimation.

4.3.3 A unified algorithm for estimating maize GPP

The model Eq. 4.1 was able to estimate maize GPP quite accurately in different irrigated and rainfed sites with the mean CV below 26% (Table 4.2) (Table 4.1). However, the reltaionships GPP vs. VI × PAR_{in} were site-specific and the coefficients of equations were different for different sites and years. But there is a need for a unified algorithm that does not require re-parameterization to estimate GPP for different fields. It is an especially important issue when using remote sensing techniques with coarse spatial resolution that are not capable of separating the signals from sites with different crop management and climatic conditions. In order to assess the accuracy of a unified algorithm for GPP estimation in different maize fields, we established one relationship GPP vs. VI × PAR_{in} with data collected over 16 site-years containing rainfed and irrigated maize from 2001 through 2008. Table 4.3 summarizes the statistical characteristics (R^2, SE and CV) of such unified relationships for twelve VI and the relationships are presented in Fig. 4.9.

By comparing Table 4.3 with Table 4.1, one can see that the accuracy of the unified relationships for GPP estimation using NDVI- and TVI-like indices (NDVI, VARI, EVI2, WDRVI, TVI, MTVI1 and MTVI2) was almost the same as the accuracy of the

relationships developed for irrigated sites; however, it was lower than the accuracy of the relationships developed for in rainfed sites. For these indices, most errors came from less accurate estimation of moderate-to-high GPP values due to their decrease in sensitivity to the moderate-to-high total Chl/green biomass. The NDVI- and TVI-like indices were more accurate for GPP estimation in rainfed maize, since much fewer samples with high GPP were available in rainfed fields than irrigated fields.

The unified algorithms, based on MTCI, SR and CIs, which are sensitive to a wide range of GPP, were able to accurately estimate GPP in both irrigated and rainfed sites. The CV of GPP estimation by SR and CIs, in irrigated and rainfed sites combined were only slightly higher (17.5% vs. 17.0% for SR, 17.4% vs. 16.6% for CI_{green} and 16.5% vs. 16.50% for $CI_{red\ edge}$) than that of irrigated and rainfed sites when treated separately. MTCI also was able to estimate GPP with CV below 18%.

Table 4.3. Determination coefficients (R^2), standard error (SE), coefficients of variation (CV) of quadratic polynomial relationships between daytime GPP and VI × PAR_{in} established using data collected in 16 irrigated and rainfed fields from 2001 through 2008. GPP ranged from 0 to 35gC/m^2/d.

	MCARI	NDVI	MTVI1	TVI	VARI	EVI2
R^2	0.67	0.80	0.82	0.82	0.82	0.82
SE, gC/m^2/d	4.61	3.71	3.44	3.41	3.40	3.34
CV (%)	30.0	24.1	22.3	22.1	22.1	21.7
	MTVI2	WDRVI	SR	CI_{green}	MTCI	$CI_{red\ edge}$
R^2	0.86	0.87	0.86	0.88	0.89	0.88
SE, gC/m^2/d	3.01	2.88	2.70	2.68	2.66	2.54
CV (%)	19.6	18.7	17.5	17.4	17.3	16.5

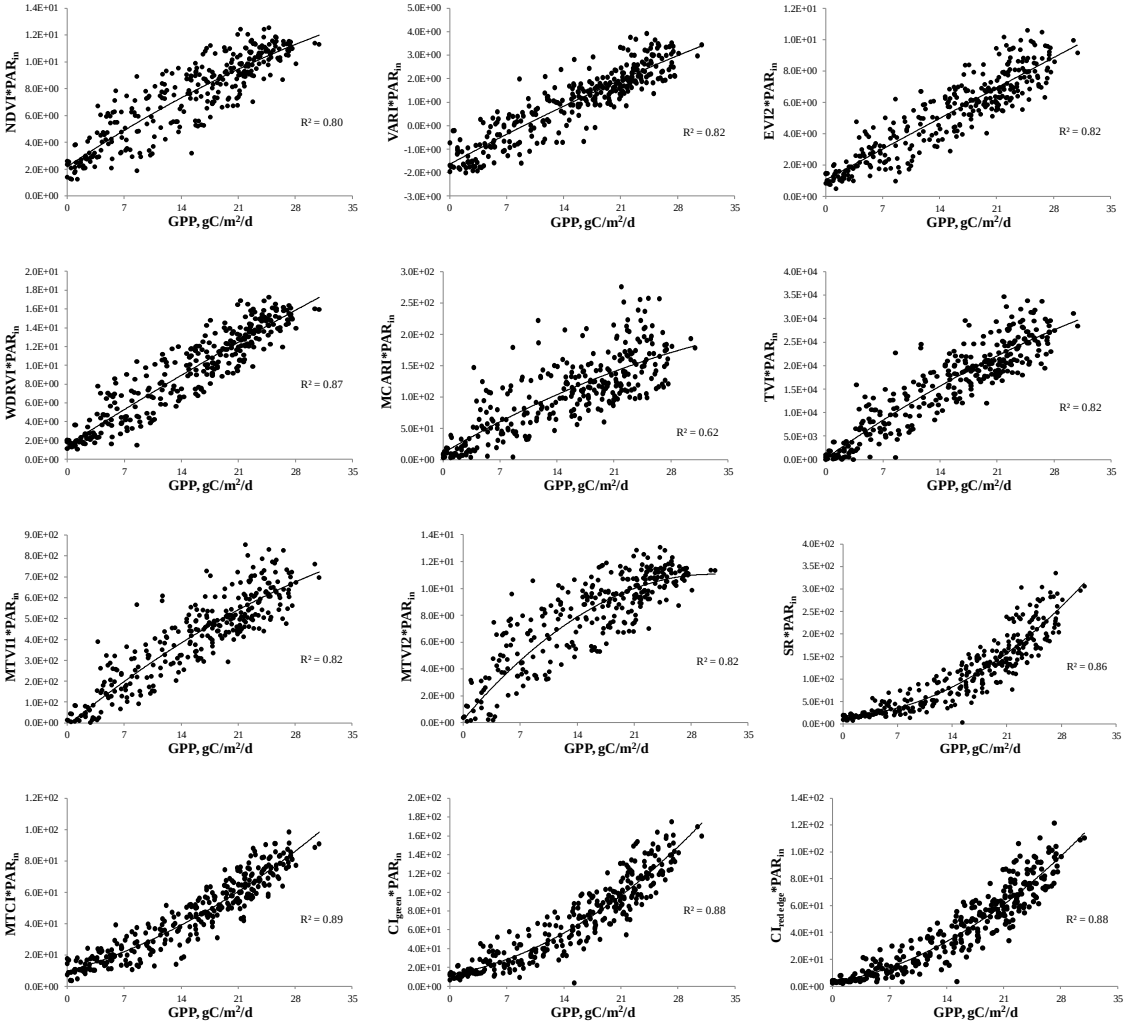

Figure 4.9 Relationship between GPP and (a) NDVI× PAR_{in}, (b) VARI × PAR_{in}, (c) EVI2 × PAR_{in}, (d) WDRVI× PAR_{in}, (e) MCARI × PAR_{in}, (f) TVI × PAR_{in}, (g) MTVI1 × PAR_{in}, (h) MTVI2 × PAR_{in}, (i) SR × PAR_{in}, (j) MTCI × PAR_{in}, (k) CI_{green} × PAR_{in}, (l) $CI_{red\ edge}$ × PAR_{in} for maize data collected in 16 irrigated and rainfed fields from 2001 through 2008.

In Fig. 4.10, the relationships between GPP and VI × PAR_{in} in 16 site-years are presented together with the best-fit function for all 16 site-years combined. Table 4.4 summarized how the unified algorithms work in estimating GPP in each of these 16

fields. Overall, the unified algorithms based on SR, MTCI, CIs, WDRVI and MTVI2 appeared to be most accurate for GPP estimation with the mean CV for 16 fields less than 23%, while the algorithms based on NDVI, VARI, EVI2, TVI and MTVI1 were less accurate (CV was between 26% to 29%). MCARI had the highest CV exceeding 35% (Fig. 4.11). Among the indices tested, SR, CIs and MTCI seemed the most accurate for estimating maize GPP.

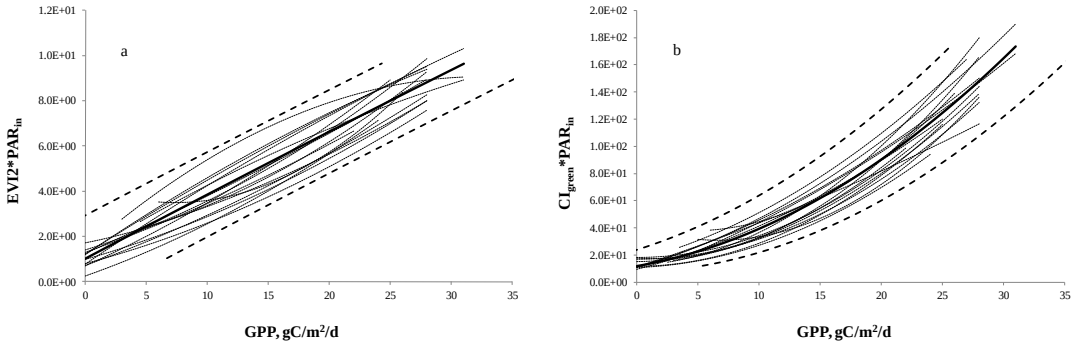

Figure 4.10 Best fit functions of the relationships between GPP and the products of (a) EVI2 × PAR_{in} and (b) CI_{green}× PAR_{in} for each of 16 fields from 2001 through 2008 (dash lines). The solid lines are the best fit functions for all data in 16 irrigated and rainfed fields combined from 2001 through 2008 (Table 4.3). The bold dash lines represent the 95% confidence interval (i.e., two standard errors of GPP estimation).

Table 4.4. Coefficients of variation (CV) of the relationship between measured GPP and GPP estimated in each of 16 different fields using relationships GPP vs. VI × PAR_{in}, established using data taken from 2001 through 2008 (Figure 4.9, Table 4.3). Details about crop management practices in each field are shown in Table 3.2.

Site #	Year	GPP, $gC/m^2/d$		CV (%)											
		max	mean	MCARI	NDVI	VARI	EVI2	MTVI1	TVI	MTVI2	WDRVI	SR	CI_{green}	MTCI	$CI_{red\ edge}$
1	2001	31.1	14.8	47.2	34.0	27.3	31.0	36.3	36.1	31.1	26.5	19.3	18.9	18.6	18.5
2	2001	33.5	13.7	54.1	37.4	36.2	38.2	45.1	44.6	40.4	32.1	24.9	24.3	21.6	24.3
3	2001	28.9	12.8	47.1	32.8	30.4	24.5	27.4	27.1	26.5	26.3	29.1	27.9	22.5	24.5
1	2002	28.8	14.3	26.7	22.5	26.3	14.6	16.3	15.9	15.7	17.8	19.9	17.5	17.0	16.8
1	2003	27.3	12.6	38.6	30.4	32.0	28.6	29.0	28.5	26.3	26.5	24.4	24.4	18.9	23.2
2	2003	28.2	13.4	35.9	28.7	25.1	26.0	27.1	26.7	23.5	22.7	18.8	20.2	18.6	18.0
3	2003	25.2	10.1	20.8	28.5	26.1	23.9	23.6	24.1	22.6	23.6	29.5	28.8	44.8	30.3
1	2004	30.4	12.9	32.9	29.0	20.7	23.6	22.9	22.7	20.5	22.5	21.4	23.5	14.0	20.2
1	2005	26.7	13.7	22.4	24.3	20.4	16.8	18.0	18.1	12.1	14.7	14.6	14.7	15.0	13.7
2	2005	27.2	14.2	26.8	25.9	22.1	18.0	18.2	18.1	15.8	18.1	16.8	15.8	16.5	14.3
3	2005	22.5	12.5	25.6	27.8	19.6	21.6	20.5	21.0	16.9	17.1	18.8	18.0	27.9	15.9
1	2006	26.2	14.4	35.5	20.7	25.0	25.8	25.3	25.3	21.2	14.4	17.7	14.7	13.0	15.0
1	2007	30.6	13.5	39.3	31.2	22.7	36.7	31.4	31.3	25.1	22.3	16.4	19.3	15.1	18.1
2	2007	27.6	12.8	49.8	29.6	31.1	31.7	29.7	29.1	24.1	20.6	17.8	17.6	11.6	17.2
3	2007	24.3	11.4	20.5	25.9	24.2	32.2	20.1	20.7	18.2	22.0	28.5	31.7	23.0	29.1
1	2008	26.9	13.4	37.3	36.9	33.9	24.6	25.5	24.9	23.3	25.7	17.5	11.9	25.1	12.9
Mean		27.8	13.2	35.0	29.1	26.5	26.1	26.0	25.9	22.7	22.5	21.0	20.6	20.2	19.5

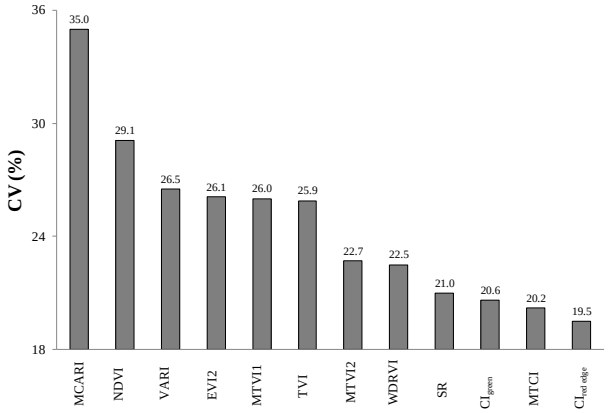

Figure 4.11 Mean coefficients of variation (CV) of relationships between measured daytime GPP and GPP estimated by a unified algorithm established using maize data taken over 16 different fields from 2001 through 2008 (Table 4.3).

To show the role of PAR_{in} in the model Eq. 4.1, we established relationships GPP vs. VI and calculated statistics of these relationships (Table 4.5). The accuracy of GPP estimation by VIs alone was much lower than using Eq. 4.1 (Table 4.3).

Table 4.5. Determination coefficients (R^2), standard errors (SE), coefficients of variation (CV) of quadratic polynomial relationships between daytime GPP and VI established using data collected in 16 irrigated and rainfed fields from 2001 through 2008. GPP ranged from 0 to 35gC/m^2/d.

	MCARI	MTVI1	TVI	EVI2	CI_{green}	MTVI2
R^2	0.52	0.70	0.70	0.71	0.75	0.75
SE, gC/m^2/d	5.58	4.40	4.39	4.32	4.03	4.01
CV (%)	36.3	28.6	28.5	28.0	26.2	26.0
	NDVI	SR	WDRVI	VARI	$CI_{red\ edge}$	MTCI
R^2	0.77	0.78	0.78	0.78	0.79	0.81
SE, gC/m^2/d	3.87	3.77	3.76	3.74	3.67	3.53
CV (%)	25.1	24.5	24.4	24.3	23.8	22.9

We also compared the performances of the product VI×PRI×PAR_{in} and VI× PAR_{in} for GPP estimation and found no improvement by using PRI as a proxy of LUE for GPP estimation for both irrigated and rainfed maize. While relationship PRI vs. total canopy Chl was significant (R^2 = 0.59, p-value < 0.01, Fig. 4.12a), the relationship of PRI with LUE = GPP/$APAR_{green}$, where $APAR_{green}$ is the radiation absorbed by green elements of plants (Hall et al., 1992), was very weak (R^2 = 0.03, p-value = 19.35, Fig. 4.12b). Thus, PRI may not be effective as a surrogate of LUE in ecosystems where Chl content closely follows the seasonal dynamic of CO_2 exchange such as croplands, deciduous forests and grasslands (Garbulsky et al., 2010; Peng et al., 2011).

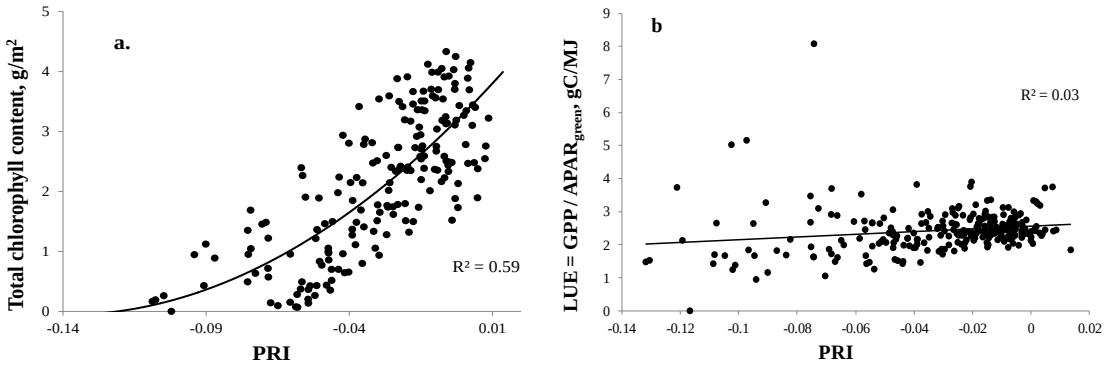

Figure 4.12 The relationship between the PRI index and (a) total chlorophyll content and (b) LUE = GPP / $APAR_{green}$, based on observations of 2001 through 2008 for irrigated and rainfed maize.

Therefore, it is feasible to develop a unified algorithm to estimate maize GPP accurately in fields that were different in crop management and climatic conditions. To calibrate and validate the algorithms for GPP estimation, we created a dataset including all data taken from 2001 through 2008 in three sites (332 samples in total), and sorted all

samples in ascending order of GPP. Data with odd numbers were used for establishing the relationships GPP vs. VI × PAR_{in} and, thus, calibrating the algorithms. The established relationships are presented in Table 4.6.

Table 4.6. The results of calibration of the algorithms for estimating daytime GPP in 16 irrigated and rainfed maize sites from 2001 through 2008: GPP = f(x), x = VI× PAR_{in}. Best fit functions and determination coefficients (R^2) are given for twelve vegetation indices.

VI	Best Fit Function	R^2
MCARI	GPP = -4.35E-4 x^2 + 0.21 * x – 0.35	0.71
NDVI	GPP = 2.37 x - 2.59	0.79
VARI	GPP = -0.154 x^2 + 5.01 x + 10.83	0.80
MTVI1	GPP = -1.27E-5 x^2 + 4.28E-2 x + 1.12	0.84
TVI	GPP = -9.49E-9 x^2 + 1.12E-3 x + 0.23	0.84
EVI2	GPP = -0.138 x^2 + 4.28 x - 3.08	0.88
MTVI2	GPP = -0.101x^2 + 3.57 x + 1.66	0.87
WDRVI	GPP = -2.88E-2 x^2 + 2.08 x -0.76	0.87
SR	GPP = 28.8 * (1 – $e^{-0.008287*x}$)	0.89
MTCI	GPP = -1.73E-3 x^2 + 0.471 x – 1.60	0.89
CI_{green}	GPP = -8E-4 x^2 + 0.2992 x – 0.1213	0.90
$CI_{red\ edge}$	GPP = -3.2E-3 x^2 + 0.56 x + 1.6074	0.90

The algorithms, presented in Table 4.6, were then validated using a validation data set (samples with even numbers). Measured reflectances in the validation dataset were used to calculate GPP values, and then these predicted GPP values were compared with GPP measured by the eddy covariance technique. Table 4.7 and Fig. 4.13 show the accuracy of GPP prediction by the established (Table 4.6) algorithms. Among the twelve indices, SR, MTCI and CIs were the most precise estimators of GPP with CV < 18%,

followed by WDRVI and MTVI2 with CV around 20%. NDVI, VARI, EVI2, TVI and MTVI1 appeared to estimate GPP less precisely with CV more than 23%, and MCARI was the worst with CV more than 31% (Fig. 4.13).

Table 4.7. The results of validation of algorithms for estimating daytime GPP in 16 irrigated and rainfed maize sites from 2001 through 2008. Slopes and offsets of the relationships between GPP predicted by algorithms (Table 4.6) and measured daytime GPP, root mean square errors (RMSE) are given for twelve vegetation indices.

	MCARI	NDVI	MTVI1	TVI	VARI	EVI2
Slope	0.66	0.74	0.79	0.79	0.80	0.81
Offset	5.13	4.12	3.22	3.13	3.03	3.01
RMSE, $gC/m^2/d$	4.92	3.80	3.60	3.58	3.57	3.55
	MTVI2	WDRVI	CI_{green}	MTCI	SR	$CI_{red\ edge}$
Slope	0.82	0.82	0.83	0.86	0.84	0.85
Offset	2.76	2.78	2.67	2.14	2.29	2.29
RMSE, $gC/m^2/d$	3.11	2.92	2.75	2.65	2.62	2.56

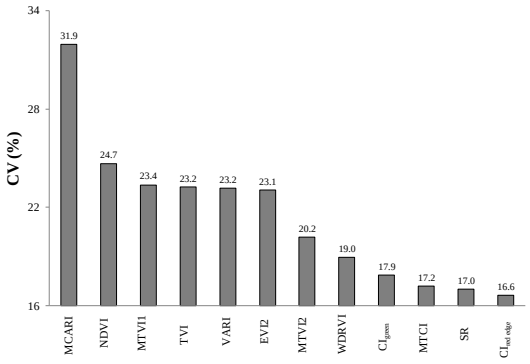

Figure 4.13 Coefficients of variation (CV) of relationships between measured daytime GPP and GPP predicted by established algorithms presented in Table 4.6.

In addition to statistical characteristics of the established relationships such as R^2, RMSE, it is also important to assess accuracy of each algorithm to GPP in whole range of GPP variation. Thus, we compared the noise equivalent (NEΔGPP) of each VI tested (Fig. 4.14). The NEΔGPP of MCARI was the highest among the VIs tested due to much higher value of SE. It can be seen that NDVI- and TVI-like indices had smaller NEΔGPP (they were more sensitive to GPP) for GPP below 10 -14 $gC/m^2/d$ than to higher GPP. Among these indices, WDRVI had the lowest and constant value of NEΔGPP. The SR, MTCI, CI_{green} and $CI_{red\ edge}$ had much NEΔGPP (they are more sensitive to GPP) when GPP exceeded 14 $gC/m^2/d$. Thus, they were more appropriate for estimating moderate-to-high GPP, while NDVI- and TVI-like indices were more sensitive to low GPP values.

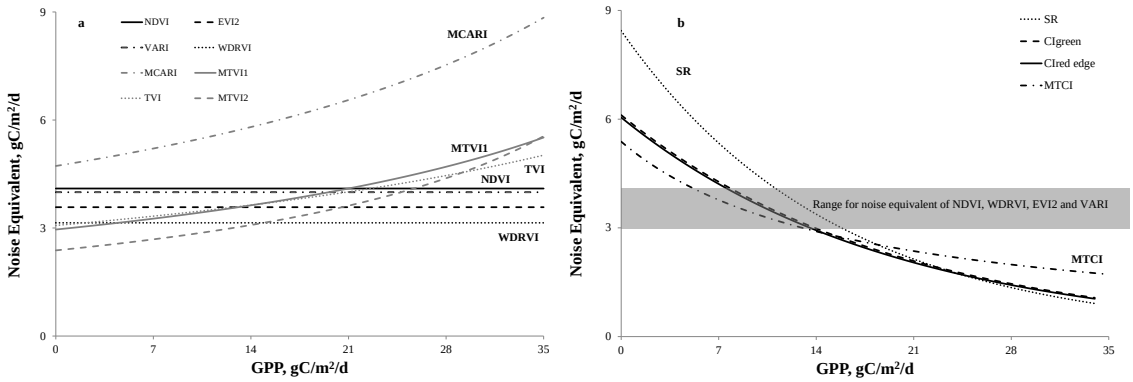

Figure 4.14 Noise Equivalent of GPP estimation by the product of $VI \times PAR_{in}$ for (a) NDVI, WDRVI, EVI2, VARI, MCARI, TVI, MTVI1and MTVI2; (b) SR, CI_{green}, $CI_{red\ edge}$ and MTCI. When GPP was above $14gC/m^2/d$, the SR, CI_{green}, $CI_{red\ edge}$ and MTCI had lower noise equivalent (i.e., more sensitivity to GPP) than indices in Fig. 4.14a.

4.3.4 GPP estimation in soybean

The soybean and maize species have very different biochemical mechanisms for photosynthesis. The maize utilizes C4 carbon fixation, while the soybean utilizes C3 carbon fixation. In addition, their canopy architectures are contrasting. The distribution of foliage in maize canopy is spherical, while it is heliotropic in soybean. Since the model Eq. 4.1 was capable to predict GPP accurately in maize (Chapter 4.3.1 – 4.3.3), we tested the performance of this model for estimating GPP in soybean.

Table 4.8 shows the best fit functions, R^2, RMSE of the relationships GPP vs. VI × PAR_{in} in irrigated and rainfed soybean sites in 2002, 2004, 2006 and 2008 (8 site-years), established using a k-fold cross validation procedure with k = 15. All twelve VIs worked well for estimating soybean GPP reaching 19 $gC/m^2/d$ with RMSE below 2.3 $gC/m^2/d$. Among the indices tested, CI_{green}, $CI_{red\ edge}$, Red edge NDVI, as well as WDRVI appeared to be the best indices for estimating GPP in soybean.

When compared with the performances of VIs for GPP estimation in maize (Table 4.7), the model based on NDVI was more accurate for soybean than for maize (Fig. 4.15). The maximal GPP of maize was at least 50% higher than that of soybean, thus, NDVI worked better for estimating low-to-moderate Chl / GPP, as in soybean, but it was less sensitive to high Chl / GPP in maize (Asrar et al., 1984; Gitelson, 2004). As shown in Fig. 3.14, CI_{green} and $CI_{red\ edge}$, which remain sensitive to the wide range of Chl / GPP (Gitelson et al., 2003a; Peng et al., 2011), were consistently the most accurate for GPP estimation in both maize and soybean. SR was much less accurate in estimating GPP in soybean than in maize, since red reflectance of soybean (in the denominator of SR) is

much smaller than of maize (below 2% for GPP above 16 $gC/m^2/d$) and it makes soybean SR much noisier than maize SR.

Table 4.8. Established relationships "GPP vs. $VI \times PAR_{in}$" in 8 irrigated and rainfed soybean sites in 2002, 2004, 2006 and 2008: $GPP = f(x)$, $x = VI \times PAR_{in}$. Best fit functions, determination coefficients (R^2) and root mean square errors (RMSE) are given for twelve vegetation indices. GPP ranged from 0 to 19 $gC/m^2/d$. All algorithms and RMSE were obtained using a k-fold cross validation procedure with k = 15.

VI	Best Fit Function	R^2	RMSE ($gC/m^2/d$)
VARI	$GPP = -5.41E\text{-}2x^2 + 2.20x + 6.39$	0.79	2.30
MTVI1	$GPP = -1.10E\text{-}5x^2 + 2.62E\text{-}2x + 0.51$	0.81	2.17
TVI	$GPP = -7.98E\text{-}9x^2 + 7.15E\text{-}4x - 0.33$	0.81	2.14
MTCI	$GPP = -3.97E\text{-}3x^2 + 0.51x - 1.33$	0.82	2.04
NDVI	$GPP = -4.87E\text{-}2x^2 + 2.08x - 2.17$	0.83	2.02
EVI2	$GPP = -0.132x^2 + 3.06x - 1.53$	0.84	1.95
MTVI2	$GPP = -8.51E\text{-}2x^2 + 2.32x + 0.90$	0.84	1.95
SR	$GPP = 4.33\ln(x) - 9.42$	0.85	1.91
WDRVI	$GPP = -3.63E\text{-}2x^2 + 1.59x - 0.37$	0.87	1.78
Red edge NDVI	$GPP = -0.178x^2 + 3.67x - 2.70$	0.87	1.76
CI_{green}	$GPP = 5.13\ln(x) - 10.4538$	0.88	1.72
$CI_{red\ edge}$	$GPP = 4.80\ln(x) - 3.80956$	0.90	1.56

Note that for both maize and soybean, Red edge NDVI was less accurate for GPP estimation than CIs. The Red edge NDVI was closely linearly related to the fraction of absorbed photosynthetically active radiation ($fAPAR_{green}$) in crops (Vina and Gitelson, 2005). Thus, in model Eq. 4.1, Red edge NDVI was less accurate in estimating GPP (assuming constant LUE) than CIs, which are proxies of total Chl content (Gitelson et al.,

2005). The total Chl content closely relates to $fAPAR_{green}$ and is indicative of light use efficiency (Houborg et al., 2011; Peng et al., 2011).

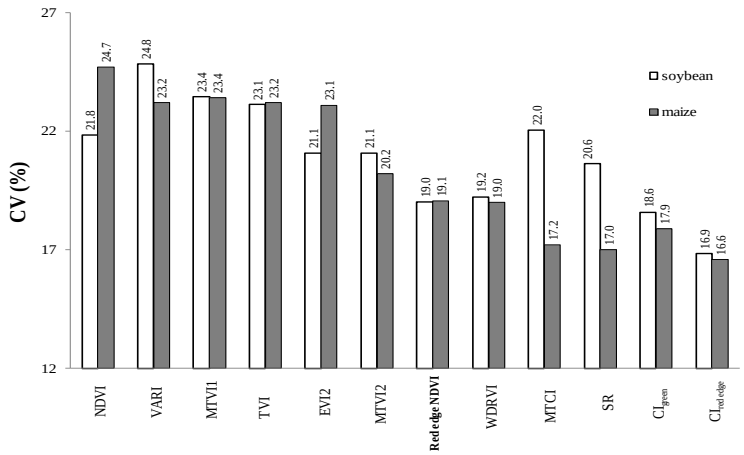

Figure 4.15 Coefficients of variation (CV = RMSE / mean GPP) of the relationships, $GPP = VI \times PAR_{in}$, established for soybean (Table 4.8) and for maize (Table 4.6).

Among the eight studied soybean site-years, four were under irrigated management (site 2 in 2002, 2004, 2006 and 2008), and the other four relied entirely on rainfall (site 3 in 2002, 2004, 2006 and 2008). The soybean cultivars and climatic conditions differed from year to year. There were obvious dry periods during reproductive stages in 2002, but no significant dry periods during the growing seasons of 2004 and 2006 (Suyker and Verma, 2010). In accord with that, the dynamic ranges of LAI, GPP and yield were different in the eight soybean fields. For example, the maximum LAI was 5.1 m^2/m^2 in site 2 in 2006, but only 3.2 m^2/m^2 in site 3 in 2002. All these differences existing among years and fields might cause differences in relationships GPP vs. $VI \times PAR_{in}$ for different fields (Fig. 4.16); however, the algorithms established by data taken over 8 fields

combined were quite accurate with RMSE below 2.3 gC/m^2/d and R^2 above 0.79 (Table 4.8).

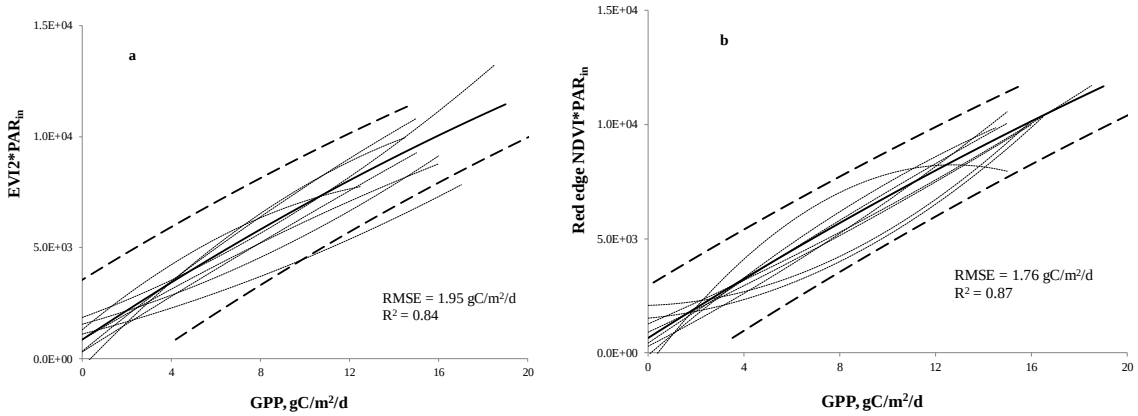

Figure 4.16 Best fit functions of the relationships between GPP and the products of (a) EVI2 × PAR_{in} and (b) Red edge NDVI × PAR_{in} for each of 8 different soybean fields in 2002, 2004, 2006 and 2008 (dash lines). The solid lines are the best fit functions for all data in 8 irrigated and rainfed fields combined. The bold dash lines represent the 95% confidential interval (i.e., two standard error of GPP estimation).

From 2006 through 2008, site 1 was under the conservation-plow tillage operation while site 2 and site 3 were under no-till management (Table 3.2). Since the reflectance of residues is much higher than that of the bare soil in Nebraska, the background reflectance was significantly lower in site 1 than in site 2 and site 3. The total canopy reflectance was more affected by the background reflectance in maize fields with spherical canopy than in soybean fields with planophile canopy. Using simulated data (Gobron et al., 1997), it was shown that MTCI, EVI2 and $CI_{red\ edge}$ were accurate in estimating green LAI despite very different soil backgrounds (Viña et al., 2011). It is also

confirmed by results of our study. For maize and soybean tilled and no-tilled fields combined, the model Eq. 4.1 explained more than 79% of GPP variation with RMSE below 2.3 $gC/m^2/d$ for soybean (GPP ranged from 0 to 19 $gC/m^2/d$) and 3.6 $gC/m^2/d$ for maize (GPP ranged from 0 to 35 $gC/m^2/d$) (Table 4.6, Table 4.7 and Table 4.8).

4.3.5 A unified algorithm for GPP estimation in maize and soybean

Relationships between GPP and the product of PAR_{in} and VIs in maize and soybean are presented in Fig. 4.17). Established relationships of GPP vs. VI $\times$ PAR_{in} for soybean (8 irrigated and rainfed site-years) and for maize (16 irrigated and rainfed site-years) were compared. For all VIs used, the relationships for these two crop types were species specific (p-value < 0.0001), and the discrepancies became more pronounced at moderate to high GPP. For the same GPP, the value of VI $\times$ PAR_{in} for soybean was consistently higher than that of maize. The relationship between GPP and the product of total Chl content and PAR_{in} in maize and soybean was found to be non-species-specific (Gitelson et al., 2006a). However, the relationship between total Chl content and VI was species-specific with consistently higher values for soybean than for maize with the same total Chl content (Gitelson et al., 2005).

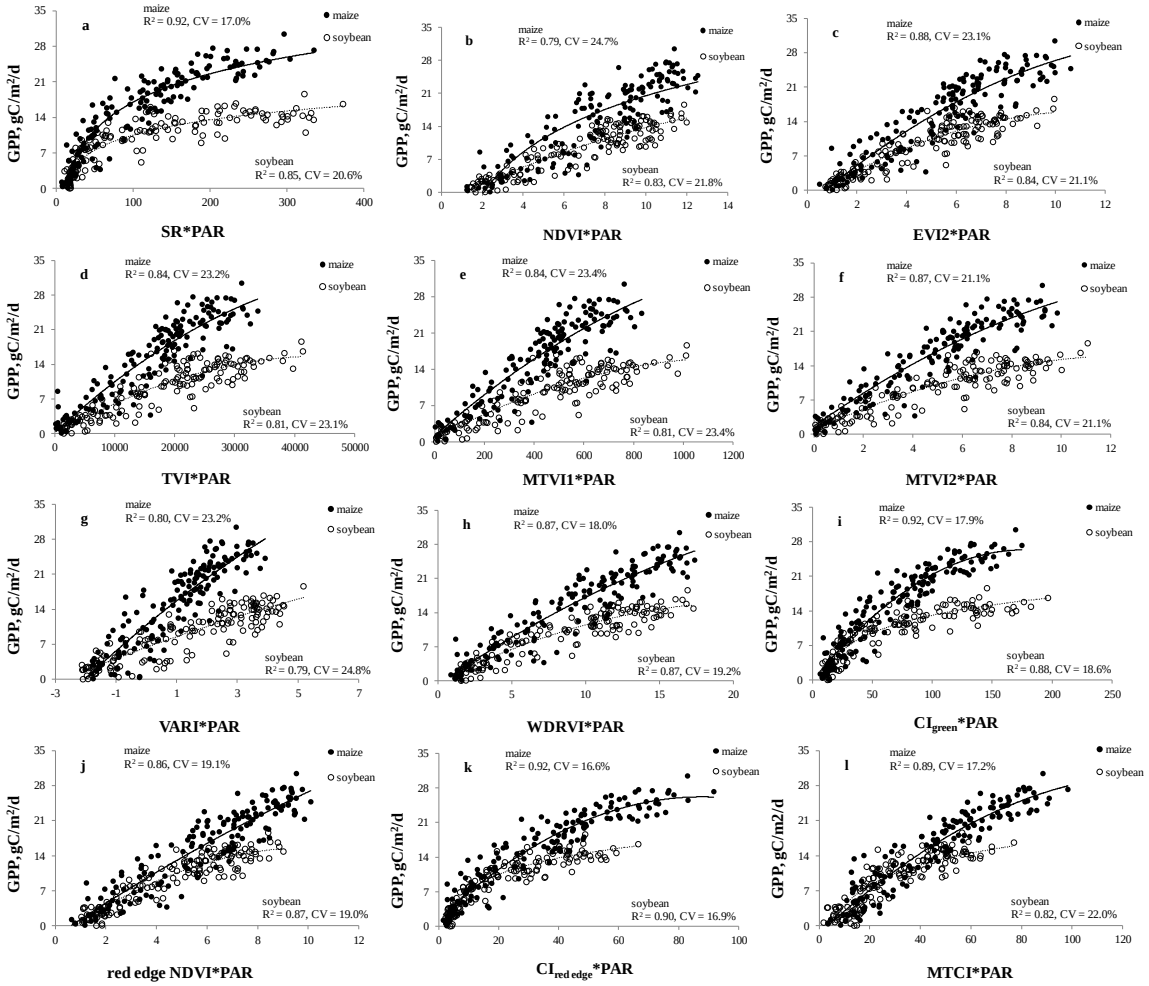

Figure 4.17 Relationships of GPP vs. (a) SR×PAR_{in}, (b) NDVI×PAR_{in}, (c) EVI2×PAR_{in}, (d) TVI ×PAR_{in}, (e) MTVI1×PAR_{in}, (f) MTVI2×PAR_{in}, (g) VARI×PAR_{in}, (h) WDRVI×PAR_{in}, (i) CI_{green}×PAR_{in}, (j) Red edge NDVI×PAR_{in}, (k) $CI_{red\ edge}$×PAR_{in}, (l) MTCI×PAR_{in} for soybean and maize. The solid lines are the best fit functions for the relationships GPP vs. VI×PAR_{in}, established for maize. The dash lines are the best fit functions for the relationships GPP vs. VI×PAR_{in}, established for soybean.

The reason for the species-specific algorithms for maize and soybean is at least twofold:

(1) The reflectance in the visible region of the spectrum is mainly affected by leaf absorption. For the same total leaf Chl content, the reflectance in the visible region is lower in a soybean leaf than in a maize leaf, since leaf Chl content of the adaxial surface of a C3 plant (i.e. soybean) is higher than a C4 plant (i.e. maize). As the visible light is predominantly absorbed by chloroplasts at the surface layer of a leaf (Fukshansky, 1981; Fukshansky et al., 1993; Merzlyak & Gitelson, 1995), the absorption in the visible region by a soybean leaf is higher than a maize leaf. Total canopy Chl content is the product of leaf Chl content and total leaf area, so in the visible region, the canopy reflectance of soybean is lower than of maize with the same total canopy Chl content (Fig. 4.18).

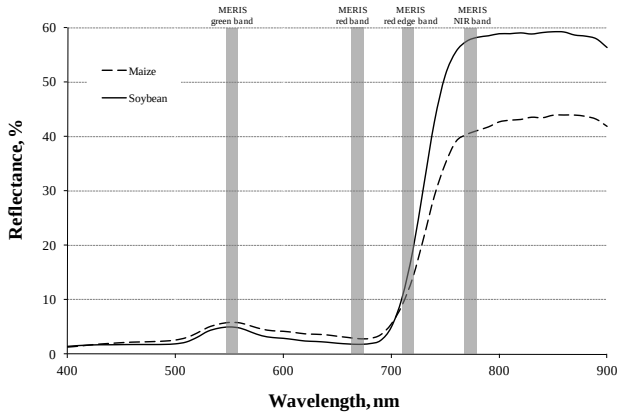

Figure 4.18. Spectral reflectance of maize and soybean canopies with total Chl content of 2.15 g/m^2. In the visible range (the green and red), reflectance of soybean is lower than that of maize, while NIR reflectance of soybean is higher than of maize. So for the same Chl content, indices using visible and NIR bands are consistently higher for sybean than for maize. Both NIR and red edge reflectance of soybean are higher than that of maize with the same Chl content. Thus, indices with NIR and red edge reflectance were less species-specific than that with NIR and either red or green reflectance.

(2) NIR reflectance is governed by leaf/canopy scattering. NIR reflectance of soybean leaf is higher than that of maize. In addition, for the same LAI, NIR reflectance of planophile canopy (soybean) is much higher than spherical canopy (maize) - Fig. 4.18. Thus, in soybean, the visible reflectance is lower and the NIR reflectance is higher than in maize. So VI based on NIR and visible reflectance produce consistently higher values for soybean than for maize.

Fig. 4.19 shows RMSE of GPP estimation for soybean, reaching 19 gC/m2/d, using relationships GPP vs. VI × PAR_{in} established for maize (Table 4.6). It is not surprising that the algorithms with VI based on NIR and visible bands (VARI, MTVI1, TVI, MTVI2, SR, CIgreen, WDRVI, NDVI and EVI2) were not accurate when applied for soybean: RMSE was above 5.3 gC/m2/d and coefficient of variation, CV = RMSE/mean GPP, was above 57%.

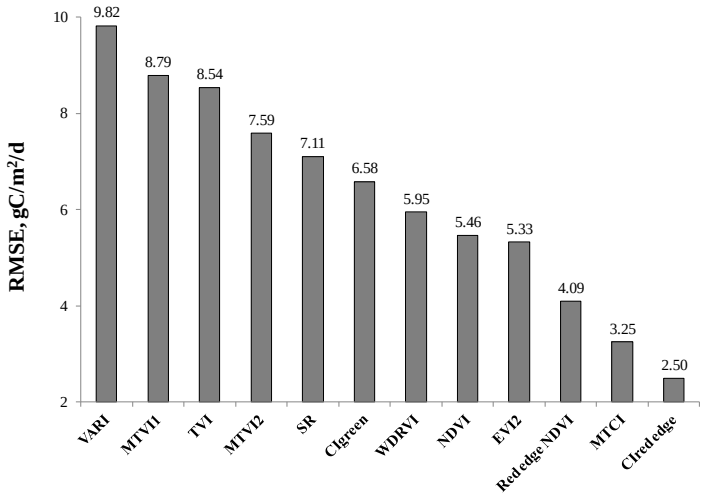

Figure 4.19 Root mean square errors (RMSE) of estimating GPP reaching 19 $gC/m^2/d$ in soybean using algorithms established for maize (Table 4.6).

However, the accuracy of GPP estimation in both crops was much higher and RMSEs were much lower (below 4.1 $gC/m^2/d$) when VIs based on NIR and MERIS red edge bands (Red edge NDVI, MTCI and $CI_{red\ edge}$) were used. The reflectance in the red edge region is affected not only by leaf absorption but also leaf and canpoy scattering. The absorption coefficient of Chl in the red edge region is much lower than in the visible region (Gitelson, 2011). The depth of light penetration into a leaf inversely relates to the Chl absorption coefficient (Merzlyak & Gitelson, 1995), so, the red edge light penetrates deeper into a leaf and chloroplasts of the whole leaf work for light absorption. Therefore, for the same total leaf Chl content, absorption of a maize leaf in the red edge region becomes equal to that of soybean leaf absorption. On the other hand, the leaf scattering in the red edge region in soybean is higher than in maize. As a result, for the same total Chl content, soybean reflectance in the red edge region becomes higher than maize reflectance, accompanied with higher NIR reflectance in soybean than in maize (Fig. 4.18). Therefore, the difference in VI values for both species with the same Chl content, when using the red edge band (703 nm–710 nm), became lower than when visible bands were used. The indices using MERIS red edge band performed quite accurately estimating GPP in maize and soybean data combined with the coefficients of variation below 26% (Table 4.9).

There is a need to increase the accuracy of the algorithms noted above when applied to both maize and soybean. This issue is particularly important when using satellite data with coarse spatial resolution that do not allow for separating signals from sites with different crop species.

Table 4.9 The algorithms based on indices using MERIS red edge band for estimating daytime GPP in 24 maize and soybean fields from 2001 through 2008: GPP=f(x), $x=VI\times PAR_{in}$. Best fit functions, determination coefficients (R^2), root mean square errors (RMSE) and coefficients of variation were obtained using a k-fold cross validation procedure with k=15.

VI	Best Fit Function	R^2	RMSE ($gC/m^2/d$)	CV (%)
Red edge NDVI	GPP = -2.51E-2 x^2 + 2.57 x – 1.04	0.81	3.17	25.5
$CI_{red\ edge}$	GPP = -2.43E-3 x^2 + 0.501x + 1.55	0.85	2.74	22.1
MTCI	GPP = -1.07E-3 x^2 + 0.405x – 0.75	0.85	2.72	22.0

In order to identify the optimal red edge band for GPP estimation in both maize and soybean with no re-parameterization, we used optimization procedure to find the minimal RMSE value of the relationship GPP vs. $VI\times PAR_{in}$ for Red edge NDVI and $CI_{red\ edge}$. Tuning the wavelength from 700 nm to 750 nm, we found the minimal RMSE value in the range around 720 nm (Fig. 4.20).

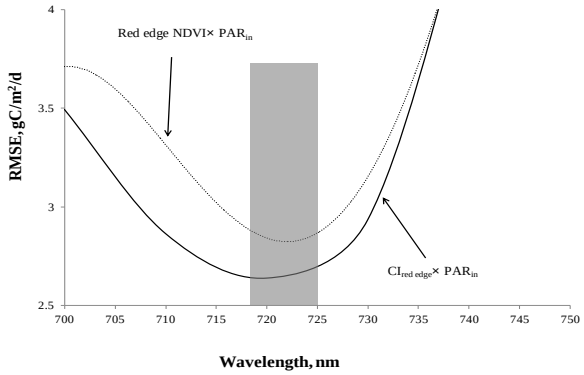

Figure 4.20 Root mean square errors (RMSE) of the relationships GPP vs. $VI\times PAR_{in}$ for Red edge NDVI and $CI_{red\ edge}$ calculated for soybean and maize data combined by tuning the red edge bands from 700 nm to 750 nm.

As the red edge band shifts towards a longer wavelength around 720 nm, the reflectance is more affected by leaf scattering than in the red region. So, in both species with the same Chl content, red edge reflectance of soybean becomes higher than that of maize. This difference in the red edge reflectances between soybean and maize compensated for the difference in their NIR reflectances. Thus, the VIs based on longer wavelength in red edge region and NIR band become non-species-specific. Both Red edge NDVI and $CI_{rededge}$ with a red edge band around 720 nm were able to estimate GPP in soybean and maize with RMSEs of less than 2.9 $gC/m^2/d$ (Fig. 4.21). This is consistent with optimal red edge band for total Chl content estimation in maize and soybean (Gitelson et al., 2005).

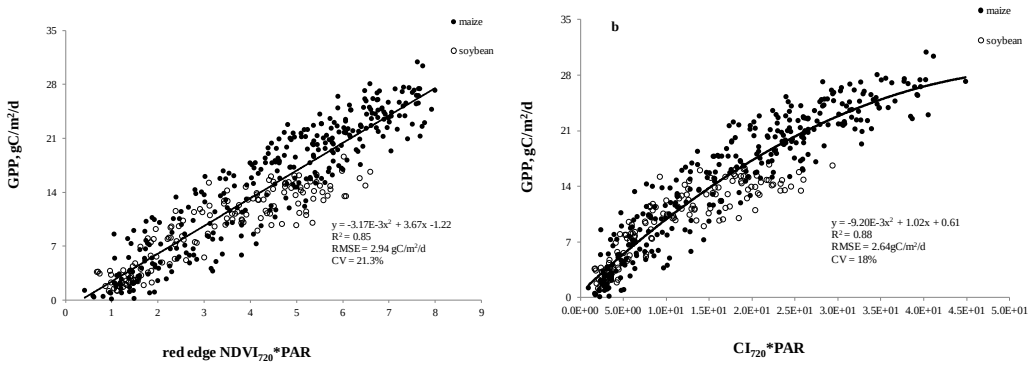

Figure 4.21 Products of (a) Red edge NDVI×PAR_{in}, and (b) $CI_{red\ edge}$×PAR_{in}, plotted versus GPP in maize (16 fields during 2001 through 2008) and soybean (8 fields in 2002, 2004, 2006 and 2008). The solid line is the best fit function for the relationship GPP vs. VI*PAR established for all soybean and maize data combined. Best fit functions, root mean square errors, RMSE, determination coefficients and coefficients of variation, R2 and CV, were obtained using a k-fold cross validation procedure with k = 46.

This study gives clear understanding of using a product of a Chl-related vegetation indices and PAR_{in} for GPP estimation. We are well aware that the presented model does not take into account GPP decline that does not relate to a decrease in Chl content. It is a case when GPP is affected by short-term (minutes to hours) environmental stresses (e.g., temperature, humidity, and soil moisture, among others), that do not affect the Chl content (i.e., crop greenness), thus, do not affect Chl-related indices. The model presented here will fail to detect a decrease in GPP related to the types of stressors mentioned. The next step in this direction should be including other biophysical characteristics (i.e., temperature) and assess the efficiency of a modified model.

4.4 Conclusions

We showed that two key physiological properties, light capture and the efficiency of the use of absorbed light, relate closely to total crop Chl content, which subsumes a broad range of processes and can be applied as an integrative diagnostic tool. GPP in crop is closely related to total canopy Chl content. As a result, a procedure was suggested to remotely assess crop GPP via estimation of total crop Chl content employing vegetation indices related to canopy Chl content. In this chapter, we tested a simple model that relates GPP to a product of ground-observed PAR_{in} and Chl-related vegetation indices retrieved from remotely sensed data collected at close range. The results demonstrated that this model was capable of accurately estimating GPP in maize and soybean, contrasting crop species, from both irrigated and rainfed fields that were different in crop management practices, field history and climatic conditions.

But the algorithms for GPP estimates were species-specific for maize and soybean due to their differences in leaf structures and canopy architectures, especially when using vegetation indices with NIR and either red or green reflectance. $CI_{red\ edge}$, MTCI and Red edge NDVI with reflectance simulated in MERIS spectral bands, were less sensitive to different crop species. The algorithms using $CI_{red\ edge}$ and Red edge NDVI, employing red edge band around 720 nm, were very accurate in estimation of GPP in maize and soybean with no need for re-parameterization for different crop types, with RMSE less than 2.9 $gC/m^2/d$ and coefficients of variation below 21%.

The approach presented here is not limited to estimating crop GPP using spectral reflectance collected by radiometers mounted on a platform close to the canopy The vegetation indices used in this chapter were calculated with canopy *in situ* reflectance simulated in the spectral bands of MODIS and MERIS satellite sensors, which could provide a theoretical framework for using satellite data to estimate GPP at regional and global scales. The choice of the VI for GPP estimation depends on the spectral characteristics of the radiometers or the specific satellite sensors used. If the red edge band around 720 nm is available, as it is in the case of many hyperspectral radiometers such as Ocean Optics, ASD as well as hyperspectral imaging spectrometers such as AISA or HYPERION, $CI_{red\ edge}$ and Red edge NDVI are recommended as non-species-specific indices that can estimate GPP accurately in both soybean and maize. If the red edge band around 700 nm is available, as in MERIS (703 nm – 712 nm), HYPERION and future satellite sensors such as Sentinel-2, -3 and Venus, $CI_{red\ edge}$, MTCI and Red edge NDVI, which are least sensitive to different crop species, are suggested for use. If a red edge band is not available, one can use CI_{green} and MTVI2 with green, red and NIR bands

available as in the case of Landsat and MODIS 500 m data. If only red and NIR bands are available, such as in MODIS 250 m data, WDRVI, SR and EVI2 are recommended for estimating crop GPP.

Chapter 5: GPP estimation based entirely on Landsat data

This chapter has been published as:

Gitelson, A.A., Peng, Y., Masek, J.G., Rundquist, D.C., Verma, S.B., Suyker, A., Baker, J.M., Hatfield, J.L. & Meyers, T. (2012) Remote estimation of gross primary productivity in crops with Landsat data. Remote Sensing of Environment, 121, 404 - 414.

5.1 Introduction

Accurate and synoptic GPP estimates based on satellite data can provide efficient and valuable information for regional and global studies of carbon budgets and environmental regulation. Since 1999, the National Aeronautics and Space Administration (NASA) has provided GPP estimates for the entire globe based on the Moderate Resolution Imaging Spectroradiometer (MODIS) 1km products (e.g., Running, et al., 2000; Running et al., 2004). The current MODIS GPP algorithm provides reasonable spatial patterns and logical temporal variability across a diverse range of biomes and climate regimes. However, continued efforts are needed to resolve significant problems in certain biomes, especially in croplands, where an accurate MODIS estimation of GPP is still elusive (e.g., Heinsch et al., 2006; Turner et al., 2005, 2006). A recent evaluation of satellite-based MODIS products revealed that the estimates of GPP and net primary production (NPP) were particularly poor for maize and soybean test sites (Turner et al., 2005). Even though the annual NPP for the maize and soybean fields was among the most accurate available ancillary data of all biomes studied, the uncertainties

of the MODIS-derived estimates for the agricultural sites were the highest; the MODIS product strongly underestimated NPP.

There are several reasons for the poor performance of the MODIS product for croplands (e.g., Heinsch et al., 2006; Turner et al., 2005; Sims et al., 2006; Zhao et al., 2005). The reasons include: (a) the use of a constant maximum LUE value within a given biome, a consequence of which is a reduced ability to detect differences in species-specific LUE among crops (e.g., C_3 vs. C_4); (b) the assumption of a single land cover class for the entire 1 km pixel even though there is a considerable discrepancy between the spatial resolution of the MODIS product (1 km) and typical smaller sizes of cropped fields in North America; and (c) the use of a generalized radiation transfer algorithm for the retrieval of fAPAR based on LAI (Myneni et al., 1997) without a site-specific approach to characterize the vegetation species. Different crops with the same LAI (e.g., soybean vs. maize: Suyker et al., 2005) have very different GPP values.

A potential alternative to MODIS are the Landsat Thematic Mapper (TM) and Landsat Enhanced Thematic Mapper (ETM) sensors, with their fine spatial resolution (30 m pixel). Landsat data may provide useful information to facilitate the analysis of CO_2 exchange in croplands. Ecophysiological differences among different crop species are well documented, so classification of crop types using the Landsat data should be particularly useful. Due to differences in canopy architectures and leaf structures, LUE varies drastically between species (C_4 vs. C_3 crops: maize LUE is nearly double that of soybean - e.g., Suyker et al., 2005), causing great uncertainties in estimating CO_2 fluxes in crops with the coarse spatial resolution (1 km) of MODIS. The use of Landsat data allows one the opportunity to overcome these limitations. With the opening of the

Landsat archives to free and web-based access, the use of the sensor data with greatly improved spatial resolution may considerably reduce the uncertainties of GPP estimation in crops.

As we discussed in chapter 4, the VI-PAR_{in}-based model Eq. 4.1 was capable of estimating crop GPP accurately using *in situ* reflectance data (Gitelson et al., 2006b; Peng et al., 2011; Peng and Gitelson, 2011a, 2011b). And this model was also successfully applied to real satellite data. The VI-PAR_{in}-based model Eq. 4.1, with MTCI derived from MERIS images, was capable of estimating GPP accurately across a variety of land cover and vegetation types (Harris and Dash, 2010; Almond et al., 2010). Wu et al. (2010b, 2011) showed that maize GPP could be estimated with high accuracy using the VI-PAR_{in}-based model with MODIS data. The VI-PAR_{in}-based model was also accurate in estimating maize GPP using Landsat-ETM data (Gitelson et al., 2008). However, in all applications discussed above, PAR_{in} measured at ground level with tower-based systems was used.

To develop algorithms based solely on remotely sensed data, one needs to find an accurate proxy for PAR_{in} that can be measured remotely. Shortwave radiation (SW) obtained from coarse scale meteorological data sets from the NASA Data Assimilation Office were used as a substitute for PAR_{in} as input to Eq.4.1 (Sakamoto et al., 2011b). However, these estimates of PAR_{in} have significant uncertainties; the coefficient of variation (CV) was 23.6% and mean normalized bias (MNB) was 13.9% (Sakamoto et al., 2011b) – Fig. 3.4.

In this study, we *did not try to find a substitute for PAR_{in}*, but replaced PAR_{in} by $PAR_{potential}$ (the maximal PAR_{in} value under conditions of minimal aerosol - details see Chapter 3.9) into the model:

$$GPP \propto VI \times PAR_{potential} \quad (5.1)$$

Our hypothesis was that $PAR_{potential}$ may be a better representative of incident radiation, affecting photosynthesis, than PAR_{in}. Thus, the model Eq. 5.1 may be entirely based on remotely sensed data.

The objectives of this Chapter are (1) to compare the accuracy of Landsat-based GPP estimation models for maize and soybean, using both $PAR_{potential}$ (Eq. 5.1) and PAR_{in} (Eq. 4.1), (2) to assess the accuracy and uncertainties of several Landsat-retrieved VIs in estimating crop GPP, and (3) to explore the possibility of using a unified algorithm for GPP estimation in study sites that are different in geographic locations, crop management practices, and climatic conditions.

5.2. Results and discussion

5.2.1 Ground-observed PAR_{in} and $PAR_{potential}$ on Landsat acquisition dates

The Landsat images, used in our work, were mostly acquired when the study sites were under cloud-free conditions. Fig. 5.1 showed that the ground-observed PAR_{in} and $PAR_{potential}$ were quite close for Nebraska sites at the Landsat acquisition dates during the 8-year period from 2001 to 2008, with the difference between PAR_{in} and $PAR_{potential}$, $(PAR_{potential} - PAR_{in})/PAR_{potential}$, at 12% on average and 40% at most. For 88% of all Landsat images, the difference was below 20%. These differences were due to varying atmospheric conditions, including aerosol scattering and absorption by water vapor.

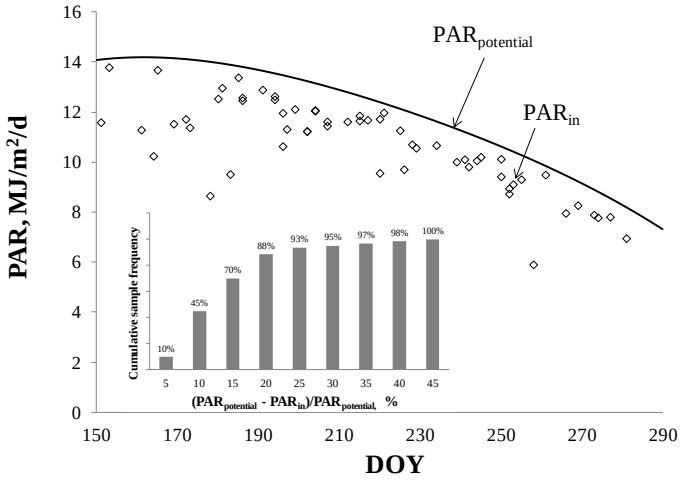

Figure 5.1 Temporal behavior of PAR_{in}, measured on the Landsat acquisition dates, and calculated $PAR_{potential}$ during the growing seasons 2001 through 2008 for Mead, Nebraska. Insert: cumulative sample frequency plotted versus difference between PAR_{in} and $PAR_{potential}$. For 88% of samples, the difference between PAR_{in} and $PAR_{potential}$ was below 20%.

5.2.2 Quality of atmospheric correction

Since spectral reflectance changed gradually across the growing season, daily canopy reflectance at close range was interpolated based on measurements taken at cloud-free sampling dates. Such interpolated reflectance, obtained at close range, was simulated in the spectral bands of Landsat for comparison to Landsat-retrieved surface reflectance at the dates of image acquisition to assess the quality of Landsat atmospheric correction. In blue, green, red and NIR bands, Landsat-retrieved surface reflectance was quite close to reflectance taken at close range for all three sites in Mead, Nebraska from 2001 through 2008 (Fig. 5.2), with maximal CV of 27.7% and maximal mean normalized bias (MNB) of 18.3% for the blue band (Fig. 5.2a) and minimal CV of 16.8% and

minimal MNB of 11.7% for NIR band (Fig. 5.2d). The points out of the range of the 95% confidential interval (3 of 140 points) were excluded from the database for the model development and calibration.

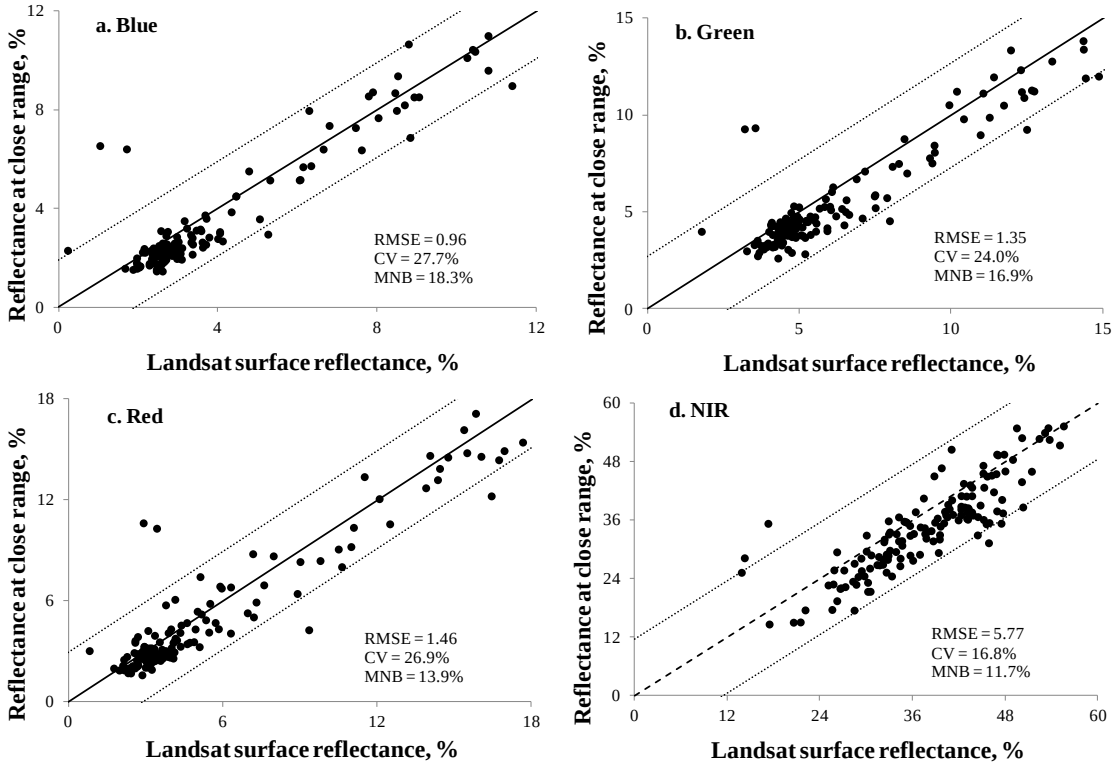

Figure 5.2 The relationships of the reflectance collected at close range, 6 m above the top of the canopy, versus Landsat-retrieved surface reflectance for Nebraska study sites from 2001 through 2008 in the Landsat (a) blue band, (b) green band, (c) red band and (d) NIR band. The solid line is the 1-by-1 line, and the dashed lines represent two standard errors of the relationships.

It is worth noting that in all spectral bands, MNB was positive indicating that close range measured reflectance was consistently lower than Landsat surface reflectance. One of the reasons for it is shadow effect that is significant when reflectance is measured at

close range. Many of 36 spectra measured in different locations in one site contain shadow component that is much more pronounced than in Landsat images. The higher Landsat surface reflectance is due to averaging reflectance values over 30 m pixels within a field, as well as strong effect of scattering by aerosol when signal travels from target to sensor.

5.2.3 Estimating total Chl content using Landsat data

To remotely estimate GPP in crops with satellite data, one needs to retrieve an accurate measure of Chl content. Many approaches for accurately estimating the total Chl content using satellite-retrieved VI have been proposed. MTCI has been specifically proposed for MERIS data to estimate total Chl content (Dash & Curran, 2004). The CI_{green}, derived from Hyperion and Landsat-TM images, was found to be closely related to maize Chl content with a R^2 above 0.86 (Wu et al., 2010a). The WDRVI, retrieved from the MODIS 250m product, appeared to be a good proxy of green LAI (Gitelson et al., 2007), which closely relates to total Chl content (Ciganda et al., 2008).

Fig. 5.3 showed that several Landsat-retrieved vegetation indices, based on five-year observations from 2001 through 2005 at three Nebraska sites, closely related to total Chl content in maize and soybean. NDVI and green NDVI were saturated for total Chl content above $1g/m^2$ in both maize and soybean. EVI2 and green WDRVI were more sensitive to moderate to high total Chl content, but still lost sensitivity dramatically for total Chl content above 2 g/m^2. SR was almost linearly related to total Chl content, but it was quite noisy. CI_{green}, which was sensitive to the whole range of total Chl content, was the most accurate for estimating total Chl content. These Landsat-retrieved indices can be used as a proxy of Chl content in the model Eq. 5.1 for GPP estimation.

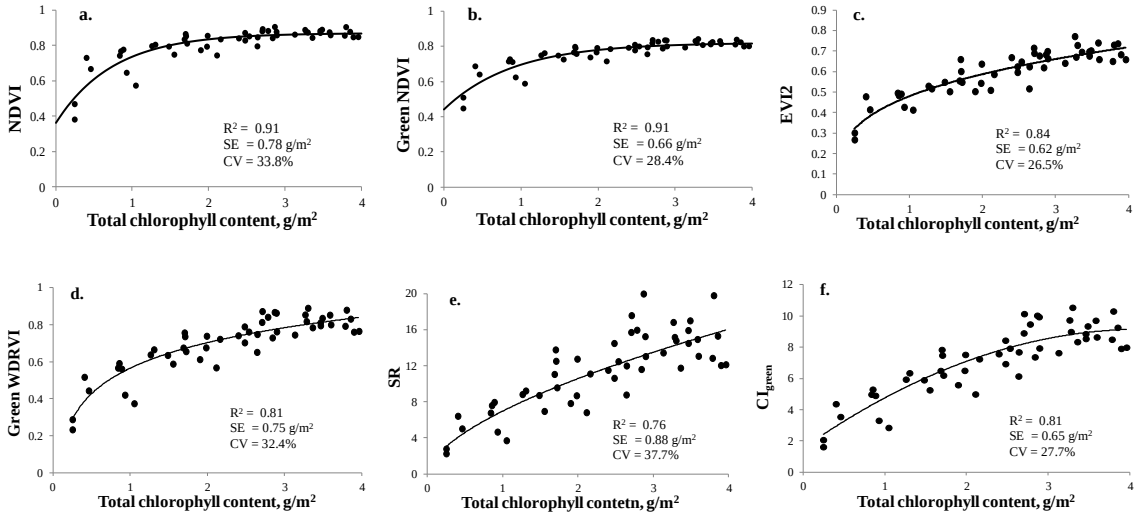

Figure 5.3a Relationship between Landsat-retrieved (a) NDVI, (b) Green NDVI, (c) EVI2, (d) Green WDRVI, (e) SR and (f) CI_{green} and total chlorophyll content in maize, based on 5-year observations during 2001 through 2005 in three Nebraska sites.

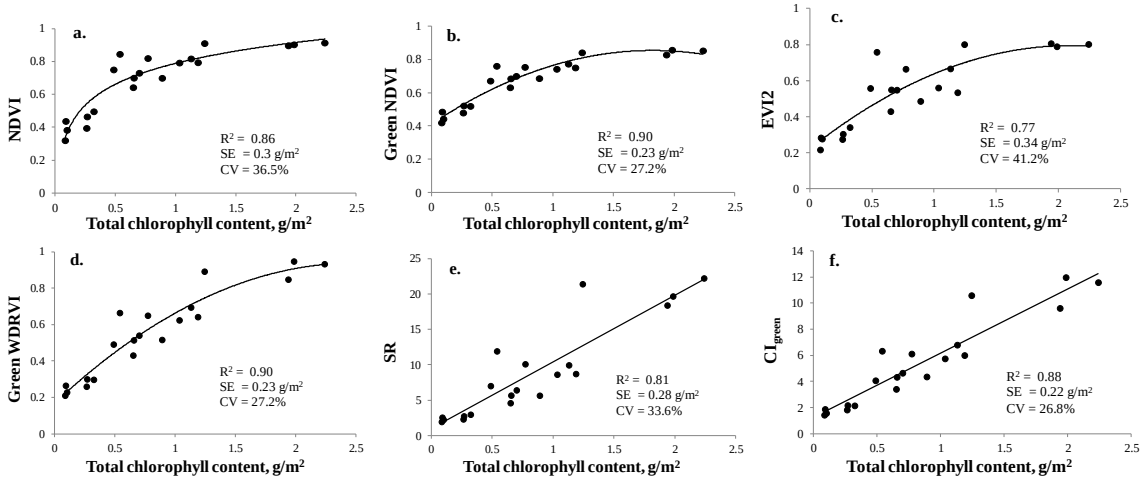

Figure 5.3b Relationship between Landsat-retrieved (a) NDVI, (b) Green NDVI, (c) EVI2, (d) Green WDRVI, (e) SR and (f) CI_{green} and total chlorophyll content in soybean, based on 5-year observations during 2001 through 2005 in three Nebraska sites.

5.2.4 GPP model with $PAR_{potential}$ vs. model with PAR_{in}

To assess the accuracy of the models that use PAR_{in} (Eq. 4.1) and $PAR_{potential}$ (Eq. 5.1), standard errors of GPP estimation by both models, SE{PAR_{in}} and SE{$PAR_{potential}$}, and their difference, ΔSE, were calculated as:

$$\Delta SE = (SE\{PAR_{in}\} - SE\{PAR_{potential}\})/SE\{PAR_{in}\} \times 100\%$$

The value of the difference is positive if the accuracy of the model Eq. 5.1 that uses $PAR_{potential}$ is higher than that of the model Eq. 4.1 that uses PAR_{in}, while the difference is negative if the accuracy of the model Eq. 5.1 is lower.

For all six VIs, retrieved from Landsat data for both maize and soybean, the accuracy of the model with $PAR_{potential}$ (Eq. 5.1) was consistently higher than that with PAR_{in} (Eq.4.1) -Fig. 5.4. The model with $PAR_{potential}$ was more accurate by at least 5% for SR to more than 20% for green NDVI Fig. 5.4.

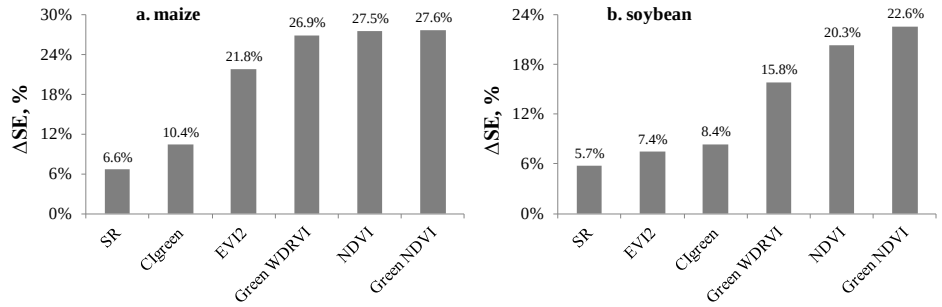

Figure5.4 Difference in standard errors of GPP estimation by two models: Eq. 4.1 that uses PAR_{in} and Eq 5.1 that used $PAR_{potential}$. $\Delta SE=(SE\{PAR_{in}\} - SE\{PAR_{potential}\}) / SE\{PAR_{in}\}\times 100\%$, where SE {$PAR_{in}$} is the standard error of the model Eq. 4.1 and SE {$PAR_{potential}$} is the standard error of the model Eq. 5.1. (a) ΔSE is for maize data and (b) ΔSE is for soybean data. The accuracy of the model Eq. 5.1 with $PAR_{potential}$ used was consistently higher than that of Eq. 4.1 with PAR_{in} used for all six VIs.

One possible reason for such accurate GPP estimation when using $PAR_{potential}$ instead of PAR_{in} is the well-documented (for maize) saturation of GPP vs. PAR_{in} relationship, indicating that a decrease in PAR_{in} may not correspond to a decrease in GPP (e.g., Ort, 2001; Suyker et al., 2005). Secondly, under water-limited conditions, photoprotection mechanisms were likely invoked to prevent damage to photosynthetic processes (e.g., Kasahara et al., 2002; Bjorkman and Powles, 1984). So with the same total Chl content, the small decrease of PAR_{in} (as on the Landsat acquisition dates) might not be accompanied with a GPP decrease in the same degree. In that case, multiplying by PAR_{in}, which fluctuated in accordance with small variations in daily weather conditions, may make the values of $VI \times PAR_{in}$ "noisier" than $VI \times PAR_{potential}$ for GPP estimation, as is illustrated in Fig. 5.5 for Green NDVI.

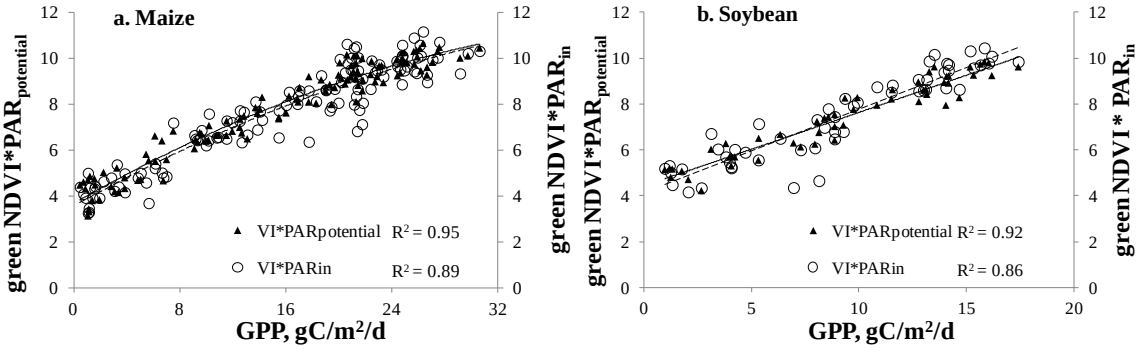

Figure 5.5 The relationships of green $NDVI \times PAR_{potential}$ ($MJ/m^2/d$) vs. GPP and green $NDVI \times PAR_{in}$ ($MJ/m^2/d$) vs. GPP for (a) maize and (b) soybean. In both maize and soybean, the values of $VI \times PAR_{potential}$ were more closely related to GPP than those of $VI \times PAR_{in}$. The solid line is the best fit function of the relationship green $NDVI \times PAR_{potential}$ vs. GPP, and the dash line is the best fit function of the relationship green $NDVI \times PAR_{in}$ vs. GPP.

5.2.5 Calibration of algorithms

Concurrent GPP and Landsat observations during 2001- 2008 over the three Nebraska sites represented a wide dynamic range of GPP variation (maize GPP ranging from 0 to 31 $gC/m^2/d$; soybean GPP ranging from 0 to 19 $gC/m^2/d$). The relationships VI × $PAR_{potential}$ vs. GPP were established for maize and soybean (Fig. 5.6). The relationship NDVI × $PAR_{potential}$ vs. GPP was nonlinear with slope decreasing as GPP increased (Fig. 5.6a). The NDVI was a good indicator of low-to-moderate GPP, but it was less accurate in detecting GPP when it exceeded 20 $gC/m^2/d$. At moderate-to-high vegetation densities, (1) red reflectance becomes almost invariant and, thus, not sensitive to change in Chl content, and (2) NIR reflectance is much higher than the red reflectance, which results in low sensitivity of NDVI to total Chl content above $1g/m^2$ (Gitelson 2004; Gitelson et al., 2005) as well as to green LAI above 2 m^2/m^2 (Vina et al., 2011). Since crop production closely relates to total Chl content and green LAI, NDVI lost its sensitivity to moderate-to-high GPP values. Note that the relationship NDVI×$PAR_{potential}$ vs. GPP for soybean was much closer to a linear relationship (Fig. 5.6b) due to a lower maximal Chl content and GPP values in soybean as compared to that for maize.

The relationship green NDVI×$PAR_{potential}$ vs. GPP was more linear than NDVI ×$PAR_{potential}$ vs. GPP, but still exhibited a decrease in sensitivity to maize GPP exceeding 23-25 $gC/m^2/d$. Green WDRVI×$PAR_{potential}$ and EVI2×$PAR_{potential}$ were linearly related to GPP, thus remained sensitive to the wide range of GPP variation. SR and CI_{green} were exponentially related to GPP with slopes increasing as GPP increases. These ratio indices were very sensitive to moderate-to-high GPP values, but much less sensitive to low GPP.

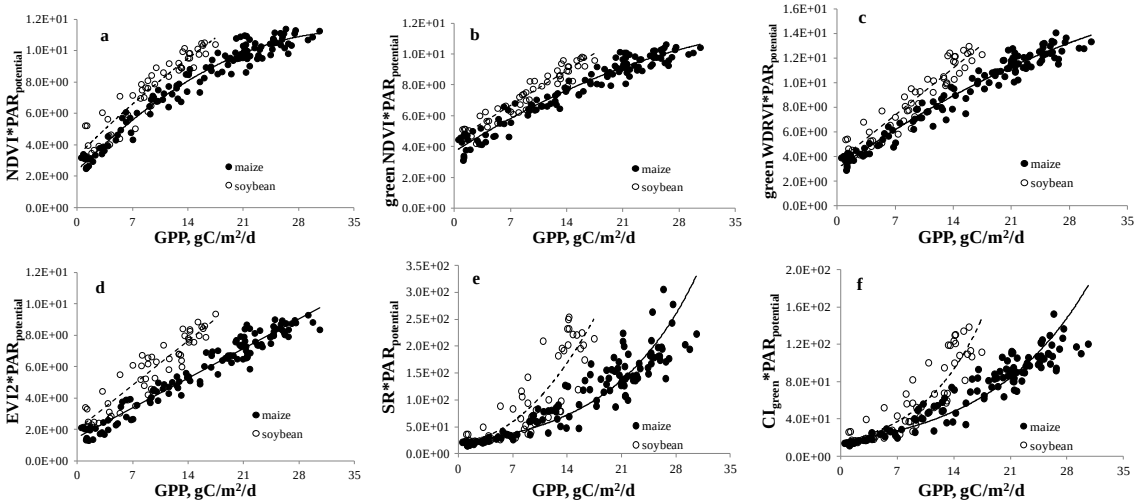

Figure 5.6 Relationship of GPP vs. (a) NDVI× $PAR_{potential}$, (b) green NDVI× $PAR_{potential}$, (c) green WDRVI × $PAR_{potential}$, (d) EVI2 × $PAR_{potential}$, (e) SR× $PAR_{potential}$, and (f) CI_{green}× $PAR_{potential}$ for maize and soybean established in Nebraska sites from 2001 through 2008.

While best-fit functions for VI×$PAR_{potential}$ vs. GPP were nonlinear for all VIs, except EVI2 and green WDRVI, they may be approximated quite accurately by linear functions. For example, the determination coefficient (R^2) of the nonlinear relationship for NDVI×$PAR_{potential}$ in maize was 0.964, while R^2 was 0.934 for the linear relationship. The R^2 was 0.916 for CI_{green}×$PAR_{potential}$ in maize with an exponential relationship and 0.905 if using a linear relationship.

To compare performances of VIs in estimating GPP, the linear relationships for all six VI×$PAR_{potential}$ were established. Table 5.1 presents the linear relationships GPP vs. VI × $PAR_{potential}$, as well as indicators of uncertainties associated with maize and soybean GPP estimation (R^2, SE and CV) in Nebraska sites from 2001 through 2008. Overall, all six VIs were quite accurate for GPP estimation with CVs below 23% in maize and below

30% in soybean. SR was less accurate than other indices for GPP estimation for both maize and soybean, since at moderate-to-high GPP the red reflectance as the denominator of SR is very low (below 3%) and noisy, thus resulting in a pronounced scattering of points away from its best-fit function.

Table 5.1a. The algorithms for daytime GPP using $VI \times PAR_{potential}$ estimating in irrigated and rainfed maize sites at Mead, Nebraska during 2001- 2008 (120 samples), with determination coefficients (R^2), standard errors (SE) and coefficients of variation (CV) presented. GPP ranged from 0 to 30 $gC/m^2/d$.

VI	GPP = ax +b ($x = VI*PAR_{potential}$)	R^2	SE, $gC/m^2/d$	CV, %
Green WDRVI	GPP = 2.63x – 8.59	0.95	1.90	12.1
EVI2	GPP = 3.54x – 4.62	0.95	1.92	12.3
Green NDVI	GPP = 4.00x – 15.4	0.94	2.20	14.0
NDVI	GPP = 3.11x – 9.22	0.93	2.22	14.2
CI_{green}	GPP = 3.57x + 9.29	0.91	2.67	17.0
SR	GPP = 0.114x + 3.02	0.84	3.49	22.2

Table 5.1b. The algorithms for daytime GPP using $VI \times PAR_{potential}$ estimating in irrigated and rainfed soybean sites at Mead, Nebraska in 2002, 2004, 2006 and 2008 (54 samples), with determination coefficients (R^2), standard errors (SE) and coefficients of variation (CV) presented. GPP ranged from 0 to 19 $gC/m^2/d$.

VI	GPP = ax +b ($x = VI*PAR_{potential}$)	R^2	SE, $gC/m^2/d$	CV, %
Green NDVI	GPP = 2.86x – 11.9	0.92	1.40	14.9
Green WDRVI	GPP = 1.66x – 4.98	0.90	1.54	16.3
NDVI	GPP = 2.07 x – 6.19	0.89	1.65	17.4
EVI2	GPP = 2.15x – 3.06	0.87	1.79	18.9
CI_{green}	GPP = 0.106x + 2.63	0.76	2.42	25.6
SR	GPP = 0.0515x + 3.91	0.67	2.79	29.5

The normalized difference VIs (NDVI, green NDVI and green WDRVI) performed better than ratio-based VIs (SR, and CI_{green}), especially for soybean data as noted in Table 5.1b (CV was above 25% for ratio indices while below 18% for normalized difference VIs). To find the reason for the discrepancy, the relationship between $GPP/PAR_{potential}$ and CI_{green} for soybean was analyzed. The relationship showed pronounced hysteresis (Fig. 5.7b): for the same CI_{green}, $GPP/PAR_{potential}$ in the green-up stage (DOY < 220) was much higher than in the late reproductive stage (DOY > 220).

a.

Sample #	A	B
Date	7/15/2008	9/17/2008
$fAPAR_{green}$	0.78	0.19
Green LAI, m^2/m^2	1.5	0.5
Total LAI, m^2/m^2	1.5	2.3
NIR, %	33	39

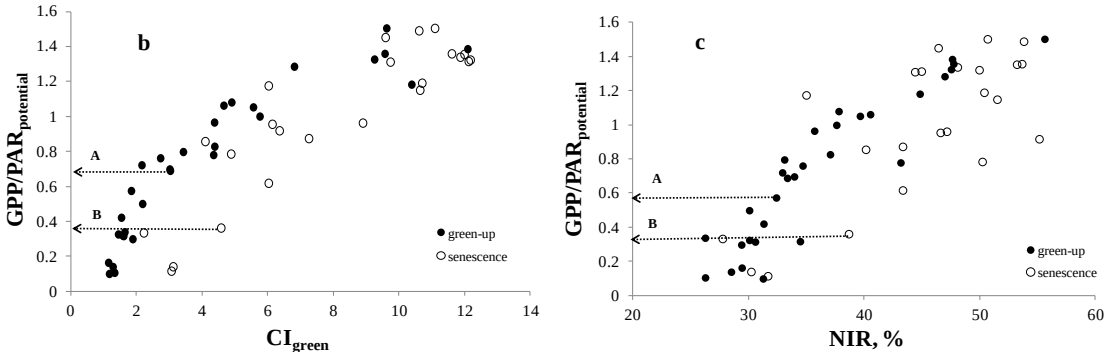

Figure 5.7 (a) Soybean biophysical characteristics for two cases: sample A at the green-up stage and sample B at the late reproductive stage. The relationship of $GPP/PAR_{potential}$ vs. (b) CI_{green} and (c) NIR reflectance.

We considered two cases taken during green up (sample A) and late reproductive (sample B) stages (Fig. 5.7a). Green LAI was 1.5 for sample A while 0.5 for sample B; fraction of absorbed radiation (i.e. $fAPAR_{green}$) in sample A was three times higher than in sample B. In contrast, the total LAI in the late reproductive stage (sample B) was higher than in sample A: 2.3 vs. 1.5 due to a higher total amount of both photosynthetic and non-photosynthetic leaves in sample B, which caused higher light scattering and higher ρ_{NIR} (Fig. 5.7c). Such hysteresis of ρ_{NIR} resulted in the hysteresis of ratio VIs for which NIR reflectance acted as a numerator (example for CI_{green} in Fig. 5.7b). For NDVI, green NDVI, and green WDRVI, the effect of NIR reflectance hysteresis was attenuated by normalization; thus they performed much better for soybean GPP estimation (CVs below 17.4%) than ratio VIs. This effect was less pronounced in maize due to a significant decrease in leaf inclination, and thus a decrease in NIR reflectance during late reproductive stage.

It is interesting to note that EVI2, which is also a normalized difference, performed very accurately in maize GPP estimation (CV = 12.3%), but less so for soybean (CV = 18.9%). In order to understand the reason for the discrepancy, the relationships EVI2 vs. ρ_{NIR} and EVI2 vs. (ρ_{NIR} - ρ_{red}) were studied (Fig. 5.8). EVI2 was closely related to the ρ_{NIR} retrieved from Landsat data as well as from radiometric data taken at close range for both maize and soybean in three irrigated and rainfed fields from 2001 through 2008 with R^2 above 0.908 (Fig. 4.8a). EVI2 was especially close to ρ_{NIR} for moderate to high vegetation density. For green LAI exceeding 2 m^2/m^2, the red reflectance is very low (below 3%) and almost invariant with respect to green LAI; thus EVI2 is solely related to NIR reflectance with R^2 exceeding 0.925. Thus, for green LAI exceeding 2, ρ_{NIR}

explained more than 92% of EVI2 variation and NIR reflectance was the main factor governing EVI2.

The relationship EVI2 vs. ρ_{NIR} - ρ_{red} was extremely close with an R^2 above 0.99 (Fig. 5.8b) in both soybean and maize. The same close relationships exist between EVI and ρ_{NIR} - ρ_{red} as well as EVI and ρ_{NIR} (not shown). These strong relationships EVI vs. ρ_{NIR} and EVI2 vs. ρ_{NIR} explain the decrease in accuracy using EVI2 for GPP estimation in soybean (Table 5.1b). In reality, EVI and EVI2 are not normalized differences, but they are essentially the difference between NIR and the red reflectance (Fig. 5.8b).

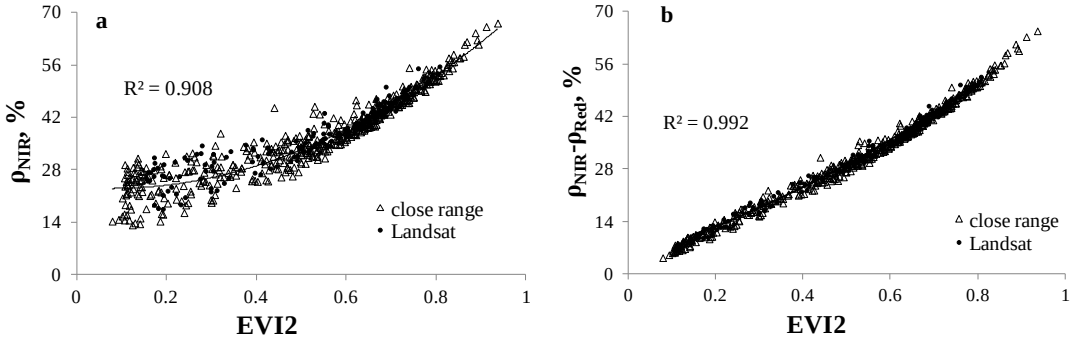

Figure 5.8 Relationship of EVI2 vs. (a) NIR reflectance, ρ_{NIR} and (b) difference between NIR and red reflectances, ρ_{NIR} - ρ_{red} in 24 irrigated and rainfed maize and soybean fields in Nebraska from 2001 through 2008 with data retrieved from Landsat data as well as radiometric data taken at close range.

This helps also to explain recent findings at three flux tower sites (Harvard Forest, Howland Forest and Morgan Monroe State Forest) that EVI was significantly affected by view angles (Sims et al., 2011). Those authors found a substantial variation in the view

angle sensitivity of EVI across seasons, and this variation was different for backscattering vs. forward scattering data.

All six VIs used in the current study were species specific for maize and soybean. For the same GPP, the value of VI× $PAR_{potential}$ in soybean was consistently higher than that in maize with VIs calculated from reflectance in NIR and either green or red bands. This result is due to contrasting leaf structures and canopy architectures of maize and soybean (Gitelson, 2011, Peng and Gitelson, 2011b). Thus, prior information about crop types is required when using Landsat data for GPP estimation. However, in the case of green NDVI, the relationships for maize and soybean were close, allowing accurate GPP estimation in both crops using the same algorithm with no re-parameterization (Fig. 5.9).

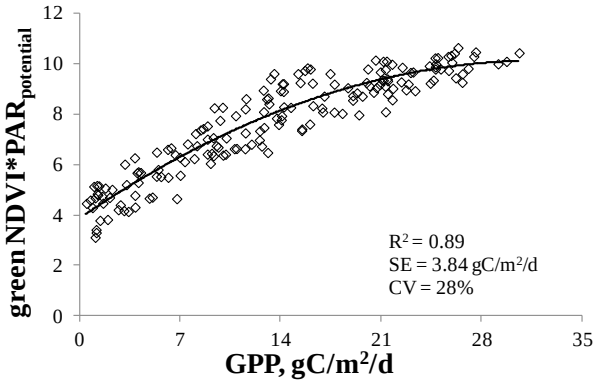

Figure 5.9 Relationship of green NDVI× $PAR_{potential}$ vs. GPP for maize and soybean data combined, established in Nebraska sites from 2001 through 2008.

5.2.6 Validation of algorithms in Minnesota, Iowa and Illinois AmeriFlux sites

The images and GPP values were obtained during an eight-year period over three irrigated and rainfed sites in Nebraska with different field histories, crop managements and weather conditions. However, the algorithms, established based on data from

different sites in different years of observations combined (16 site-years combined for maize and 8 site-years combined for soybean), were accurate in estimating GPP (Table 5.1, Figure 5.6). In order to explore the possibility of using a unified algorithm for GPP estimation, one needs to examine whether the algorithm, established in Nebraska, works for study sites located in different geographic regions with no re-parameterization of their coefficients, and assess the associated uncertainties of GPP estimation.

Fig. 5.10 presents the relationships between GPP measured in Minnesota, Iowa and Illinois sites and the product $VI \times PAR_{potential}$ for VIs that were found to be the best in Nebraska sites (Table 5.1, green WDRVI for maize, and green NDVI for soybean). These VIs were calculated using surface reflectance retrieved from Landsat images taken over MN, IA and IL sites. Best-fit linear functions, established in Nebraska sites (Table 5.1), with two standard errors of GPP estimation, are also included.

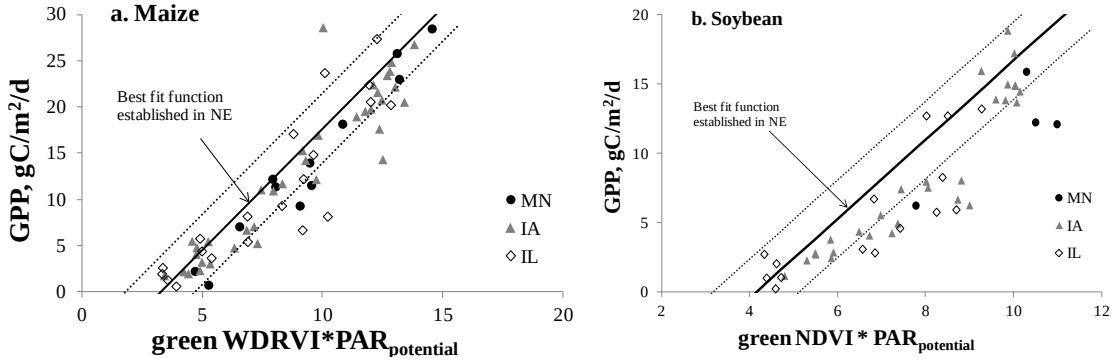

Figure 5.10 Relationships between GPP, measured in Minnesota, Iowa and Illinois sites, and the product $VI \times PAR_{potential}$ for VIs that were found to be the best in Nebraska sites for (a) maize and (b) soybean. The solid lines represent best-fit linear functions established in Nebraska sites (Table 5.1). The dotted lines represent two standard errors of the relationships.

Despite the differences in climatic conditions and geographic locations among study sites from four states, more than 84% of the maize samples and 62% of the soybean samples fell within the 95% confidential interval of the algorithms calibrated at Nebraska sites. This result shows potential for estimating GPP across the nation or even across the globe using satellite data and a unified algorithm based on the model Eq. 5.1.

However, there was consistent overestimation of GPP in MN, IA and IL when using the algorithm established in Nebraska (MNB was 30.1% for maize and 52.1% for soybean). One possible explanation for the error was the different planting density in MN, IL and IA sites: it was approximately 15% higher than in Nebraska sites (for maize: 86000 pl/ha in MN, IL and IA vs. 75000 pl/ha in Nebraska; for soybean: 340000 pl/ha in MN, IL and IA and around 300000 pl/ha in Nebraska). Plant density affects vertical light profile and, thus, the light climate inside the canopy, as well as $fAPAR_{green}$ values. For the same total Chl content and amount of incoming radiation, more light may be absorbed and used for photosynthesis by the sparsely distributed plants due to more open areas available and less shadows of nearby plants (Peng and Gitelson, 2011a). Thus, at the same value of $VI \times PAR_{potential}$, the site with lower planting density, as in Nebraska, produces more GPP than sites with higher planting densities, e.g., MN, IA and IL. In addition, the solar radiation availability for the growing season differed among sites in Nebraska, MN, IA and IL. For the same crop total Chl content in different geographic locations, $PAR_{potential}$ varies as site latitude changes; however, it is not clear how locational difference affects GPP and whether algorithms calibrated in one geographic region could be used for very different latitudes with no re-parameterization. Further

studies are required to identify sources of uncertainties when the unified algorithms are applied to different geographic locations and crop management systems.

The model Eq. 5.1, which relies on the product of crop total Chl and $PAR_{potential}$, can be accurately applied to estimate GPP in maize and soybean based entirely on Landsat data. However, the procedures of calibration and validation of the model are far from perfect and contain several uncertainties. One of them is due to the incongruity of time scales between Landsat observations and GPP data used in the model. The Landsat image was obtained around 10 am for each orbital passage, while GPP was calculated on a daylong basis. During a day, although crop Chl content remains the same, instantaneous GPP may change significantly due to changes in incoming radiation. Another uncertainty of the model Eq. 5.1 arises because of its failure to detect the variation in GPP related to short-term (minutes to hours) changes in controlling factors, such as high temperatures and/or a decrease in soil moisture, which do not immediately affect crop Chl content.

5.2.7 GPP estimation using raw Landsat data

Since Landsat data are now freely available, it is convenient to use Landsat at-sensor radiance data. However, atmospheric correction is required to convert Landsat at-sensor radiances to surface reflectance. The procedure of atmospheric correction is quite complicated and challenging, which may be impractical for users with little or no appropriate software experience. So, we decided to address the following question: how accurately does the model Eq.5.1 work for estimating crop GPP with Landsat top-of-atmosphere radiance retrieved from images without atmospheric correction?

Table 5.2 provides measures of accuracy for the model Eq.5.1, R^2, SE and CV, for GPP estimation using VIs retrieved from Landsat atmospherically corrected images, as

well as raw, uncorrected images for maize and soybean at the Nebraska sites from 2001 through 2008. All six indices, calculated using top of atmosphere, TOA, reflectance, were able to estimate GPP reasonably well, with CVs below 20% in maize and CVs below 30% in soybean. One reason for such an accurate GPP estimation using the Landsat TOA reflectance is that Landsat images, used in this study, were mostly taken on clear days, when reflectance was not strongly affected by atmospheric gases and aerosols. In addition, VI was calculated as mathematical combinations of reflectance ratios or as normalized differences to reduce the dependence on atmospheric effects. Further analyses are needed to confirm these findings.

Table 5.2a. Determination coefficients (R^2), Standard errors (SE) and coefficients of variation (CV) for relationships GPP vs. VI× $PAR_{potential}$ with VIs from Landsat atmospherically corrected and raw (uncorrected) images taken over maize sites in Nebraska from 2001 through 2008.

Vegetation index	Surface reflectance			TOA reflectance		
	R^2	SE, $gC/m^2/d$	CV, %	R^2	SE, $gC/m^2/d$	CV, %
Green WDRVI	0.95	1.90	12.1	0.93	2.23	14.2
EVI2	0.95	1.92	12.3	0.95	2.03	13.0
Green NDVI	0.94	2.20	14.0	0.93	2.36	15.0
NDVI	0.93	2.22	14.2	0.93	2.24	14.3
CI_{green}	0.91	2.67	17.0	0.81	2.62	16.7
SR	0.84	3.49	22.2	0.88	2.95	18.8

Table 5.2b. Determination coefficients (R^2), Standard errors (SE) and coefficients of variation (CV) for relationships GPP vs. VI× $PAR_{potential}$ from VIs with Landsat atmospherically corrected and raw(uncorrected) images taken over soybean sites in Nebraska in 2002, 2004, 2006 and 2008.

Vegetation index	Surface reflectance			TOA reflectance		
	R^2	SE, $gC/m^2/d$	CV, %	R^2	SE, $gC/m^2/d$	CV, %
Green NDVI	0.92	1.40	14.9	0.78	2.21	23.5
Green WDRVI	0.90	1.54	16.3	0.77	2.33	24.7
NDVI	0.89	1.65	17.4	0.84	1.96	20.7
EVI2	0.87	1.79	18.9	0.77	2.33	24.7
CI_{green}	0.76	2.42	25.6	0.70	2.69	28.5
SR	0.67	2.79	29.5	0.69	2.74	29.0

5.3. Conclusions

The model based on total crop Chl content and potential PAR was tested for estimating GPP in maize and soybean, crops with contrasting leaf structures and canopy architectures. Several vegetation indices were used as proxies of Chl content. The model was capable of estimating GPP using atmospherically corrected Landsat data with coefficients of variation below 23% for maize and below 30% for soybean. The indices using green and NIR Landsat bands were found to be the most accurate in GPP estimation. Our results showed that the model, which may be based solely on satellite data, is robust in estimating GPP and represents a significant improvement over MODIS GPP for croplands. The model was also capable of estimating GPP using raw imagery; i.e., top of atmosphere reflectance. The algorithms established in the Nebraska were validated for the maize and soybean in Minnesota, Iowa and Illinois. More than 84% of the maize samples and 62% of the soybean samples, collected in MN, IA and IL study

sites, falling within the 95% confidential interval of the algorithms calibrated at Nebraska sites.

Chapter 6: GPP estimation based on MODIS 250 m data

6.1 Introduction

The VI-$PAR_{potential}$-based model using a product of Chl-related vegetation index and $PAR_{potential}$ (incident PAR under a condition of minimal atmospheric aerosol loading) to estimate GPP in crops was proposed recently (Gitelson et al., 2012). This model may be based solely on remotely sensed data not requiring any ground-observed values, thus, it is easy to implement. It was successfully applied to Landsat data, and represents a significant improvement over GPP estimates based on MODIS 1 km products provided by NASA (Details in Chapter 5). But one drawback of Landsat data is its poor temporal resolution (one scene per 16 days), which may be an issue for real-time monitoring vegetation dynamics.

The MODIS product provides daily observations for the globe, and with its 250 m spatial resolution, it may be feasible to monitor vegetation dynamic changes for typical cropped fields in North America. With the free web-based access to MODIS data, the MODIS 250 m products, a combination of high temporal resolution and moderate spatial resolution, have been increasingly used for crop mapping and monitoring. Brown et al., (2007) employed MODIS 250 m vegetation index data to study processes of intensification of mechanized agriculture in an Amazonian soy-producing municipality. Wardlow and Egbert (2008) applied time-series of MODIS 250 m NDVI product for large-area-crop-related mapping over the U.S. Central Great Plains. Sakamoto et al., (2010b) used time-series of MODIS 250 m data to detect maize and soybean phenology.

Based on the VI-PAR_{in}-based model (details in Chapter 4), Sakamoto et al., (2011b) accurately estimated GPP in maize using a product of MODIS WDRVI data and shortwave radiation (SW) of NLDAS-2 reanalysis dataset, which is a substitute for $PAR_{in.}$ This technique allowed estimating daily GPP based only on remote sensing and reanalysis data. However, SW and PAR_{in} are not closely related and thus, there is a potential of significant uncertainties in GPP estimation. On the other hand, using a VI-PAR_{in}-based model may introduce noise to GPP estimation, as shown in results when using a product of Landsat-retrieved VI and PAR_{in} for estimating crop GPP (details in Chapter 5.2.4).

The objectives of Chapter 6 are with MODIS 250 m data: (1) to explore the uncertainties of a VI-PAR_{in}-based model Eq. 4.1 for GPP estimation; (2) to apply a VI-$PAR_{potential}$-based model Eq. 5.1 for estimating GPP in maize and soybean; (3) to compare the accuracy of GPP estimation models with $PAR_{potential}$, PAR_{in} and SW.

6.2. Background

6.2.1 $PAR_{potential}$ and PAR_{in} on daily basis

The ground-observed daily PAR_{in} values and the $PAR_{potential}$ profile created for Nebraska sites (details in Chapter 3.9) during the growing seasons 2001 through 2008 was shown in Fig. 6.1. Fig. 6.2a presented the histogram of the departure of PAR_{in} from $PAR_{potential}$, $(PAR_{potential}-PAR_{in})/PAR_{potential}$ *100%, for Mead, Nebraska during growing seasons 2001 through 2008. The eastern part of Nebraska (e.g. study sites in Mead) has a humid continental climate, with hot and sunny summers, which are the main growing seasons for maize and soybean. 1554 out of 2834 days during growing seasons 2001

through 2008 were under quite clear atmospheric conditions with ($PAR_{potential}$ − PAR_{in})/$PAR_{potential}$ smaller than 20%, as was the condition for most Landsat acquisition dates (details in Chapter 5.2.1). And 2235 out of 2834 days were in condition of ($PAR_{potential}$ – PAR_{in})/$PAR_{potential}$ smaller than 40%, as was the maximum difference between PAR_{in} and $PAR_{potential}$ that could occur for Landsat acquisition dates. But in collectedr Landsat dataset, only a few clear images were acquired during the growing season (around 6 – 10 images per growing season, less than 9% of the daily MODIS dataset). In contrast, as shown in Fig. 6.2b, for daily MODIS 250 m data, 55% of images were obtained when ($PAR_{potential}$ – PAR_{in})/$PAR_{potential}$ was below 20%, and 78% of images were obtained when ($PAR_{potential}$ – PAR_{in})/$PAR_{potential}$ was below 40%.

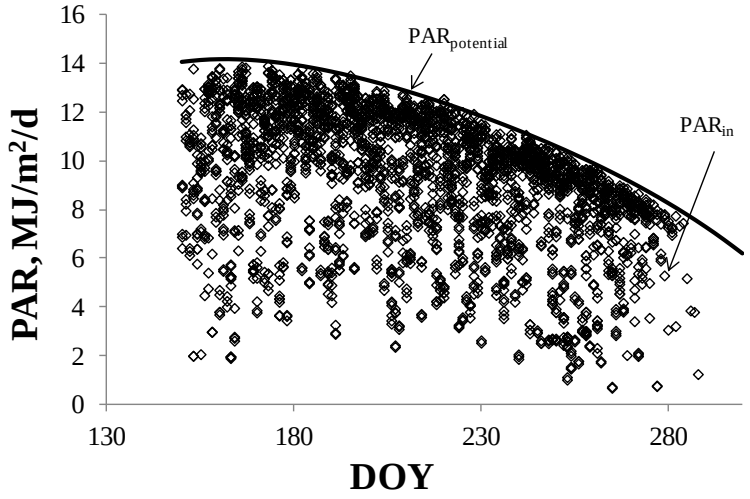

Figure 6.1 Temporal behavior of daily PAR_{in} during the growing seasons 2001 through 2008 and the $PAR_{potential}$ profile (solid line) created for Mead, NE.

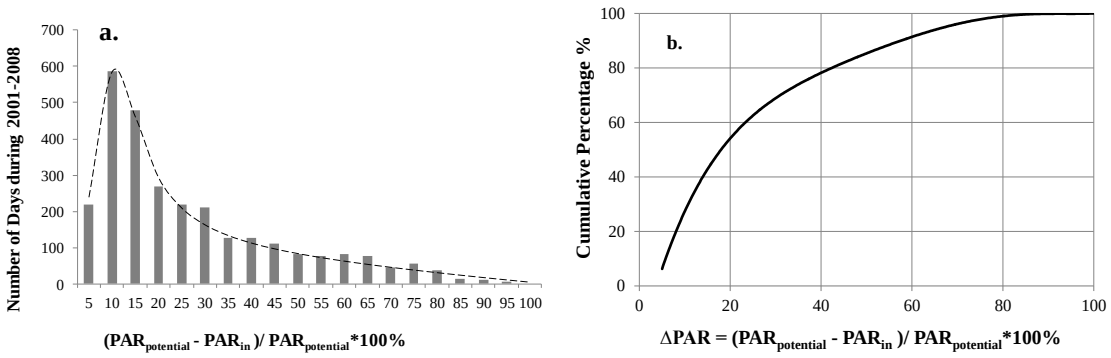

Figure 6.2 (a) Number of days and (b) cumulative percentage distribution plotted versus the departure of PAR_{in} from $PAR_{potential}$, $(PAR_{potential}-PAR_{in})/PAR_{potential}$ *100%, for Mead, Nebraska during growing seasons 2001 through 2008. For 55% of days, the difference between PAR_{in} and $PAR_{potential}$ was below 20%.

6.2.2 Limitation of VI-PAR_{in}-based model for GPP estimation

The VI-PAR_{in}-based model Eq. 4.1 is developed based on Monteith's model Eq. 2.2, which assumes that for the same fraction of absorbed photosynthetically active radiation, fAPAR, (1) GPP linearly relates to PAR_{in} and (2) light use efficiency (LUE) is constant for the same crop species. However, some studies have shown that these assumptions do not hold in many cases (e.g., Suyker et al., 2005).

To investigate how PAR_{in} affects GPP, daily available GPP and PAR_{in} data were used in conjunction with daily MODIS VI products. To analyze the response of GPP to variation of PAR_{in}, pairs of events when crop greenness / fAPAR remained almost the same were selected. It was done for an irrigated maize field (site 2, 2003) and for a rainfed maize field (site 3, 2003). The selection of each pair needs to meet the following conditions:

(1) Variation of crop Chl content has to be minimal;

(2) For each pair of events, the difference ($PAR_{potential} - PAR_{in}$)/$PAR_{potential}$ should be below 20%, thus under a cloud-free condition when clear satellite images can be obtained.

To meet the first requirement, pairs were selected with the difference of vegetation indices, which is a proxy of Chl content, below 1%. Usually, such events were collected at two close dates (time interval was less than 3 days), so the crop growing situations for both events were quite similar. Therefore, it was assumed that *for each pair, the variation of GPP was related only to variation of PAR_{in} and LUE*. In total, 35 pairs data from the irrigated field and 24 pairs data from the rainfed field were selected.

For each pair, the GPP variation (ΔGPP) and PAR_{in} variation (ΔPAR_{in}) in terms of a percentage were calculated and compared. Generally, there may be six cases for GPP response to PAR_{in} variation when crop Chl content did not change:

(a) GPP decreases / increases by the same proportion as PAR_{in} decrease / increase: $\Delta PAR_{in} \approx \Delta GPP$ (Fig. 6.3a). This is in accord with Monteith's model.

(b) PAR_{in} is almost invariable, while GPP varies: $\Delta PAR_{in} \approx 0$, $\Delta GPP \ncong 0$ (Fig. 6.3b). In this case, the variation of GPP is due to LUE variations. Even for the same crop species in very similar environment, LUE was not a constant as claimed by PEM models (details in Chapter 2.1).

(c) The GPP decrease / increase follows PAR_{in} decrease / increase, but not in the same proportion: $\Delta PAR_{in} \ncong \Delta GPP$ (Fig. 6.3c). This may be due to the well-documented saturation of GPP vs. PAR_{in} relationship (e.g., Suyker et al., 2005).

(d) As PAR_{in} decreases / increases, GPP almost remains the same: $\Delta PAR_{in} \ncong 0$, $\Delta GPP \approx 0$ (Fig. 6.3d). In this case, crop could adjust itself to variation of the

incoming radiation, thus not causing immediate changes of GPP. For example, photoprotection mechanisms were likely invoked to prevent excess light damage to photosynthetic processes (Kasahara et al., 2002; Bjorkman and Powles, 1984).

(e) As PAR_{in} increases, GPP decreases: $\Delta PAR_{in} > 0$, $\Delta GPP < 0$ (Fig. 6.3e). In this case, plant is possibly stressed (e.g., high temperature or low soil moisture) and incident light is excessive. It may result in decrease of LUE, thus reducing production.

(f) As PAR_{in} decreases, GPP increases: $\Delta PAR_{in} < 0$, $\Delta GPP > 0$ (Fig. 6.3f). With decreased PAR_{in} and possible change in composition of incident light (increase in the ratio of diffuse to direct radiation), more radiation available to be absorbed by the crop, which results in higher production.

Table 6.1 summarized the numbers of events for each case. As incoming radiation fluctuated with daily weather conditions, there are quite a lot of uncertainties in GPP variation, which may relate to many factors such as crop stress and light climate inside the canopy that affect LUE. Interestingly, proportional change of PAR_{in} and GPP ($\Delta PAR_{in} \approx \Delta GPP$), in accord with Monteith's model, rarely happened (it has small probability) in both irrigated and rainfed fields (9% in irrigated field, and 13% in rainfed field). Therefore, the use of PAR_{in} in VI-PAR-based model, may introduce noise and unpredictable uncertainties in GPP estimation model. Also worth to note that the increase of GPP as PAR_{in} decreases occurred more often in the rainfed field where crops were under water-limited conditions.

a. GPP decreases / increases by the same proportion as PAR_{in} decrease / increase:
$\Delta PAR_{in} \approx \Delta GPP$

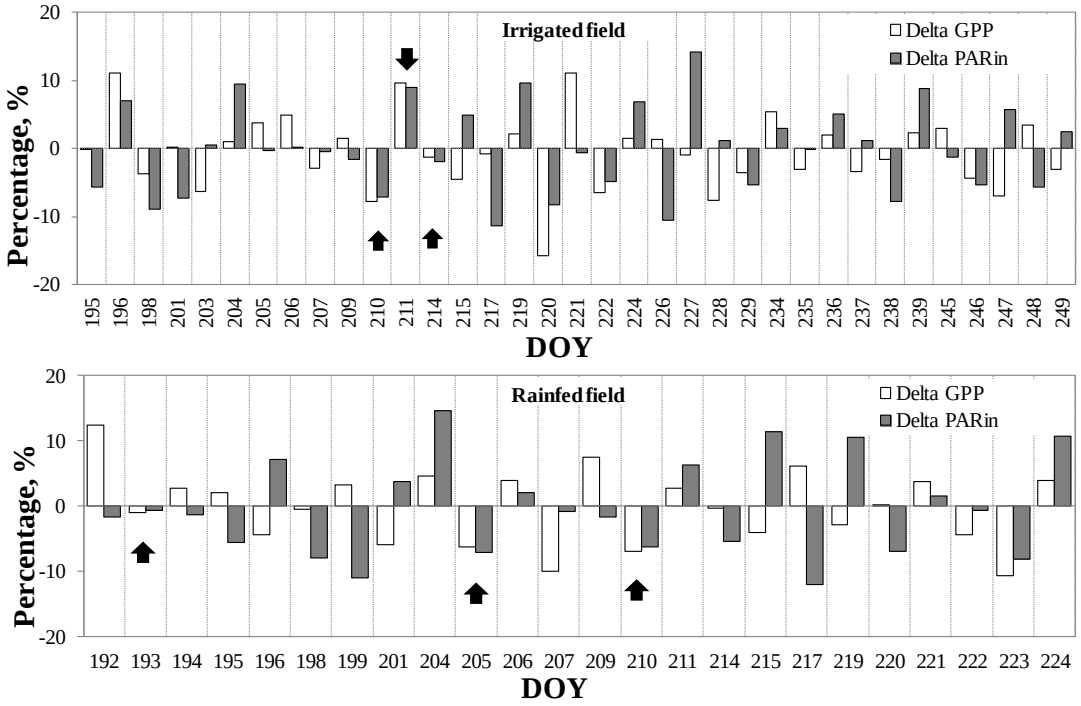

b. PAR_{in} is almost invariable, while GPP varies:
$\Delta PAR_{in} \approx 0, \Delta GPP \not\approx 0$

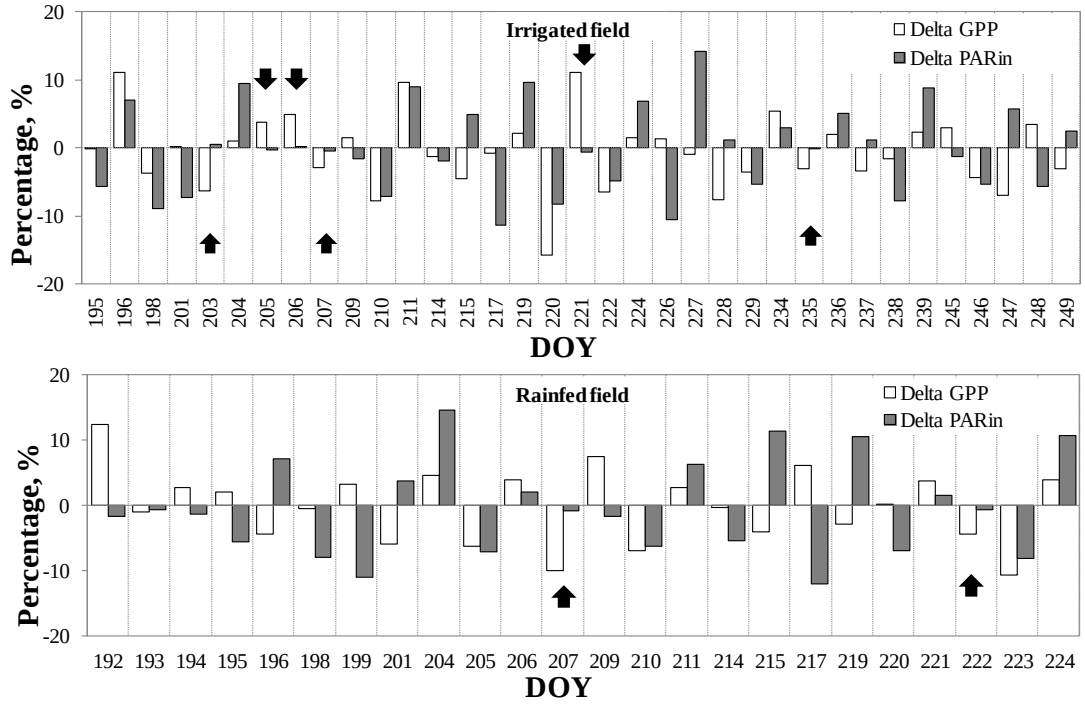

c. The GPP decrease / increase follows PAR_{in} decrease / increase, but not in the same proportion: $\Delta PAR_{in} \ncong \Delta GPP$

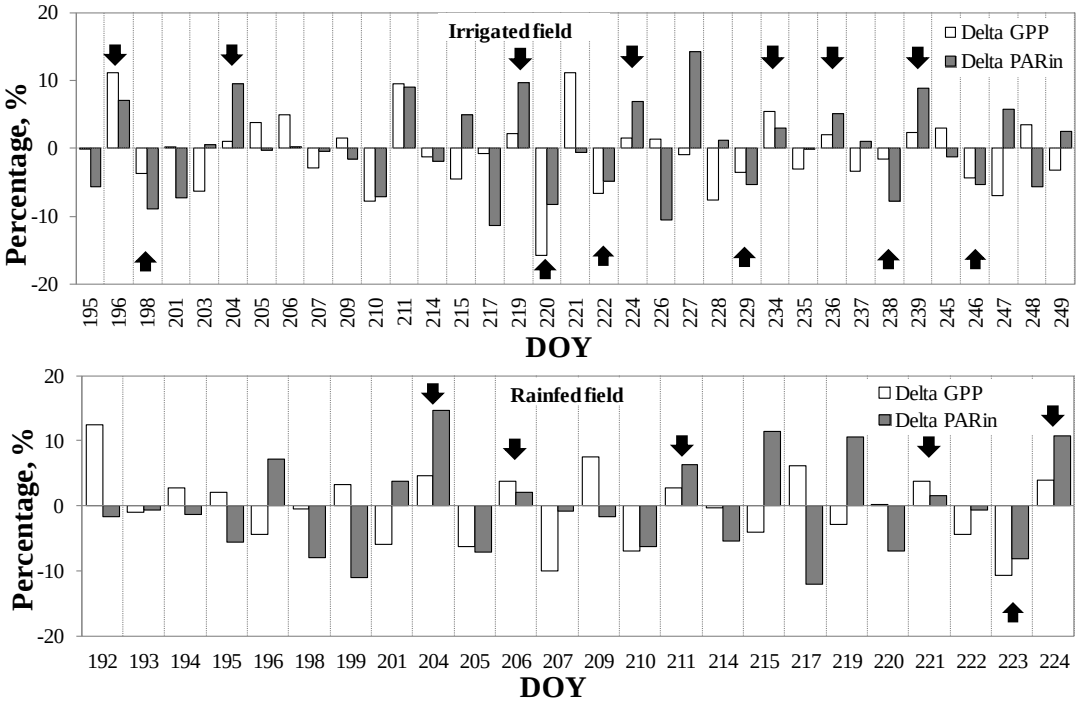

d. As PAR_{in} decreases / increases, GPP almost remains the same: $\Delta PAR_{in} \ncong 0$, $\Delta GPP \approx 0$

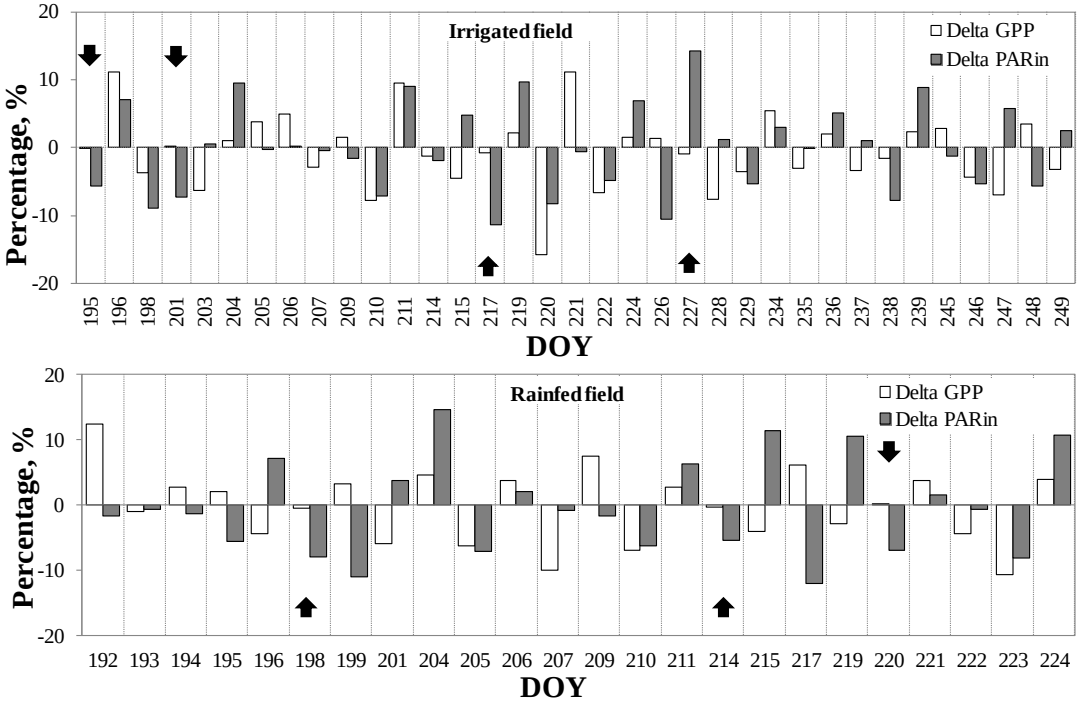

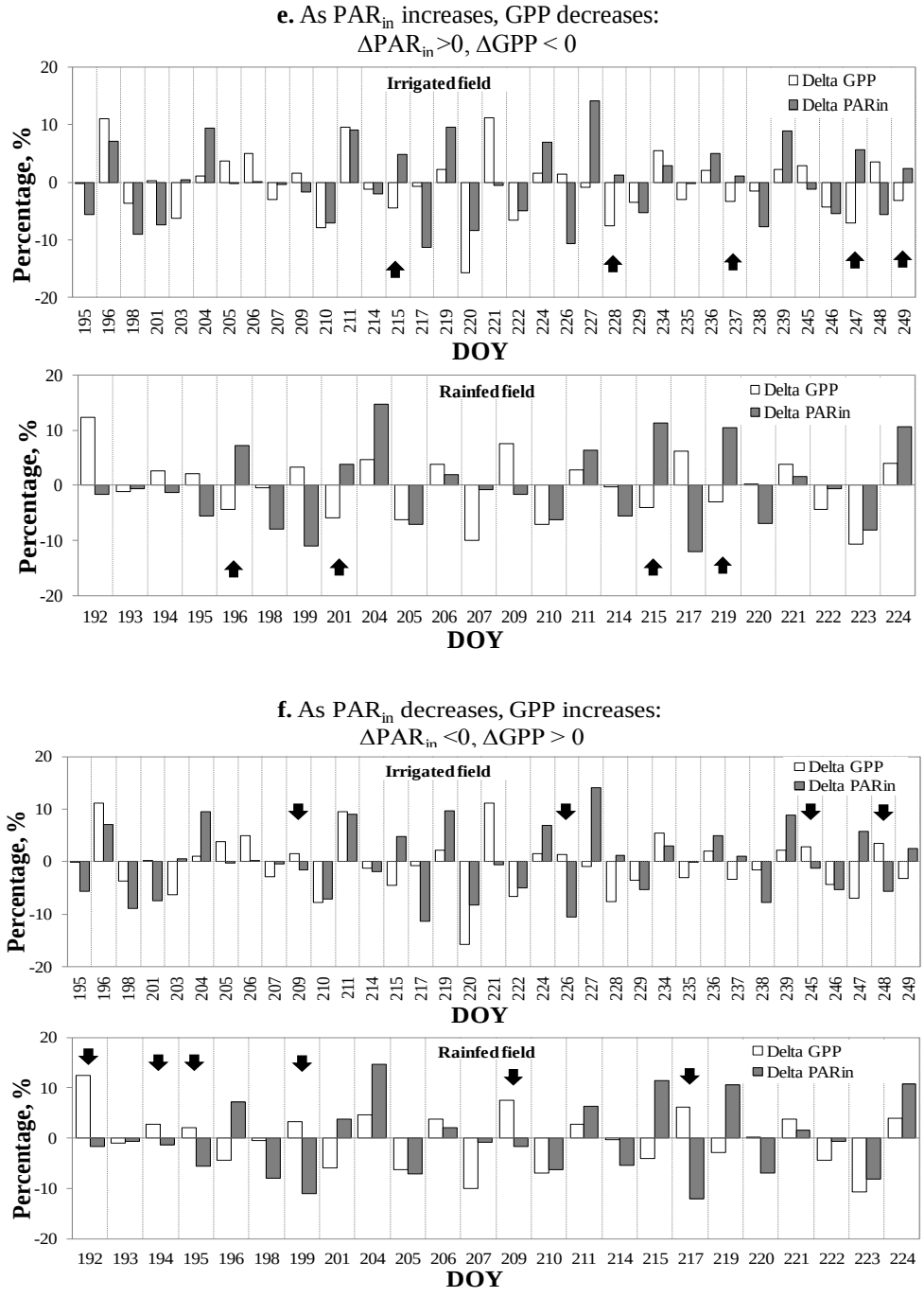

Figure 6.3 Six cases of GPP response to PAR_{in} variations, each for two events in maize with the same chlorophyll content in an irrigated field (site 2, 2003) and a rainfed field (site 3, 2003). The black arrows indicate the pairs when certain case occurred.

Table 6.1 Summary of six cases for GPP response to PAR_{in} variation.

GPP response to PAR_{in} variation	Irrigated field (35 pairs in total)		Rainfed field (24 pairs in total)	
	Number	Percentage	Number	Percentage
a. $\Delta PAR_{in} \approx \Delta GPP$	3	9%	3	13%
b. $\Delta PAR_{in} \approx 0$, $\Delta GPP \not\approx 0$	6	17%	2	8%
c. $\Delta PAR_{in} \not\approx \Delta GPP$	13	37%	6	25%
d. $\Delta PAR_{in} \not\approx 0$, $\Delta GPP \approx 0$	4	11%	3	13%
e. $\Delta PAR_{in} > 0$, $\Delta GPP < 0$	5	14%	4	17%
f. $\Delta PAR_{in} < 0$, $\Delta GPP > 0$	4	11%	6	25%

6.3. Results and discussion

In Chapter 5, $PAR_{potential}$ was introduced in the GPP estimation model Eq. 5.1 as a better representative of incident radiation affecting photosynthesis than PAR_{in}. It is shown that the model Eq. 5.1 using a product of VI and $PAR_{potential}$ was robust in estimating GPP in maize and soybean with Landsat data (Fig. 5.6, Table 5.1), and yielded higher accuracy than the model Eq. 4.1 using a product of VI and PAR_{in} (Fig. 5.4). In this chapter, we examined whether this model Eq. 5.1 can be applied to MODIS 250 m data. We had much more MODIS images on the days when $(PAR_{potential} - PAR_{in})/PAR_{potential}$ was below 20% than Landsat images (1553 MODIS 250 m images vs. 175 Landsat images for the three Nebraska study sites during 2001 through 2008).

6.3.1. GPP estimation with MODIS-retrieved VI

Based on the observations in Nebraska sites on the days when $(PAR_{potential} - PAR_{in})/PAR_{potential}$ was below 20% during growing seasons 2001 through 2008, we established the relationships $VI \times PAR_{potential}$ vs. GPP for both maize (1059 samples) and soybean (494 samples) with MODIS-retrieved vegetation indices. Due to limited spectral resolution (only red and NIR bands are presented in 250 m MODIS data), three indices were examined: NDVI, EVI and WDRVI.

Firstly, we assessed uncertainties of GPP estimation by MODIS-retrieved WDRVI, optimizing α value (Fig. 6.4). The weight coefficient α ($0 < \alpha < 1$) is used in WDRVI to attenuate the contribution of NIR reflectance at moderate-to-high vegetation density, and to make it comparable to red reflectance.

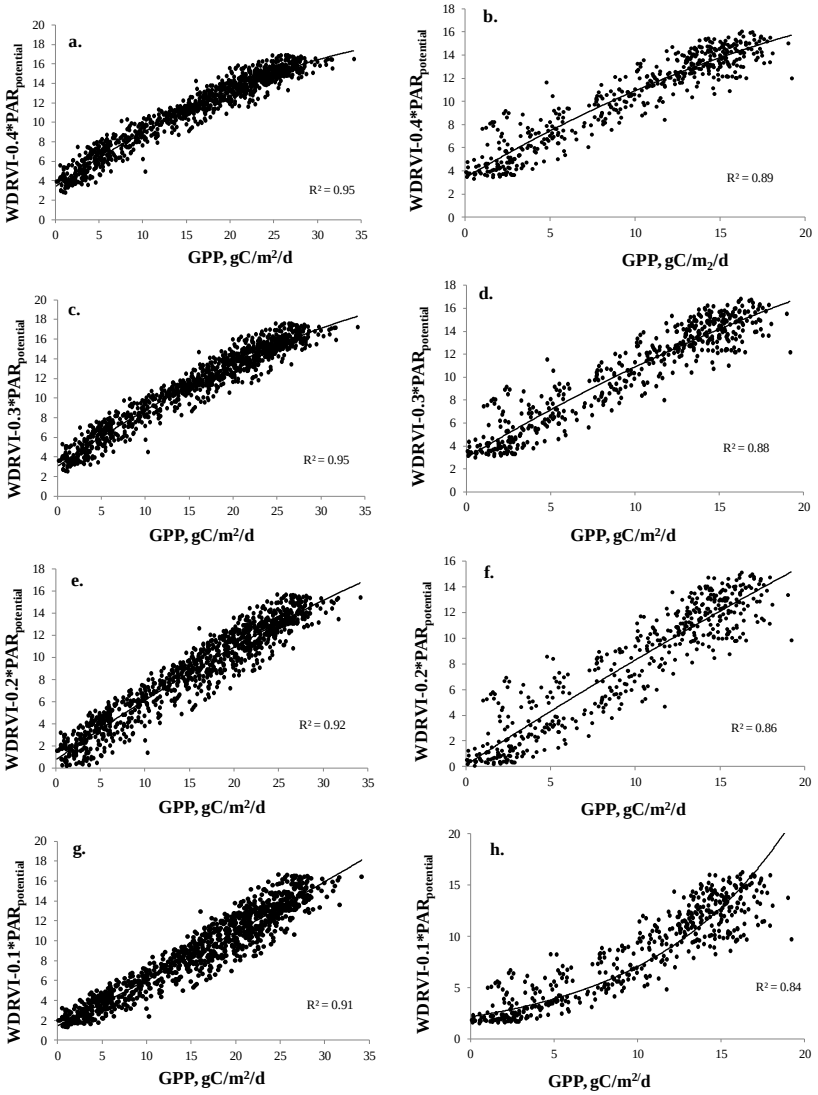

Figure 6.4 The relationship WDRVI*$PAR_{potential}$ vs. GPP for (a) α=0.4 in maize, (b) α=0.4 in soybean, (c) α=0.3 in maize, (d) α=0.3 in soybean, (e) α=0.2 in maize, (f) α=0.2 in soybean, (g) α=0.1 in maize, (h) α=0.1 in soybean.

As α value decreases, WDRVI showed increasing sensitivity to moderate to high GPP while decreasing sensitivity to low GPP. Therefore, with decrease of α, NEΔGPP of WDRVI decreased for moderate to high GPP, but NEΔGPP increased for low GPP (Fig. 6.5). Note that for the small values of α, such as 0.1 and 0.2, the small sensitivity of WDRVI to low GPP resulted in more scattering of the relationship (Fig. 6.4e, Fig. 6.4f, Fig. 6.4g and Fig. 6.4h). Among the tested α values, α=0.3 was selected: WDRVI with α=0.3 very closely related to GPP (R^2 = 0.95 for maize, and 0.88 for soybean) and remained sensitive to the wide range of GPP variation.

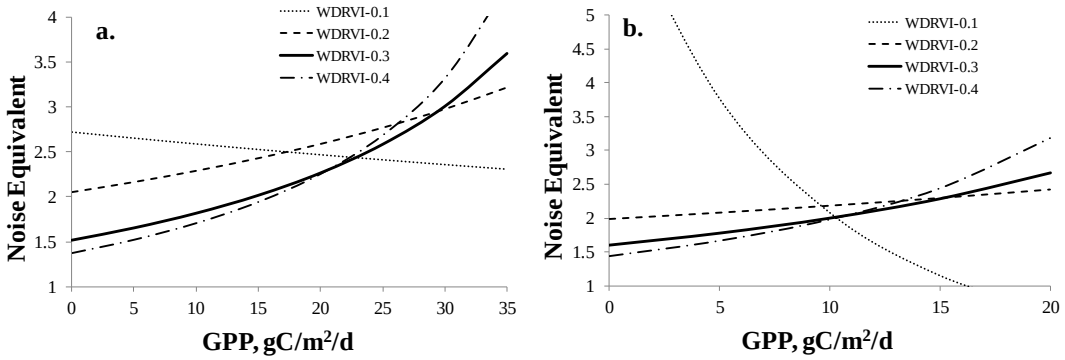

Figure 6.5 The Noise Equivalent (NEΔGPP) for relationships WDRVI×$PAR_{potential}$ (α =0.1, 0.2, 0.3 and 0.4) vs. GPP for (a) maize and (b) soybean.

Overall, the products of the MODIS-retrieved indices (NDVI, WDRVI and EVI) and $PAR_{potential}$ were all closely related to GPP (Fig. 6.6). Fig. 6.7 showed accuracy of GPP estimation in terms of noise equivalent. NDVI was most accurate estimating low GPP, but exhibited decreased accuracy at moderate to high GPP values: sharp increase of NEΔGPP values when GPP exceeding 20 gC/m^2/d for maize and 10 gC/m^2/d for soybean.

EVI was closely and linearly related to GPP. However, there were more outliers for EVI than for other indices (Fig. 6.6e and Fig. 6.6f), because NIR reflectance plays the main role in EVI formulation (Chapter 5.2.5, Fig. 5.8) and NIR reflectance may be affected by many factors (e.g., view angle, leaf orientations, canopy architecture). Aslo worth to note that points of the relationship for soybean were more scattered from best fit function than in maize, which was consistent with our observation with Landsat data. This may be explained by above mentioned (Chapter 5.2.5, Fig. 5.7) hysteresis of $GPP/PAR_{potential}$ vs. NIR reflectance relationship.

Among the indices tested, MODIS-retrieved EVI and WDRVI remained sensitive to the whole range of GPP variation (Fig. 6.7), and they appeared to be the best indices for estimating GPP in both maize and soybean.

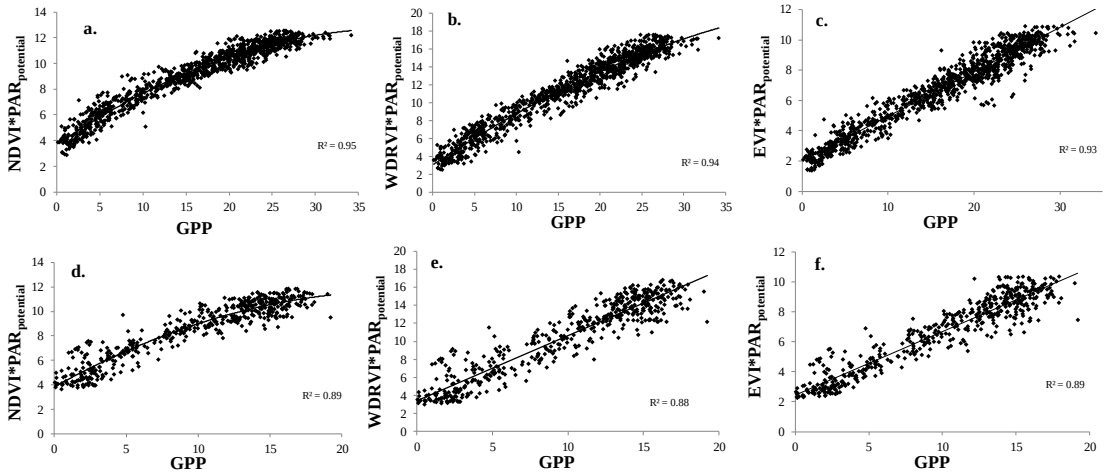

Figure 6.6 The relationship $VI \times PAR_{potential}$ vs. GPP for (a) NDVI in maize, (b) WDRVI in maize, (c) EVI in maize, (d) NDVI in soybean, (e) WDRVI in soybean, and (f) EVI in soybean.

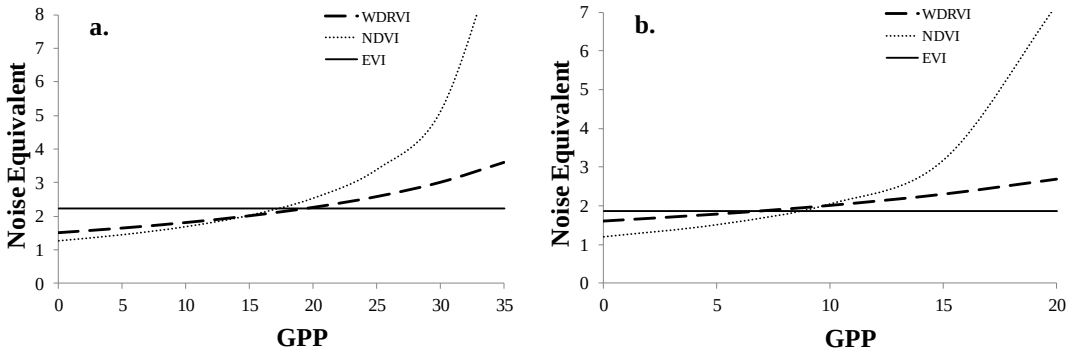

Figure 6.7 The Noise Equivalent (NEΔGPP) for relationships VI×$PAR_{potential}$ vs. GPP for NDVI, WDRVI and EVI in (a) maize and (b) soybean.

6.3.2 GPP estimation with $PAR_{potential}$, PAR_{in} and SW

Fig. 6.8 presents the relationships between GPP and the product of (1) VI×$PAR_{potential}$, (2) VI×PAR_{in} and (3) VI×SW established for Nebraska sites on days when ($PAR_{potential}$ – PAR_{in})/$PAR_{potential}$ was below 20%, using EVI and WDRVI. These indices appeared to be the best among the tested MODIS-retrieved indices for GPP estimation.

In both maize and soybean, the R^2 was much lower when using VI×SW for GPP estimation than that when using VI×PAR_{in} or VI×$PAR_{potential}$ (R^2 was 0.89 vs. 0.92 for maize, and 0.83 vs. 0.87 for soybean). The products VI×$PAR_{potential}$ and VI×PAR_{in} were both related to GPP very closely with a little higher R^2 for relationship with $PAR_{potential}$, and points appeared to be more scattered from the best fit function for VI×PAR_{in} than for VI×$PAR_{potential}$.

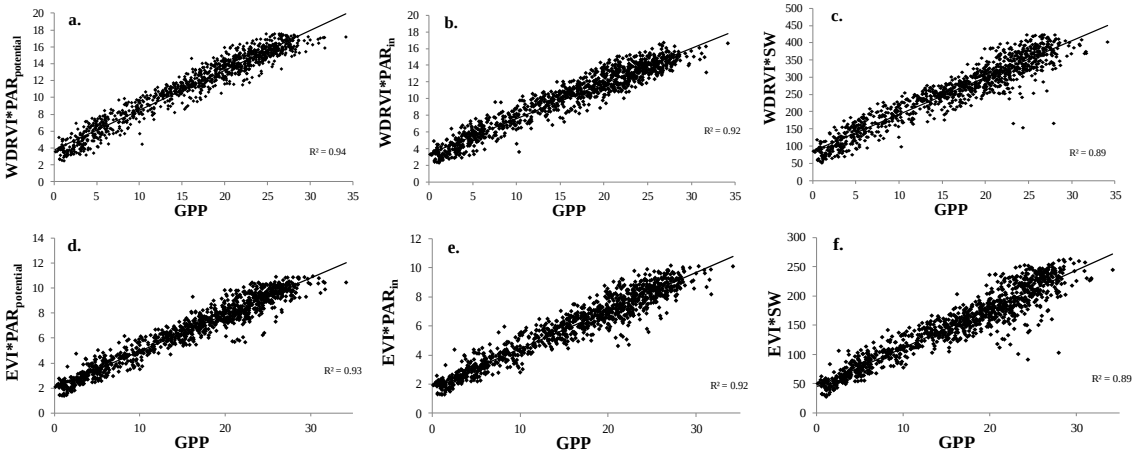

Figure 6.8a Relationships between GPP and the product of (a) WDRVI×$PAR_{potential}$, (b) WDRVI×PAR_{in} , (c) WDRVI×SW, (d) EVI×$PAR_{potential}$, (e) EVI×PAR_{in} and (f) EVI×SW established from the observations in Nebraska maize sites when ($PAR_{potential}$ − PAR_{in})/$PAR_{potential}$ below 20%.

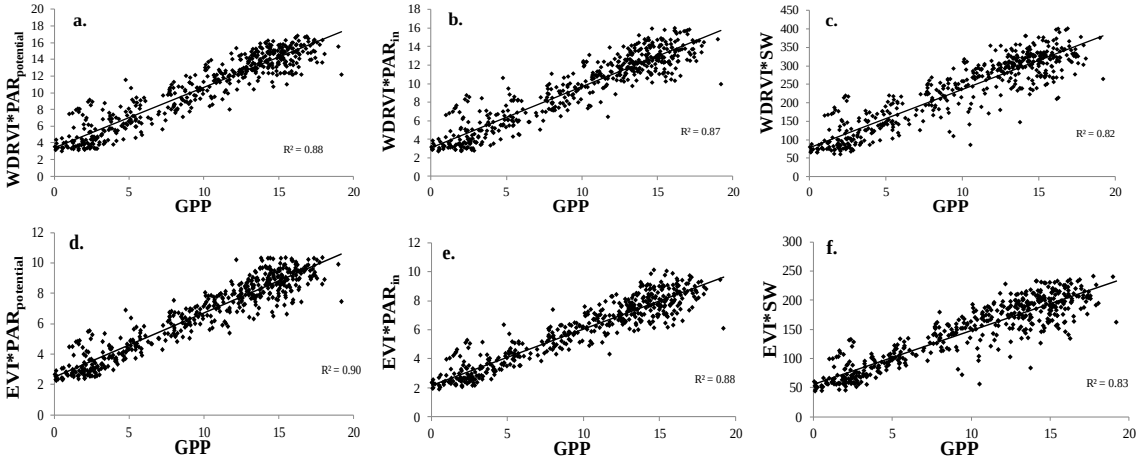

Figure 6.8b Relationships between GPP and the product of (a) WDRVI×$PAR_{potential}$, (b) WDRVI×PAR_{in} , (c) WDRVI×SW, (d) EVI×$PAR_{potential}$, (e) EVI×PAR_{in} and (f) EVI×SW established from the observations in Nebraska soybean sites when ($PAR_{potential}$ − PAR_{in})/$PAR_{potential}$ below 20%.

The accuracy of three models for GPP estimation: GPP = VI×$PAR_{potential}$ (Eq. 5.1), GPP = VI×PAR_{in} (Eq. 4.1) and GPP = VI×SW (Sakamoto et al., 2011b) were compared (Table 6.2). The model that used SW (Sakamoto et al., 2011b) was substantially less accurate for GPP estimation than the model that used $PAR_{potential}$ or PAR_{in}. This is due to the uncertainties of using SW as a proxy of PAR_{in} in the model, which would cause many outliers thus much higher SE. For both indices (EVI and WDRVI) tested for maize and soybean data, the model with $PAR_{potential}$ (Eq. 5.1) was consistently more accurate than the model with PAR_{in} (Eq. 4.1). As shown in Table 6.2, the model using $PAR_{potential}$ has lower SE value by at least 6% for EVI in soybean data (1.86 vs. 1.75 $gC/m^2/d$) to more than 15% for WDRVI in maize data (2.31 vs. 2.04 $gC/m^2/d$). This coincides with results obtained from Landsat data (Fig. 5.4).

Table 6.2a Established relationships GPP = VI×PAR_{in}, GPP = VI×SW and GPP = VI×$PAR_{potential}$ for maize data in Mead, Nebraska during 2001 through 2008 on days when ($PAR_{potential}$ – PAR_{in})/$PAR_{potential}$ below 20%. Best fit functions, determination coefficients (R^2), standard errors (SE) were given. GPP ranged from 0 to 30 $gC/m^2/d$.

Model	GPP ∝ VI × SW	GPP ∝ VI × PAR_{in}	GPP ∝ VI × $PAR_{potential}$
WDRVI			
Best fit function	GPP = 0.0838x -5.3954	GPP = 0.4217x + 3.39	GPP = 0.4722x + 3.78
R^2	0.89	0.92	0.94
SE, $gC/m^2/d$	**2.70**	**2.31**	**2.04**
EVI			
Best fit function	GPP = 0.1336x – 4.1739	GPP = 3.4897x - 4.9201	GPP = 3.1776x – 5.2892
R^2	0.89	0.92	0.93
SE, gC/m2/d	**2.77**	**2.40**	**2.15**

Table 6.2b Established relationships GPP = VI×PAR_{in}, GPP = VI×SW and GPP = VI×$PAR_{potential}$ for soybean data in Mead, NE during 2001 through 2008 on days when ($PAR_{potential}$ – PAR_{in})/$PAR_{potential}$ below 20%. Best fit functions, determination coefficients (R^2), standard errors (SE) were given. GPP ranged from 0 to 19 $gC/m^2/d$.

Model	GPP ∝ VI × SW	GPP ∝ VI × PAR_{in}	GPP ∝ VI × $PAR_{potential}$
WDRVI			
Best fit function	GPP = 0.0523x-2.351	GPP = 1.3117x – 2.6942	GPP = 1.2223x – 3.0386
R^2	0.82	0.87	0.88
SE, $gC/m^2/d$	**2.24**	**1.97**	**1.84**
EVI			
Best fit function	GPP = 0.0891x-3.2226	GPP = 2.2624x – 3.7331	GPP = 2.1099x – 4.1225
R^2	0.83	0.88	0.90
SE, gC/m2/d	**2.23**	**1.86**	**1.75**

The model using $PAR_{potential}$ appeared to be the most accurate for GPP estimation in both maize and soybean under conditions when the difference between PAR_{in} from $PAR_{potential}$ was below 20%. The same pattern can be seen when the difference between PAR_{in} from $PAR_{potential}$ was below 50% (Fig. 6.9). The product of VI×$PAR_{potential}$ was an accurate proxy of crop GPP when the concentrations of atmospheric gases and aerosols were low-to-moderate. As the difference between $PAR_{potential}$ and PAR_{in} exceeded 50% (cloudy or hazy weather conditions), the discrepancy between GPP estimates by a product of VI×$PAR_{potential}$ and measured GPP became significant (red points in Fig. 6.9). Fig. 6.10 showed that the model for GPP estimation that used $PAR_{potential}$ consistently outperformed the model that used PAR_{in} or SW when ($PAR_{potential}$ – PAR_{in})/$PAR_{potential}$ was below 60%. Future work needs to be done to study how this VI-$PAR_{potential}$-based model works for all weather conditions.

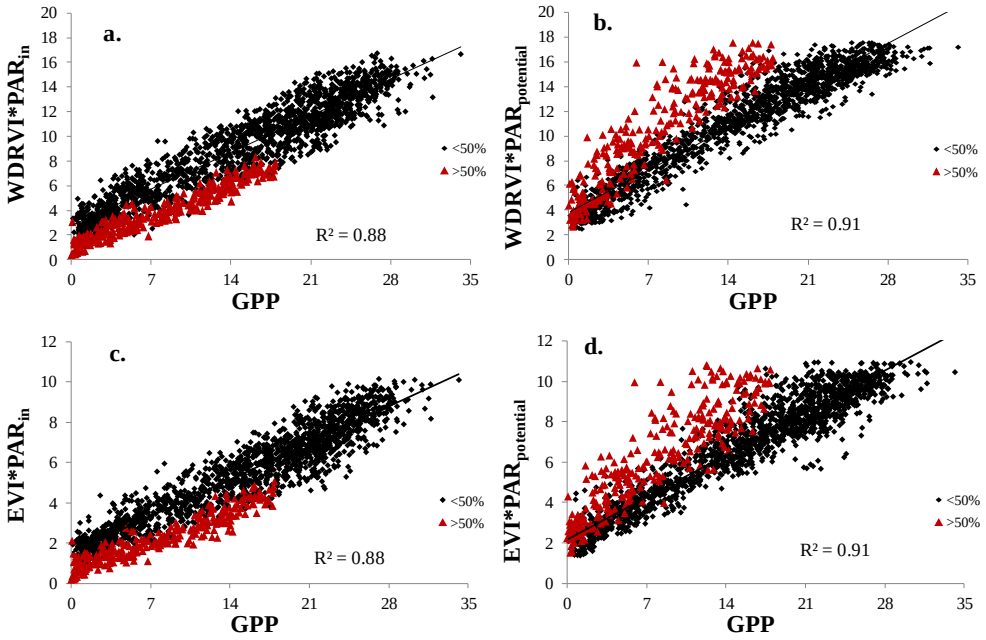

Figure 6.9 Relationships between GPP and the product of (a) WDRVI×PAR_{in}, (b) WDRVI×$PAR_{potential}$, (c) EVI×PAR_{in}, and (d) EVI×$PAR_{potential}$ established from the daily observations in Nebraska maize sites. The black points represented the observations when ($PAR_{potential}$ – PAR_{in})/$PAR_{potential}$ was below 50%. The solid lines are best-fit-functions established for relationships as ($PAR_{potential}$ – PAR_{in})/$PAR_{potential}$ was below 50%. The model using $PAR_{potential}$ appeared to be more accurate for GPP estimation in maize under a condition when concentrations of atmospheric gases and aerosols were low-to-moderate. The red points represented the observations on days when ($PAR_{potential}$ – PAR_{in})/$PAR_{potential}$ was more than 50%. On cloudy or hazy weather conditions associated with low value of PAR_{in}, the discrepancy between GPP estimates by a product of VI×$PAR_{potential}$ and measured GPP became significant.

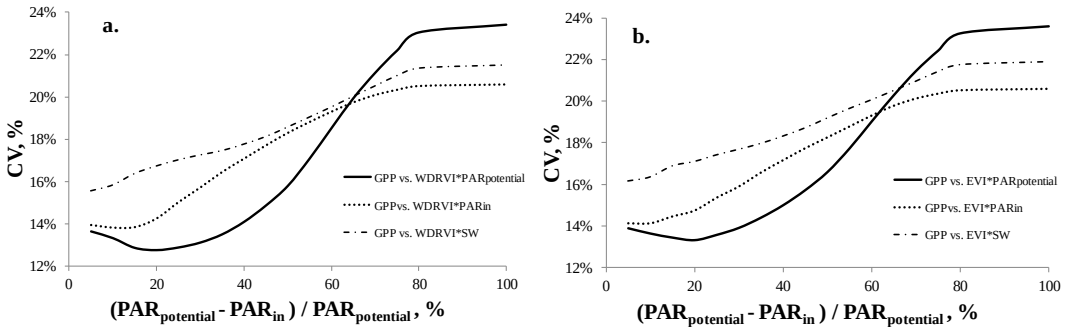

Figure 6.10 Coefficients of variation of relationships of GPP vs. VI×PAR_{in}, GPP vs. VI×SW and GPP vs. VI×$PAR_{potential}$, plotted with ($PAR_{potential}$ – PAR_{in})/$PAR_{potential}$ for (a) maize and (b) soybean.

6.4. Conclusions

The model using the product of MODIS-retrieved vegetation indices and potential PAR is able to estimate GPP very accurately on days when the decrease in PAR from potential PAR was less than 20%. Among the MODIS-250 m retrieved indices tested, EVI and WDRVI were the most accurate for GPP estimation with SE below 2.15 $gC/m^2/d$ and CV less than 15.2% for maize, and SE below 1.75 $gC/m^2/d$ and CV less than 20.1% for soybean. The GPP estimation model with $PAR_{potential}$ was more accurate than the model with PAR_{in} or SW under a condition when concentrations of atmospheric gases and aerosols were low-to-moderate. This approach allows monitoring crop GPP accurately using solely MODIS 250 m data with high temporal resolution.

Chapter 7: Summary and recommendations for future work

Total crop Chl content closely relates to the two key physiological properties, light capture and the efficiency of the use of absorbed light, which includes a broad range of processes and can be applied as an integrative diagnostic tool. It is observed that crop GPP is closely related to total Chl content. Thus, in this study a procedure was considered to remotely assess GPP in crops via estimation of total Chl content, by employing chlorophyll-related vegetation indices that can be calculated from reflectance spectra of vegetation collected by remote sensors. Besides total Chl content, crop GPP is also affected by incident photosynthetically active radiation (PAR). Therefore, a simple model, relating crop GPP to a product of chlorophyll-related VI and PAR (namely, VI-PAR-based model), was considered.

In this study, the model using a product of VI and PAR_{in} (VI-PAR_{in}-based model) was applied to estimate crop GPP with in situ collected reflectance data. VI was calculated from reflectance spectra collected at close range, 6 m above the canopy, and used as a proxy of total Chl content. PAR_{in} was measured by the ground-mounted sensors, which represented variation of incident radiation intensity due to seasonally changes in day length as well as short-period changes in atmospheric optical thickness. This model was able to accurately estimate GPP in maize and soybean that were different in crop managements and climatic conditions. Among the tested indices, chlorophyll indices (CI_{green} and $CI_{red\ edge}$) appeared to be the most accurate for estimating GPP in both maize and soybean, with RMSE below 2.55 $gC/m^2/d$ for maize (GPP ranging from 0 to 35 $gC/m^2/d$) and RMSE below 1.72 $gC/m^2/d$ for soybean (GPP ranging from 0 to 20 $gC/m^2/d$). But the algorithms for GPP estimates were species-specific for maize and

soybean due to their different leaf structures and canopy architectures, especially when using VI with NIR and either red or green reflectance. However, the indices employing red edge reflectance, simulated in MERIS spectral bands, $CI_{red\ edge}$, MTCI, Red edge NDVI, were least sensitive to different crop species. The algorithm with $CI_{red\ edge}$ or Red edge NDVI using red edge band around 720 nm was able to estimate GPP in maize and soybean combined with no need for re-parameterization for different crop types, with RMSE below 2.9 $gC/m^2/d$ and CV below 21%.

To estimate GPP entirely based on remotely sensed data, $PAR_{potential}$, which is PAR_{in} in conditions of minimal aerosol loadings, was used in the VI-PAR-based model as a better representative of incident radiation affecting crop photosynthesis than PAR_{in}. This model, relating crop GPP to a product of VI and $PAR_{potential}$ (VI-$PAR_{potential}$-based model) was successfully applied to atmospherically corrected Landsat data, and showed higher accuracy than VI-PAR_{in}-based model for GPP estimation. It was capable of estimating GPP in crops with SE below 3.5 $gC/m^2/d$ for maize and 2.8 $gC/m^2/d$ for soybean. And the indices using green and NIR Landsat bands were found to be the most accurate in GPP estimation. The algorithms established in the Nebraska study sites were validated for the same crops in Minnesota, Iowa and Illinois showing acceptable accuracy. This model was also capable of estimating GPP using raw Landsat imagery, i.e., imagery with no atmospheric correction.

The VI-$PAR_{potential}$-based GPP estimation model was also applied to MODIS 250 m data, which has much higher temporal resolution than Landsat data. The results showed that the model can accurately estimate crop GPP on days when the decrease in PAR_{in} from $PAR_{potential}$ was less than 50%. Among the MODIS-250 m retrieved indices tested,

EVI and WDRVI were the most accurate for GPP estimation with SE below 2.15 $gC/m^2/d$ in maize and 1.75 $gC/m^2/d$ in soybean. The VI-$PAR_{potential}$-based model is based solely on satellite data not requiring any ground-observed values, and represents a significant improvement over GPP estimates based on MODIS 1 km products provided by NASA.

This study provides a tool for accurate estimation crop GPP using the model based on a product of total Chl content and incident radiation, with remotely sensed data taken at close range and from satellite altitudes. However, it is recognized that this model contains several limitations:

(1) The model does not take into account GPP variation that does not affect crop Chl content. This is the case when GPP is affected by short-term (minutes to hours) environmental stresses (e.g., temperature, humidity, and soil moisture, among others), which do not immediately affect the Chl content (i.e., crop greenness), thus, do not affect chlorophyll-related indices. The model will fail to detect such GPP variations related to the types of stressors mentioned;

(2) It is observed that the use of PAR_{in} may introduce noise and unpredictable uncertainties in GPP estimation model. When the total Chl content remains the same, the quantitative prediction of GPP response to PAR_{in} variation is yet to be explored.

(3) When PAR_{in} is more than 60% below PARpotential, the use of $PAR_{potential}$ in the model may introduce the overestimation of GPP.

(4) In different geographic locations $PAR_{potential}$ varies as latitude changes. It is not clear how location difference affects GPP estimation model that uses $PAR_{potential}$ and

whether algorithms calibrated in one geographic region could be used for very different latitudes with no re-parameterization.

The approach presented in this study is easy to implement, and showed a great potential to remotely assess crop production at local, regional and global scales, which will no doubt provide valuable information for future agricultural applications and carbon studies, and will aid in policy decisions related to carbon budget, food security, and environmental regulation. There is still a long way to go to validate and improve the model, and a few recommendations for future work are summarized below:

(1) Other ancillary parameters that affect GPP need to be included in the GPP estimation model (e.g., temperature, soil moisture) to help detecting the GPP variation related to short-term stresses that do not affect crop Chl content instantly.

(2) Explore more how GPP will response to the variation of incident radiation when Chl content does not change.

(3) In this study, $PAR_{potential}$ was calculated as an empirical function of DOY. It is worthy to explore the method to retrieve $PAR_{potential}$ from remotely sensed data.

(4) Determine uncertainties of established algorithms for GPP estimation for crops other than maize and soybean with no re-parameterization.

(5) It is essential to test accuracy the GPP estimation model, presented in this study, for other geographic locations with very different latitudes.

(6) Apply the model to other satellite data that contain red edge spectral bands (e.g. MERIS and Sentinel-2, -3).

References

Ahl, D. E., Gower, S. T., Mackay, D. S., Burrows, S. N., Norman, J. M. & Diak, G. R. (2004). Heterogeneity of light use efficiency in a northern Wisconsin forest: implications for modeling net primary production with remote sensing. *Remote Sensing of Environment*, 93, 168-178.

Almond, S., Boyd, D.S., Dash, J., Curran, P.J., Hill, R.A., & Foody, G.M. (2010). Estimating terrestrial gross primary productivity with the Envisat Medium Resolution Imaging Spectrometer (MERIS) Terrestrial Chlorophyll Index (MTCI). *Geoscience and Remote Sensing Symposium (IGARSS) 2010 IEEE International*, 4792 – 4795, Honolulu, HI.

Alton, P. B., North, P. R. & Los, S. O. (2007), The impact of diffuse sunlight on canopy light-use efficiency, gross photosynthetic product and net ecosystem exchange in three forest biomes. *Global Change Biology*, 13, 776– 787.

Anderson, M. A., Norman, J. M., Meyers, T. P., & Diak, G. R. (2000). An analytical model for estimating canopy transpiration and carbon assimilation fluxes based on canopy light-use efficiency. *Agricultural and Forest Meteorology*, 100, 265– 289.

Asrar, G., Fuchs, M., Kanemasu, E.T., & Hatfield, J.H. (1984). Estimating absorbed photosynthetic radiation and leaf area index from spectral reflectance in wheat. *Agronomy Journal*, 76, 300-306.

Baker, J. & T. Griffis. (2005). Examining Strategies to Improve the Carbon Balance of Corn/soybean Agriculture Using Eddy Covariance and Mass Balance Techniques. *Agricultural and Forest Meteorology*, 128, 163-177.

Baldocchi, D.D. (2003). Assessing the eddy covariance technique for evaluating carbon dioxide exchange rates of ecosystems: past, present and future. *Global Change Biology*, 9, 479-492.

Barclay, H.J. (1998). Conversion of total leaf area to projected leaf area in Lodgeploe pine and Douglas-fir. *Tree Physiology*, 18, 185-193.

Baret, F., Houles, V. & Guerif, M. (2007). Quantification of plant stress using remote sensing observations and crop models: the case of nitrogen management. *Journal of Experimental Botany*, 58, 4, 869–880, doi:10.1093/jxb/erl231.

Barford, C. C., Wofsy, S. C., Goulden, M. L., Munger, J. W., Hammond, P. E., Urbanski, S. P., Hutyra, L., Saleska, S. R., Fitzjarrald, D. & Moore, K. (2003). Factors controlling long- and short-term sequestration of atmospheric CO_2 in a mid-latitude forest. *Science*, 294, 1688-1691.

Binkley, D., Stape, J. L. & Ryan, M. G. (2004). Thinking about efficiency of resource use in forests. *Forest Ecology and Management*, 193, 5 –16.

Bjorkman, O. & Powles, S. B. (1984). Inhibition of photosynthetic reactions under water stress: Interaction with light level, *Planta*, 161, 490–504.

Borras, L., Maddonni, G.A. & Otegui, M.E. (2003). Leaf senescence in maize hybrids: plant population, row spacing and kernel set effects. *Field Crops Research*. 82, 13-26.

Bouman, B.A.M. (1995). Crop modeling and remote sensing for yield prediction. *Netherlands Journal of Agricultural Science*, 43: 143-161.

Bradford, J. B., Hicke, J. A. & Lauenroth, W. K. (2005). The relative importance of light-use efficiency modifications from environmental conditions and cultivation for

estimation of large-scale net primary productivity. *Remote Sensing of Environment*, 96, 246– 255.

Broge, N.H. & Leblanc, E. (2000). Comparing prediction power and stability of broadband and hyperspectral vegetation indices for estimation of green leaf area index and canopy chlorophyll density. *Remote Sens. Environ.*, 76, 156 – 172.

Brown, J. C., Jepson, W. E., Kastens, J. H., Wardlow, B. D., Lomas, J. M. & Price, K. P. (2007). Multitemporal, moderate-spatial-resolution remote sensing of modern agricultural production and land modification in the Brazilian Amazon. *Giscience & Remote Sensing*, 44, 117−148.

Burba, G. (2005), Water and energy fluxes in native tallgrass prairie and cultivated wheat ecosystems, *Ph.D. dissertation*, AAI3163986, University of Nebraska-Lincoln, Lincoln.

Buschmann, C., & Nagel, E. (1993). In vivo spectroscopy and internal optics of leaves as basis for remote sensing of vegetation. International *Journal of Remote Sensing*, 14, 711 – 722.

Cassman, K.G. & Wood, S. (2005). Cultivated systems. In: Millennium Ecosystem Assessment: Global Ecosystem Assessment Report on Conditions and Trends. *Island Press*, Washington, DC, 741–789.

Ciganda, V., Gitelson, A.A. & Schepers, J. (2008). Vertical Profile and Temporal Variation of Chlorophyll in Maize Canopy: Quantitative “Crop Vigor” Indicator by Means of Reflectance-Based Techniques. *Agronomy Journal*, 100, 1409–1417, doi:10.2134/agronj2007.0322.

Ciganda, V., Gitelson, A.A. & Schepers, J. (2009). Non-destructive determination of maize leaf and canopy chlorophyll content. *Journal of Plant Physiology*, 166, 157-167.

Chappelle, E.W., Kim, M.S., & McMurtrey, J.E. (1992). Ratio analysis of reflectance spectra (RARS): an algorithm for the remote estimation of the concentrations of chlorophyll A, chlorophyll B, and carotenoids in soybean leaves. *Remote Sensing of Environment*, 39, 239-247.

Dash, J. & Curran, P.J. (2004). The MERIS terrestrial chlorophyll index. *International Journal of Remote Sensing*, 25, 5003-5013.

Dawson, T. P., North, P. R. J., Plummer, S. E. & Curran, P. J. (2003). Forest ecosystem chlorophyll content: implications for remotely sensed estimates of net primary productivity. *International Journal of Remote Sensing*, 24, 611-617.

Daughtry, C. S. T., Walthall, C. L., Kim, M. S., Brown de Colstoun, E. & McMurtrey III, J.E. (2000). Estimating corn leaf chlorophyll concentration from leaf and canopy reflectance. *Remote Sens. Environ.* 74, 229– 239.141– 152.

DeLucia, E. H., Drake, J. E., Thomas, R. B. & Gonzalez-Melers, M. (2007). Forest carbon use efficiency: Is respiration a constant fraction of gross primary production? *Global Change Biology*, 13, 1157–1167.

Dixon, R.K., Brown, S. R., Houghton, A., Solomon, A. M., Trexler, M. C. & Wisniewski, J. (1994). Carbon pools and flux of global forest ecosystems. *Science*, 263, 185-190.

Fang, H. (2009). Readme document for North America Land Data Assimilation System Phase 2 (NLDAS-2) Products. *Goddard Earth Sciences Data and Information Service*

Center, Available at: http://hydro1.sci.gsfc.nasa.gov/data/s4pa/NLDAS/README.NLDAS2.pdf.

Feng, M., C. Huang, S. Channan, E. Vermote, J. Masek, & Townshend, J.R. (2011). Quality assessment of Landsat surface reflectance products using MODIS data, *Computers & Geoscience*, 38, 9-22.

Fielding, A.L., & Bell, J.F. (1997). A review of methods for the assessment of prediction errors in conservation presence/absence models. *Environmental Conservation*, 24, 38 – 49.

Field, C. B. & Mooney, H. A. (1986). The photosynthesis-nitrogen relationship in wild plants. *in On the Economy of Plant Form and Function*, edited by T. J. Givnish, 25– 55, Cambridge University, Press, New York.

Fukshansky, L. (1981). Optical properties of plant tissue. In H. Smith (Ed.), *Plants and the daylight spectrum*, 253–303. Berlin: Springer.

Fukshansky, L. A., Remisowsky, A. M., McClendon, J., Ritterbusch, A., Richter, T., & Mohr, H. (1993). Absorption spectra of leaves corrected for scattering and distributional error: A radiative transfer and absorption statistics treatment. *Photochemistry and Photobiology*, 57, 538–555.

Gamon, J. A., Penuelas, J. & Field, C. B. (1992). A narrow waveband spectral index that tracks diurnal changes in photosynthetic efficiency. *Remote Sensing of Environnement*, 4, 35-44.

Garbulsky, M.F., Penuelas, J., Gamon, J., Inoue, Y. & Filella, I. (2010). The photochemical reflectance index (PRI) and the remote sensing of leaf, canopy and

ecosystem radiation use efficiencies. *Remote Sensing of Environment*, doi:10.1016/j.rse.2010.08.023

Gitelson, A. A. (2004). Wide dynamic range vegetation index for remote quantification of biophysical characteristics of vegetation. *J. Plant Physiol*. 161, 2, 165-173.

Gitelson, A.A. (2011). Non-destructive estimation of foliar pigment (chlorophylls, carotenoids and anthocyanins) contents: espousing a semi-analytical three-band model. Chapter 6 in Hyperspectral Remote Sensing of Vegetation, Thenkabail, P.S., Lyon, J.G., Huete, A., Eds, 141-165, Taylor and Francis.

Gitelson, A.A., & Merzlyak, M. (1994). Quantitative estimation of chlorophyll-a using reflectance spectra: experiments with autumn chestnut and maple leaves. *Journal of Photochemistry and Photobiology B: Biology*, 22, 247 – 252.

Gitleson, A.A., & Merzlyak, M. (1997). Remote estimation of chlorophyll content in higher plant leaves. *International Journal of Remote Sensing*, 18, 12, 291 – 298.

Gitelson, A., Kaufman, Y., & Merzlyak, M. (1996). Use of a Green Channel in Remote Sensing of Global Vegetation from EOS-MODIS. *Remote Sensing of Environment*, 58, 289-298.

Gitelson, A.A., Kaufman, Y.J.; Stark, R.. & Rundquist, D. (2002). Novel algorithms for remote estimation of vegetation fraction. *Remote Sens. Envron*. 80, 76-87.

Gitelson, A.A., Gritz, U. & Merzlyak M.N. (2003a). Relationships between leaf chlorophyll content and spectral reflectance and algorithms for non-destructive chlorophyll assessment in higher plant leaves. *Journal of Plant Physiology*, 160, 3, 271-282.

Gitelson, A. A., Verma, S. B., Viña, A., Rundquist, D. C., Keydan, G., Leavitt, B., Arkebauer, T. J., Burba, G. G. & Suyker, A. E. (2003b). Novel technique for remote estimation of CO_2 flux in maize. *Geophysical Research Letter*, 30, 9, 1486, doi:10.1029/2002GL016543.

Gitelson, A.A., Viña, A., Arkebauer, T.J., Rundquiste, D.C., Keydan, G. & Leavitt, B. (2003c). Remote estimation of leaf area index and green leaf biomass in maize canopies. *Geophysical Research Letters*, 30, 5, 1248, doi: 10.1029/2002GL016450.

Gitelson, A. A., Viña, A., Ciganda, V., Rundquist, D. C. & Arkebauer, T. J. (2005). Remote estimation of canopy chlorophyll content in crops, *Geophysical Research Letter*, 32, L08403, doi:10.1029/2005GL022688.

Gitelson, A. A., Keydan, G. P., & Merzlyak, M. N. (2006a). Three-band model for noninvasive estimation of chlorophyll, carotenoids, and anthocyanin contents in higher plant leaves, *Geophysical Research Letter*, 33, L11402, doi:10.1029/2006GL026457.

Gitelson, A. A., Viña, A., Verma, S. B., Rundquist, D. C., Arkebauer, T. J., Keydan, G., Leavitt, B., Ciganda, V., Burba, G. G., & Suyker, A. E. (2006b). Relationship between gross primary production and chlorophyll content in crops: Implications for the synoptic monitoring of vegetation productivity. *Geophysical Research Letter*, 111, D08S11, doi:10.1029/2005JD006017.

Gitelson, A.A., Wardlow, B. D., Keydan, G. P. & Leavitt, B. (2007). An Evaluation of MODIS 250-m Data for Green LAI Estimation in Crops, *Geophys. Res. Lett.*, 34, L20403, doi:10.1029/2007GL031620.

Gitelson, A.A., Viña, A., Masek, J.G., Verma, S. B., & Suyker, A. E. (2008). Synoptic Monitoring of Gross Primary Productivity of Maize Using Landsat Data, *IEEE Geoscience and Remote Sensing Letters*, 5, 2, 10.1109/LGRS.2008.915598.

Gitelson, A.A., Peng, Y., Masek, J.G., Rundquist, D.C., Verma, S.B., Suyker, A., Baekr, J.M., Hatfield, J.L. & Meyers, T. (2012). Remote estimation of crop gross primary production with Landsat data. *Remote Sensing of Environment*. 121, 404-414.

Gobron, N., Pinty, B., Verstraete, M. M., & Govaerts, Y. (1997). A semidiscrete model for the scattering of light by vegetation. *Journal of Geophysical Research-atmospheres*, 102, 9431–9446.

Goward, S. N. & K. F. Huemmrich. (1992). Vegetation canopy PAR absorptance and the normalized difference vegetation index: an assessment using the SAIL model. *Remote Sens. Environ.*, 39, 119-140.

Gower, S.T., Kucharik, C.J., & Norman, J.M. (1999). Direct and indirect estimation of leaf area index, fAPAR and net primary production of terrestrial ecosystems. *Remote Sensing of Environment*, 70, 29-51.

Haboudane, D., Miller, J.R., Tremblay, N., Zarco-Tejada, P.J. & Dextraze, L. (2002). Integrated narrow-band vegetation indices for prediction of crop chlorophyll content for application to precision agriculture. *Remote Sens. Environ.*, 81, 416 – 426.

Haboudane, D., Miller, J.R., Pattey, E., Zarco-Tejada, P.J. & Strachan, I.B. (2004). Hyperspectral vegetation indices and novel algorithms for predicting green LAI of crop canopies: Modeling and validation in the context of precision agriculture. *Remote Sens. Environ*. 90, 337 – 352.

Hall, F. G., Huemmrich, K. F., Goetz, S. J., Sellers, P. J. & Nickeson, J. E. (1992). Satellite remote sensing of surface energy balance: Success, failures and unresolved issues in FIFE. *Journal of Geophysical Research*, 97, 19,061 –19,089.

Hanan, N.P., Burba, G., Verma, S.B., Berry, J.A., Suyker, A. & Walter-Shea, E.A. (2002). Inversion of net ecosystem CO_2 flux measurements for estimation of canopy PAR absorption. *Global Change Biology*, 8, 563-574.

Harris, A. & Dash, J. (2010). The potential of the MERIS Terrestrial chlorophyll Index for carbon flux estimation. *Remote Sensing of environment*, 114, 1856 – 1862.

Hatfield, J. L., Jaynes, D. B., Burkart, M. R., Cambardella, C. A., Moorman, T. B., Prueger, J. H., & Smith, M. A. (1999). Water quality in Walnut Creek Watershed: setting and farming practices. *J. Environ. Qual*., 28, 11-24.

Heinsch, F. A., Zhao, M., Running, S. W., Kimball, J. S., Nemani, R. R., Davis, K. J., Bolstad, P. V., Cook, B. D., Desai, A. R., Ricciuto, D. M., Law, B. E., Oechel, W. C., Kwon, H. J., Luo, H., Wofsy, S. C., Dunn, A. L., Munger, J. W., Baldocchi, D. D., Xu, L., Hollinger, D. Y., Richardson, A. D., Stoy, P. C., Siqueira, M. B. S., Monson, R. K., Burns, S. P., & Flanagan, L. B. (2006). Evaluation of remote sensing based terrestrial productivity from MODIS using regional tower eddy flux network observations. *IEEE Trans. Geosci. Remote Sens.,* 44, 1908-1925, doi: 10.1109/TGRS.2005.85396.

Hollinger, D. Y., Aber, J., Dail, B., Davidson, E. A., Goltz, S. M., Hughes, H., Leclerc, M. Y., Lee, J. T., Richardson, A. D., Rodrigues, C., Scott, N. A., Achuatavarier, D. & Walsh, J. (2004). Spatial and temporal variability in forest-atmosphere CO_2 exchange. *Global Change Biol.,* 10, 1689-1706.

Hollinger, S.E., Bernacchi, C.J. & Meyers, T. P. (2005). Carbon budget of mature no-till ecosystem in North Central Region of the United States. *Agricultural and Forest Meteorology*, 130, 59-69.

Houborg, R., Anderson, M.C., Daughtry, C.S.T., Kustas, W. P. & Rodell, M. (2010). Using leaf chlorophyll to parameterize light-use-efficiency within a thermal-based carbon, water and energy exchange model. *Remote Sensing of Environment*, 115, 1694-1705.

Houle`s, V., Gue´rif, M., Mary, B., Gate, P., Machet, JM & Moulin, S. (2006). Elaboration d'un indicateur de nutrition azote´e du ble´ base´ sur l'indice foliaire et la teneur en chlorophylle pour la pre´conisation de doses d'azote. *In: Gue´re´f M, King D*, eds. He´te´roge´neite´ parcellaire et gestion des cultures; vers une agricolture de pre´cision. Editions QUAE. 179–198.

Huete, A. R., Liu, H. Q., Batchily, K. & van Leeuwen, W. (1997). A comparison of vegetation indices global set of TM images for EOS-MODIS. *Remote Sensing of Environment*, 59, 440-451.

Jiang, Z., Huete, A. R., Didan, K. & Miura, T. (2008). Development of a two-band enhanced vegetation index without a blue band. *Remote Sens. Environ*. 112, 3833-3845.

Jordan, C. F. (1969). Derivation of leaf area index from quality of light in the forest floor. *Ecology*, 50, 663-666.

Kanemasu, E.T. (1974). Seasonal canopy reflectance patterns of wheat, sorghum, and soybean. *Remote Sens. Environ.*, 3, 43-47.

Kasahara, M., Kagawa, T., Oikawa, K., Suetsugu, N., Miyao, M., & Wada, M. (2002) Chloroplast avoidance movement reduces photodamage in plants, *Nature*, 420, 829–832.

Kaufman, Y. J., Wald, A. E., Remer, L. A., Gao, B.-C., Li, R.-R., & Flynn, L. (1997). The MODIS 2.1-μm channel—Correlation with visible reflectance for use in remote sensing of aerosol. *IEEE Trans. Geosci. Remote Sens.*, 35, 5, 1286–1296.

Kergoat, L., Lafont, S., Arneth, A., Le Dantec, V., & Saugier, B. (2008). Nitrogen controls plant canopy Light-Use-Efficiency in temperate and boreal ecosystems. *Journal of Geophysical Research*, 113, G04017, 1-19, DOI: 10.1029/2007JG000676.

Kohavi, R. (1995). A study of cross-validation and bootstrap for accuracy estimation and model selection. In C.S. Mellish (Ed.). *International joint conference on artificial intelligence (IJCAI),* 1137 – 1143, Montreal, Quebec, Canada : Morgan Kuafmann, Los Altos, CA.

Kotchenova, S. Y., & Vermote, E. (2007). Validation of a vector version of the 6S radiative transfer code for atmospheric correction of satellite data. Part II: Homogeneous Lambertian and anisotropic surfaces, *Applied Optics*, 46, 20, 4455-4464.

Law, B. E., Falge, E. Baldocchi, D. D., Bakwin, P., Berbigier, P., Davis, K., Dolman, A. J., Falk, M., Fuentes, J. D., Goldstein, A., Granier, A., Grelle, A., Hollinger, D., Janssens, I. A., Jarvis, P., Jensen, N. O., Katul, G., Mahli, Y., Matteucci, G., Monson, R., Munger, W., Oechel, W., Olson, R., Pilegaard, K., Paw U, K. T., Thorgeirsson, H., Valentini, R., Verma, S., Vesala, T., Wilson, K., & Wofsy, S. (2002). Carbon dioxide and water vapor exchange of terrestrial vegetation in response to environment. *Agric. For. Meteorol.*, 113, 97-120.

Law, B.E., Arkebauer, T., Campbell, J.L., Chen, J., Sun, O., Schwartz, M., van Ingen, C. & Verma S. (2008). Terrestrial Carbon Observations: Protocols for Vegetation Sampling and Data Submission. *Global Terrestrial Observing System*, FAO, Rome, Report 55, 87.

Lee, D.S., Storey, J. C., Choate, M.J., & Hayes, R. (2004) Four years of Landsat-7 on-orbit geometric calibration and performance. *IEEE Transactions on Geoscience and Remote Sensing*, 42, 2786-2795.

Lichtenthaler, H., Gitelson, A., & Lang, M. (1996). Non-destructive determination of chlorophyll content of leaves of a green and an aurea mutant of tobacco by reflectance measurements. *Journal of Plant Physiology*, 148, 483-493.

Lieth, H., & Whittaker, R. H. (1975). Primary productivity of the biosphere. *Ecological Studies*, 14, Springer-Verlag, 7-16.

Lyapustin, A. (2003). Interpolation and Profile Correction (IPC) method for shortwave radiative transfer in spectral intervals of gaseous absorption. *J. Atmos. Sci.,* 60, 865-871.

Malmstrom, C. M., Thompson, M. V., Juday, G. P., Los, S. O., Randerson, J. T., & Field, C. B. (1997). Interannual variation in global-scale net primary production: Testing model estimates. *Global Biogeochemical Cycles*, 11, 367–392.

Masek, J. G., Vermote, E. F., Saleous, N., Wolfe, R., Hall, F. G., Huemmrich, F., Gao, F., Kutler, J., & Lim, T. K. (2006). A Landsat surface reflectance data set for North America. 1990-2000, *Geoscience Remote Sens. Lett.,* 3, 68-72.

Medina, E. & H. Lieth. (1964). Die Beziehungen zwischen Chlorophyllgehalt, assimilierender Flaeche und Trockensubstanzproduktion in einigen

Pflanzengemeinschaften. (The relationships between chlorophyll content, assimilating area and dry matter production in some plant communities.) *Beitraege zur Biologie der Pflanzen,* 40, 451-494.

Medlyn, B. E. (1998). Physiological basis of the light use efficiency model. *Tree Physiology*, 18, 167– 176.

Merzlyak, M., & Gitelson, A. A. (1995). Why and what for the leaves are yellow in autumn? On the interpretation of optical spectra of senescing leaves (Acer platanoides L.). *Journal of Plant Physiology*, 145, 3, 315–320.

Monteith, J. L. (1972). Solar radiation and productivity in tropical ecosystems. *Journal of Applied Ecology*, 9, 744-766.

Monteith, J. L. (1977). Climate and the efficiency of crop production in Britain. *Philosophical Transactions of the Royal society of London*, 281, 277-294.

Myneni, R. B., Keeling, C. D., Tucker, C. J., Asrar, G. & Nemani, R. R. (1997). Increased plant growth in the northern high latitudes from 1981 to 1991. *Nature,* 386, 698-702.

Myneni, R. B., Dong, J. C., Tucker, J., Kaufmann, R. K., Kuppi, P. E., Liski, J., Zhou, L., Alexyev, V. & Hughes, M. K. (2001). A large carbon sink in the woody biomass of Northern forests. *Proceedings of the National Academy of Science,* 98, 14784-14789.

Ort, D.R. (2001). When there is too much light. *Plant Physiology*, 125, 1, 29-32.

Osborne, B. A. & Raven, J. A. (1986). Light absorption by plants and its implications for photosynthesis. *Biological Reviews*, 61, 1, 1-60. doi: 10.1111/j.1469-185X.1986.tb00425.x

Peng, Y. & Gitelson, A.A. (2011a) Application of chlorophyll-related vegetation indices for remote estimation of maize productivity. Agricultural and Forest Meteorology, 151, 1267 – 1276.

Peng, Y. & Gitelson, A.A. (2011b) Remote estimation of gross primary productivity in soybean and maize based on total crop chlorophyll content. Remote Sensing of Environment, 117, 440-448.

Peng, Y., Gitelson, A.A., Keydan, G.P., Rundquist, D.C., Leavitt, B., Verma, S.B., & Suyker, A. E. (2010) Remote estimation of Gross Primary Production in Maize. Proceedings of 10th International Conference on Precision Agriculture, July 18-21, Denver, Colorado, USA, *10th ICPA Proceedings CD*, 1-15.

Peng, Y., Gitelson, A.A., Keydan, G., Rundquist, D.C. & Moses, W. (2011) Remote estimation of gross primary production in maize and support for a new paradigm based on total crop chlorophyll content. *Remote Sensing of Environment*, 115, 978-989.

Reeves, M.C., Zhao, M., & Running, S.W. (2004). Usefulness and limits of MODIS GPP for estimating wheat yield. *International Journal of Remote Sensing*, 26, 7, 1403-1421.

Prince, S. D. (1991). A model of regional primary production for use with coarse resolution satellite data. *International Journal of Remote Sensing*, 12, 1313– 1330.

Rondeaux, G., Steven, M. & Baret, F. (1996). Optimization of Soil-adjusted vegetation indices. *Remote Sens. Environ*. 55, 95-107.

Rouse, J.W., Haas, RH Jr., Schell, J.A. & Deering, D.W. (1974). Monitoring vegetation systems in the Great Plains with ERTS. NASA SP-351, *Third ERTS-1 Symposium NASA Washington DC*, 1, 309-317.

Rundquist, D., Schalles, J. & Peake, J. (1995). The response of volume reflectance to manipulated algal concentrations above bright and dark bottoms at various depths in an experimental pool. *GeoCarto International,* 10, 5–14.

Rundquist, D. C., Perk, R., Leavitt, B., Keydan G. P., & Gitelson, A. A. (2004). Collecting spectral data over cropland vegetation using machine-positioning versus hand-positioning of the sensor. *Computers and Electronics in Agriculture,* 43, 173-178.

Ruimy, A., Saugier, B. & Dedieu, G. (1994). Methodology for the estimation of terrestrial net primary production from remotely sensed data. *Journal of Geophysical Research*, 99, 5263–5283.

Ruimy, A., Kergoat, L. & Bondeau, A. (1999). Comparing global models of terrestrial net primary productivity (NPP): Analysis of differences in light absorption and light-use efficiency. *Global Change Biology*, 5, 56-64.

Running, S. W., P. E. Thornton, R. Nemani & Glassy, J. M. (2000). Global terrestrial gross and net primary productivity from the Earth Observing System. In O.E. Sala, R.B. Jackson, H.A. Mooney and R.W. Howarth (Eds.). *Methods in ecosystem science*. Springer-Verlag, New York, 44-57.

Running, S. W., Nemani, R. R., Heinsch, F. A., Zhao, M. S., Reeves, M. & Hashimoto, H. (2004). A continuous satellite-derived measure of global terrestrial primary production. *Bioscience*, 54, 547-560.

Sakamoto, T., Shibayama, M., Takada, E., Inoue, A., Morita, K., Takahashi, W., Miura,S. & Kimura, A. (2010a). Detecting seasonal changes in crop community structure using day and night digital images. *Photogrammetric Engineering and Remote Sensing*, 76, 6, 713–726.

Sakamoto, T., Wardlow, B.D., Gitelson, A.A., Verma, S.B., Suyker, A.E. & Arkebauer, T.J. (2010b). A two-step filtering approach for detecting maize and soybean phenology with time-series MODIS data. *Remote Sensing of Environment*, 114, 2146-2159.

Sakamoto, T., Gitelson, A.A., Wardlow, B.D., Arkerbauer, T.J., Verma, S.B, Suyker, A.E. & Shibayama, M. (2011a). Application of day and night digital photographs for estimating maize biophysical characteristics, Precision Agriculture, doi: 10.1007/s11119-011-9246-1.

Sakamoto, T., Gitelson, A.A., Wardlow, B.D., Verma, S.B., & Suyker, A.E. (2011b). Estimating daily gross primary production of maize based only on MODIS WDRVI and shortwave radiation data - IN PRESS. *Remote Sensing of Environment*, doi:10.1016/j.rse.2011.06.015.

Sakamoto, T., Gitelson, A.A., Nguy-Robertson, A.L., Arkerbauer, T.J., Wardlow, B.D., Suyker, A.E., Verma, S.B & Shibayama, M. (2012). An alternative method using digital cameras for continuous monitoring of crop status. *Agricultural and Forest Meteorology*, 154-155: 113-126.

Schimel, D.S. (1998). Climate change: The carbon equation. *Nature*, 393, 208-210.

Sims, D. A., Rahman, A. F., Cordova, V. D., El-Masri, B. Z., Baldocchi, D. D., Flanagan, L. B., Goldstein, A. H., Hollinger, D. Y., Mission, L., Monson, R. K., Oechel, W. C., Schmid, H. P., Wofsy, S. C. & Xu, L. (2006). On the use of MODIS EVI to assess gross primary productivity of North American ecosystems. *Journal of Geophysical Research*, 111, G04015, doi:10.1029/2006JG000162.

Sims, D. A., Rahman, A. F., Cordova, V. D., El-Masri, B. Z., Baldocchi, D. D., Bolstad, P. V. et al. (2008). A new model of gross primary productivity for North American

ecosystems based solely on the enhanced vegetation index and land surface temperature from MODIS. *Remote Sensing of Environment*, 112, 1633−1646.

Sims, D.A., Rahman, A.F., Vermote, E.F. & Jing, Z. (2011). Seasonal and inter-annual variation in view angle effects on MODIS vegetation indices at three forest sites. *Remote Sensing of Environment,* 115, 3112-3120.

Stark, R. & Gitelson, A. (2000). Radiation regime in irrigated wheat. *In: Proceedings of the Second International Conference on Geospatial Information in Agriculture and Forestry*, 89–96.

Suyker, A.E., Verma, S..B., Burba, G.G., & Arkebauer, T.J. (2005). Gross primary production and ecosystem respiration of irrigated maize and irrigated soybean during a growing season. *Agric. For. Meteorol*. 131, 180-190.

Suyker, A. E., & Verma, S. B. (2010). Coupling of carbon dioxide and water vapor exchanges of irrigated and rainfed maize-soybean cropping systems and water productivity. *Agricultural and forest Meteorology*, 150, 553 – 563.

Terry, N. (1980). Limiting factors in photosynthesis. I. Use of iron stress to control photochemical capacity in vivo. *Plant Physiology*, 65, 114 – 120.

Terry, N. (1983). Limiting factors in photosynthesis. IV. Iron stress-mediated changes in light harvesting and electron transport capacity and its effects on photosynthesis in vivo. *Plant Physiology*, 71, 855 – 860.

Thomas, J. R., & H. W. Gaussman. (1977). Leaf reflectance vs. leaf chlorophyll and carotenoid concentration for eight crops, *Agronomy Journal*, 69: 799– 802.

Turner, D. P., Urbanski, S., Bremer, D., Wofsy, S., Meyers, T., Gower, S. T., et al. (2003). A cross-biome comparison of daily light use efficiency for gross primary production.*Global Change Biology*, 9, 383–395.

Turner, D. P., Ritts, W. D., Cohen, W. B., Maeirsperger, T. K., Gower, S. T., Kirschbaum, A. A., Running, S. W., Zhao, M., Wofsy, S. C., Dunn, A. L., Law, B. E., Campbell, J. L., Oechel, W. C., Kwon, H., Meyers, T. P., Small, E. E., Kurc, S. A., , & Gamon, J.A. (2005). Site-level evaluation of satellite-based global terrestrial GPP and NPP monitoring. *Global Change Biol.*, 11, 666-684.

Turner, D., Ritts, W., Zhao, M., Kurc, S. A., Dunn, A., Wofsy, S., Small, E. E. & Running, S.W. (2006). Assessing interannual variation in MODIS-based estimates of gross primary production. *IEEE Trans. Geosci. Remote Sens.,* 44, 7, 1899-1907.

Ustin, S.L., Smith, M. O., Jacquemoud, S., Verstraete, M. M. & Govaerts, Y. (1998). GeoBotany: Vegetation Mapping for Earth Sciences. *In Manual of Remote Sensing: Remote Sensing for the Earth Sciences,* A.N. Rencz, ed., Third Edition, 3, 189-248.

Verma, S. B., Dobermann, A., Cassman, K. G., Walters, D. T., Knops, J. M., Arkebauer, T. J., Suyker, A. E., Burba, G. G., Amos, B., Yang, H., Ginting, D., Hubbard, K. G., Gitelson, A. A. & Walter-Shea, E. A. (2005). Annual carbon dioxide exchange in irrigated and rainfed maize-based agroecosystems. *Agricultural and Forest Meteorology*, 131, 77-96.

Vermote, E.F., Tanré, D., Deuzé, J.L., Herman, M., & Morcrette, J.J., (1997a). Second Simulation of the Satellite Signal in the Solar Spectrum: an overview, *IEEE Transactions on Geoscience and Remote Sensing,* 35, 3, 675-686.

Vermote, E. F., Saleous, N. El, Justice, C. O., Kaufman, Y. J., Privette, J. L., Remer, L., Roger, J. C. & Tanré, D. (1997b). Atmospheric correction of visible to middle-infrared EOS-MODIS data over land surfaces: Background, operational algorithm, and validation. *J. Geophys. Res.*, 102, 17131-17141.

Vermote, E. F., El Saleous, N. Z., & Justice, C. O. (2002). Atmospheric correction of MODIS data in the visible to middle infrared: First results. *Remote Sensing of Environment*, 83, 97−111.

Viña, A. (2004). Remote estimation of leaf area index and biomass in corn and soybean. *Ph.D dissertation*, AAI3131566, University of Nebraska-Lincoln, Lincoln, NE.

Viña, A., Henebry, G. M., & Gitelson A. A. (2004). Satellite Monitoring of Vegetation Dynamics: Sensitivity Enhancement by the Wide Dynamic Range Vegetation Index. *Geophysical Research Letters*, 31, L04503, doi:10.1029/2003GL019034.

Viña, A & Gitelson, A.A. (2005). New developments in the remote estimation of the fraction of absorbed photosynthetically active radiation in crops, *Geophysical Research Letters*, 32, L17403, doi:10.1029/2005GL023647.

Viña, A., Gitelson, A.A., Nguy-Robertson, A.L. & Peng, Y. (2011). Comparison of different vegetation indices for the remote assessment of green leaf area index of crops. *Remote Sensing of Environment*, 115, 3468-3478.

Wardlow, B. D., & Egbert, S. L. (2008). Large-area crop mapping using time-series MODIS 250 m NDVI data: An assessment for the US Central Great Plains. *Remote Sensing of Environment*, 112, 1096−1116.

Weiss, A. & Norman, J.M. (1985). Partitioning solar radiation into direct and diffuse, visible and near-infrared components. *Agricultural and Forest Meteorology*, 34, 205-213.

Whittaker, R. H. & Marks, P. L. (1975). Methods of assessing terrestrial productivity. In H. Lieth and R. H. Whittaker (Eds.). Primary productivity of the biosphere. *Ecological Studies,* 14, Springer-Verlag, 55-118.

Wood, S., Sebastian, K. & Scherr, S.J. (2000). Pilot Analysis of Global Ecosystems (Agroecosystems). *International Food Policy Research Institute and World Resources Institute*, Washington, DC, 110.

Wullschleger, S. D. (1993). Biochemical limitations to carbon assimilation in C3 plants—A retrospective analysis of the A/Ci curves from 109 species. *Journal of Experimental Botany*, 44, 907– 920.

Wu, C., Niu, Z., Tang, Q., Huang, W., Rivard, B. & Feng, J. (2009). Remote estimation of gross primary production in wheat using chlorophyll-related vegetation indices. *Agricultural and Forest Meteorology,* 149, 1015-1021.

Wu, C., Wang, L., Niu, Z., Gao, S., &Wu, M.Q. (2010a). Nondestructive estimation of canopy chlorophyll content using Hyperion and Landsat/TM images. *International Journal of Remote Sensing*, 31: 8, 2159 – 2167.

Wu, C., Niu, Z., & Gao, S. (2010b). Gross primary production estimation from MODIS data with vegetation index and photosynthetically active radiation in maize. *Journal of Geophysical Research*, 115, D12127, doi:10.1029/2009JD013023.